1983

Boundary Layer Flow In Streamwise Concave Corners

Steven Ray Wilkinson

CANADIAN THESES ON MICROFICHE

I.S.B.N.

THESES CANADIENNES SUR MICROFICHE

National Library of Canada
Collections Development Branch

Canadian Theses on
Microfiche Service

Ottawa, Canada
K1A 0N4

Bibliothèque nationale du Canada
Direction du développement des collections

Service des thèses canadiennes
sur microfiche

NOTICE

The quality of this microfiche is heavily dependent upon the quality of the original thesis submitted for microfilming. Every effort has been made to ensure the highest quality of reproduction possible.

If pages are missing, contact the university which granted the degree.

Some pages may have indistinct print especially if the original pages were typed with a poor typewriter ribbon or if the university sent us a poor photocopy.

Previously copyrighted materials (journal articles, published tests, etc.) are not filmed.

Reproduction in full or in part of this film is governed by the Canadian Copyright Act, R.S.C. 1970, c. C-30. Please read the authorization forms which accompany this thesis.

THIS DISSERTATION
HAS BEEN MICROFILMED
EXACTLY AS RECEIVED

AVIS

La qualité de cette microfiche dépend grandement de la qualité de la thèse soumise au microfilmage. Nous avons tout fait pour assurer une qualité supérieure de reproduction.

S'il manque des pages, veuillez communiquer avec l'université qui a conféré le grade.

La qualité d'impression de certaines pages peut laisser à désirer, surtout si les pages originales ont été dactylographiées à l'aide d'un ruban usé ou si l'université nous a fait parvenir une photocopie de mauvaise qualité.

Les documents qui font déjà l'objet d'un droit d'auteur (articles de revue, examens publiés, etc.) ne sont pas microfilmés.

La reproduction, même partielle, de ce microfilm est soumise à la Loi canadienne sur le droit d'auteur, SRC 1970, c. C-30. Veuillez prendre connaissance des formules d'autorisation qui accompagnent cette thèse.

LA THÈSE A ÉTÉ
MICROFILMÉE TELLE QUE
NOUS L'AVONS REÇUE

NL-339 (r. 82/08)

Canada

BOUNDARY LAYER FLOW IN STREAMWISE CONCAVE CORNERS

by

Steven Ray Wilkinson

Department of Applied Mathematics

Submitted in partial fulfillment
of the requirements for the degree of
Doctor of Philosophy

Faculty of Graduate Studies
The University of Western Ontario
London, Ontario

January, 1983

ORIGINAL

ABSTRACT

Laminar boundary-layer theory has been correctly developed for streamwise corners using singular perturbation techniques. Similarity appears as a basic assumption and provides needed simplification. Any theoretical investigation of similarity breakdown, however, would require examination of the cross-flow behavior, which is examined thoroughly in this thesis.

The formulation of the boundary-layer equations is reviewed beginning with time-independent Navier-Stokes equations. Tensor analysis is used so that the resulting equations are generally applicable to any similar flow configuration. A non-orthogonal Cartesian coordinate system is chosen to deal with streamwise concave corners (i.e. with corner angles less than 180°). Coordinate and flow-variable transforms are then used to define bounded quantities.

The computational procedures for obtaining the boundary conditions and solving the main equations are described briefly, noting some pitfalls that would hinder numerical computation. Results characterizing the mainstream flow and the secondary cross-flow are displayed and discussed for corners with angles of 30°, 60°, 90°, 120° and 150°. Ways to proceed with further investigation, while keeping the mathematical model simple, are then suggested.

ACKNOWLEDGEMENTS

In the production of this work, thanks are due to Dr. Mair Zamir for making it possible, the University and the NSERC for making it worthwhile, and my wife Susan for making it livable from beginning to end.

TABLE OF CONTENTS

LIST OF FIGURES

LIST OF FIGURES (continued)

1. INTRODUCTION

1.1 Three-Dimensional Boundary Layer Theory

The broad purpose of boundary-layer theory is to make the difficult problem of solving the Navier-Stokes equation simpler. The classical problem of the flow past a flat plate is perhaps the simplest of such problems, mainly because the flow is two-dimensional. Although the vast majority of practical situations are of course three-dimensional, various features resulting from the two-dimensional problem can be used to good approximation in situations where surface curvature is small. The normal to the surface at some point, for example, can be assumed to be the direction of the maximum velocity gradient with the result that velocity gradients in other directions are negligable. From the potential flow problem associated with the boundary layer problem in question, the pressure distribution is found. It is applicable within the boundary layer by virtue of the pressure gradient along the surface normal being zero. These results are taken advantage of by specifying a coordinate system in which one of the coordinate directions is normal to the surface and other coordinate directions parallel to the surface. The velocity gradient in the normal direction dominates those in the parallel directions, and the pressure gradient in the normal direction

is zero. It is now known that certain terms in the flow equations can be neglected compared with others.

With three-dimensional problems it is possible that there exists velocities in the lateral direction (i.e. perpendicular to the flow direction yet parallel to the surface). For problems which are axially symmetric with respect to the streamwise direction, the lateral coordinate is periodic and can be eliminated from the problem by a transformation (see Schlicting (1955)). Otherwise one must assume the lateral curvature to be small so that the lateral velocity component is small enough to be of secondary importance compared to the mainstream velocity.

Large curvatures in the solid boundary present different problems. Sharp corners perpendicular to the flow cause the boundary layer to separate from the boundary. In these cases the fundamental assumption that the boundary layer is thin breaks down and other theories must deal with the situation. Stewartson (1974) presents a theory for this case. Large curvatures in the lateral direction present different problems again since lateral velocities can be large and must be considered, which further complicates the problem. The question arises of how boundary layer theory can be used to simplify the problem.

The basic flow configuration to be considered now and for the remainder of this work is that of flow moving parallel to the intersection of two infinite planes or, in other words, streamwise corner flow. This problem serves well to illustrate the basic features of flow near surface regions of large lateral curvature. In this case the curvature is infinite at the corner. Such flow features arise in many practical situations such as wing-fuselage junctions, tail assemblies of aircraft and corners of air intakes for jet engines. The solution to the problem can also be more directly applied to providing details of flow near corners of high Reynolds number channel flows and square air ducts in which the extent of the walls is large compared to the domain of interest near the corner. Physical properties one may wish to predict in streamwise corner flow are boundary layer separation and transition from laminar to turbulent flow. This implies that the flow is laminar to begin with, therefore the problem in laminar incompressible flow is here considered.

Having chosen the streamwise corner flow problem as specified above, it is necessary to consider how the features of two-dimensional boundary layer theory can be carried over into this three-dimensional problem. The arguments of velocity gradients normal to the surface dominating or constant pressure along surface normals clearly cannot apply in the region near the corner. What has been suggested by

Zamir (1970) and Eichelbrenner (1973) is that a coordinate system be adopted such that one family of coordinate surfaces be streamlines and other be orthogonal to these. Along the orthogonals one assumes constant pressure or maximum velocity gradients. Zamir (1970) developed a system of equations that would apply in the boundary region without referring to a specific coordinate system by means of tensor analysis. A serious problem arises when one requires a specific coordinate system to work in. Neither the streamline surfaces nor the corresponding orthogonal coordinate surfaces are known beforehand. One may choose the corresponding coordinate surfaces resulting from the associated potential flow problem as being close approximations to those within the boundary region, but the coordinate system thus imposed may be very complicated to work in. The system proposed by Zamir (1970) is a case in point. The theory of curvilinear boundary layers therefore involves fewer terms in the flow equations but, since a complicated coordinate system is used, the terms themselves become complicated. Very little progress has been made in this direction for this reason.

Another method that has met with greater success, as far as streamwise corner flow is concerned, is that which regards the problem as a singular perturbation expansion. Van Dyke (1975) discusses two-dimensional boundary layer flow over a flat plate in detail by such a method. It is pointed out by this author that the conventional Blasius solution has long been known to be the first order inner

solution of a perturbation upon the potential flow, but the derivation of higher-order expansions was lacking until the method of matched asymptotic expansions was developed. By treating streamwise corner flow in terms of singular perturbations with matched asymptotic expansions, equations of the boundary region have been obtained.

In summary, the fundamental aspects of boundary layer theory, applicable in either two or three dimensions, can be applied using the singular perturbation process. As with boundary layer flow over a flat plate, the basic assumption of the boundary layer being thin makes it necessary to define new independent variables that are the same order of magnitude. This can be called rescaling the independent variables. Writing the Navier-Stokes equations in these new variables and dropping the terms that are very small in comparison with the others, one obtains a set of boundary layer equations. Upon examining this simpler set of equations it is seen that in physical terms one has assumed that the normal pressure gradient is zero and that the velocity gradients parallel to the surface are negligable compared with the normal velocity gradients. These assumptions can be applied directly in curvilinear boundary layer theory for three dimensional situations, but since the assumptions arise as a result of rescaling variables and dropping negligable terms as in the two-dimensional case, proper rescaling of variables in the three-dimensional case leads to the same results. Curvilinear boundary layer

theory and singular perturbation boundary layer theory thus apply the same approximations in different ways. Using the singular perturbation method makes it unnecessary to use a complicated curvilinear coordinate system.

1.2 Theoretical Streamwise Corner Flow in Review

A formulation for three-dimensional flow was first developed by Stewartson (1961) for viscous flow over a quarter-infinite plate. Rubin (1966) adopted this formulation for streamwise corner flow as a singular perturbation problem. Region I of Figure 1 denotes the area of zeroth-order potential flow (i.e. undisturbed mainstream flow). Perturbation leads to first-order Blasius boundary layer solutions of regions II and III. Outflow predicted by the Blasius solutions provides matching conditions for first-order potential flow of region I, implying that the effective displacement body is two intersecting plates with parabolic profiles. The induced cross flow in II and III due to first-order potential flow leads to the second-order boundary layer of those regions which do not appear in two-dimensional theory. Solutions of the flow equations can be found for these regions for distances far from the corner. Rubin (1966) deduced what form the corner boundary region equations of region IV would take. Boundary conditions for this region are the no-slip conditions at the walls, matching conditions of regions II and III and mainstream conditions far from the solid boundaries.

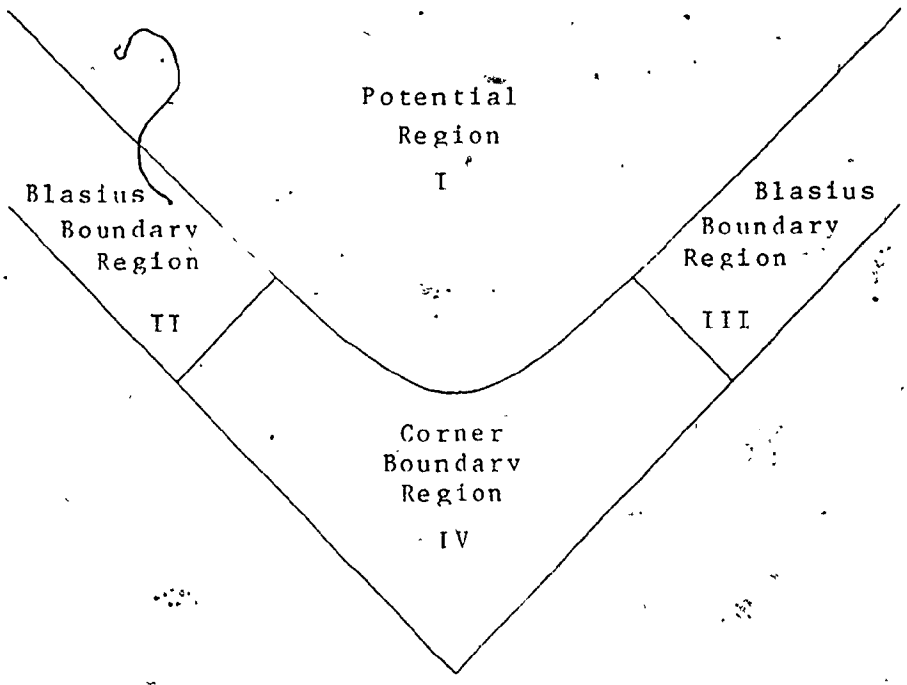

Figure 1
Corner Boundary Regions

Rubin (1966) made the assumption that the flow properties decayed exponentially into regions II and III. In a later paper Pal and Rubin (1971) discovered that in fact algebraic decay into these regions applies. These algebraic conditions were determined as an asymptotic series with respect to distance from the corner and presented by the authors. The fact that this asymptotic series could be continued to any desired number of terms proved important for the numerical solution of the streamwise corner flow equations as presented by Rubin and Grossman (1971) since values on the outer boundary (a finite distance from the corner) were required. Greater accuracy could be had by using several terms of the expansion at the cost of progressively greater difficulty in solution of each term. With the outer boundary conditions in hand the governing equations of the corner region were solved by a Gauss-Seidel numerical method.

Ghia and Davis (1974a) demonstrated that the first order potential flow of streamwise corner flow can be found by visualizing the displacement effects of the corner region as the superposition of the displacement effects of the two semi-infinite flat plates forming the corner*. Since any vector can be represented as the vector product of the gradients of two scalar functions, the velocity vector of the potential region can be written as:

$$\bar{V} = \nabla\Psi_1 \times \nabla\Psi_2 \qquad (1.2.1)$$

* This is obvious from the analysis of Rubin (1966) although it was not explicitly stated in that paper.

where Ψ_1 and Ψ_2 are the stream functions associated with flow past each plate comprising the corner as if the other plate were not present. These are known from boundary layer theory applied to flat plates as found in Van Dyke (1975). An understanding of the first-order potential flow is important since the solution will dictate what forms the velocity expressions of the corner region will take.

Ghia (1975) presented a method of dealing with the far-field boundaries based on the knowledge of the algebraically decaying asymptotic expressions of Pal and Rubin (1971). Based on an independent variable transform of Sills (1969), the boundary at infinity was mapped onto unity so that the domain of the problem was mapped from quarter-infinite to a unit square. By redefining the dependent variables so that they remain bounded, it was possible to find Dirichlet-type boundary conditions for the dependent variables at the far-field boundary. Ghia and Davis (1974b) had developed an alternating direction implicit method for solving numerically the finite corner problem of Rubin and Grossman (1971). Ghia (1975) used an improved version of this ADI method. The results reproduced in the main are the results of previous finite corner solutions. Differences in the secondary flow were attributed to the better treatment of the outer boundary, since the need to determine higher orders of the asymptotic solution of the outer boundary to obtain better accuracy at large but finite distances from the corner is eliminated.

Weinberg and Rubin (1972) considered compressible flow behavior in the corner boundary region. Mikhail and Ghia (1978) also studied this situation using the far-field boundary treatment of Ghia (1975).

Desai and Mangler (1974) derived the streamwise corner flow equations in a general curvilinear coordinate system with the intention of applying them to corners of arbitrary angle. Once a particular coordinate system was chosen, asymptotic solutions were found for the equations at large distances from the corner, but close to the wall. With the boundary conditions at infinity available in this manner, this boundary was then mapped onto a finite value. Numerical results were then obtained using a Gauss-Seidel method for 90° and 135° corners for which experimental as well as theoretical results existed.

Barclay and Ridha (1980) formulated the streamwise corner flow problem so that solutions for corner angles between 0° and 360° could be obtained. Unlike Desai and Mangler (1974), a simple non-orthogonal Cartesian coordinate system was used as well as far-field conditions, which are generalizations of those found by Pal and Rubin (1971) with the corner angle parameter appearing explicitly. The far-field boundary was mapped onto a finite value with a transform very similar to that presented by Sills (1969) and used for the streamwise corner flow problem by Ghia (1975) for the same reasons. Solutions were obtained

using a Gauss-Seidel method for angles of 90°, 135°, 180°, 225° and 270°. For the 90° corner the results corresponded very closely to the existing solutions of Rubin and Grossman (1971) and especially so to those of Ghia (1975). Differences do occur in the cross flow velocities at distances far from the solid boundary. These differences were explained in Barclay and Ridha (1980) as resulting from the treatment of the potential flow boundary of the domain. This boundary at infinity was not mapped onto a finite value in Barclay and Ridha (1980) since it was argued that vorticity and streamwise velocity decay exponentially to conditions of the potential flow region. Instead the boundary was taken at a finite distance from the surface. This was justified since excellent agreement with the results of Ghia was obtained. Comparisons of the results at different angles were made by examining the mainstream and cross-stream velocities in the symmetry plane as well as skin friction along the wall in the cross-flow plane and cross-flow directions.

1.3 Theoretical Considerations

It is useful to examine the similarities and differences of the various treatments of the streamwise corner flow discussed above. The major similarity is that the cross-flow coordinates are all scaled as before indicated so that they are of order $R^{-\frac{1}{2}}$ compared with the mainstream coordinate where

$$R = \frac{U\ell}{\nu} \qquad (1.3.1)$$

is the Reynolds number based on an arbitrary length ℓ. In addition to the rescaling, the boundary region is assumed to be similar with respect to the streamwise variable x so that a factor of 2x also appears in the new cross-flow coordinates so that the final rescaling is

$$x = X$$
$$y = \left(\frac{2\nu x}{U}\right)^{\frac{1}{2}} Y \qquad (1.3.2)$$
$$z = \left(\frac{2\nu x}{U}\right)^{\frac{1}{2}} Z$$

Here the assumptions of boundary layer theory are applied to obtain boundary layer equations as approximations of the full Navier-Stokes equations near the wall. The new coordinates Y and Z can be functions of still other variables so that a chosen coordinate system can be used (as was the case in Desai and Mangler (1974) and Barclay and Ridha (1980)) to deal with corners of different angles.

Since the velocity magnitudes of the first-order potential flow are known from Ghia and Davis (1974a), when written in terms of the boundary region coordinates of (1.3.2), these velocities become

$$V^{(x)} = u(Y,Z)\ U$$
$$V^{(y)} = v(Y,Z)\ UR_x^{-\frac{1}{2}} \qquad (1.3.3)$$
$$V^{(z)} = w(Y,Z)\ UR_x^{-\frac{1}{2}}$$

where $V^{(x)}$, $V^{(y)}$ and $V^{(z)}$ are the physical velocity components; u, v and w are the scaled velocity components; and

$$R_x = \frac{2Ux}{\nu} \qquad (1.3.4)$$

is the Reynolds number based on length x. When these scaled coordinates and velocities are substituted into the Navier-Stoke's equations and only first orders in terms of R_x kept, one obtains the first-order corner boundary region equations. Because of similarity being assumed, these equations are independent of x. The expansion for pressure can be assumed to have the form

$$P = P_1(x) + R_x^{-1} P_2(Y,Z) + \ldots . \qquad (1.3.5)$$

The first-order term disappears from the top-order equations and the R_x^{-1}-term can be eliminated by cross-differentiation.

The velocity components of (1.3.3) are used by all authors mentioned in this section and the corner boundary region equations are obtained as described. The computational domains used are all closed and have Dirichlet boundary conditions available either directly, by iteration, or from a simplified set of equations applying at a boundary. The treatment of these boundaries and the method of obtaining boundary conditions, however, constitute the major differences. A less important source of difference is the coordinate system used in a particular case. In dealing with right-angled corners, Rubin and Grossman (1971) and Ghia and Davis (1974b) used Cartesian coordinates. The boundary conditions

far from the corner were obtained by Pal and Rubin (1971). These far-field conditions were applied at a finite distance from the corner and not at true infinity. Ghia (1975) used a variable transform in order to apply the boundary conditions at true infinity. Corners of arbitrary angle were studied by Desai and Mangler (1974) and Barclay and Ridha (1980). Desai and Mangler (1974) used a curvilinear yet non-orthogonal coordinate system that allowed corner angles up to and including 180° while Barclay and Ridha (1980) used a non-orthogonal Cartesian coordinate system that could represent corner angles between 0° and 360°. Both of these papers used coordinate transforms so that far-field boundary conditions could be applied at true infinity. However, while Barclay and Ridha (1980) used far-field equations of Pal and Rubin (1971), generalized so that they applied for different angles, Desai and Mangler (1974) assumed zero velocity component parallel to the solid boundary so that the boundary layer far from the corner corresponds exactly to that of the flat plate. Along with this point Barclay and Ridha (1980) also point out that the boundary equations of Desai and Mangler (1974) provide only gradients of flow quantities instead of the quantities themselves. These differences are sufficient to account for the lack of agreement in results between Desai and Mangler (1974) on the one hand and Rubin and Grossman (1971), Ghia (1975) and Barclay and Ridha (1980) on the other, according to the latter paper.

Experimental measurements have been made of the mainstream velocity in several streamwise corner flow situations, but differences exist between various experimental results as well as between theory and experiment. As well as presenting new experimental results, Zamir (1981) examined these differences and concluded that the boundary layer in a rectangular corner does not exist in a stable, laminar form for Reynolds numbers greater than about 10^4 unless there is a favorable streamwise pressure gradient. As the gradient is reduced to zero the instability appears, the manner of which depends upon such factors as free stream disturbances and the form of the corner leading edge. Such instability is not apparent in the boundary layer far from the corner. When the corner boundary layer is stable the mainstream velocity profiles show a high degree of similarity. Unstable corner boundary layers, however, show a breakdown of similarity. All of the theoretical analyses assume similarity explicitly in the manner in which the independent variables are rescaled (eg: see (1.3.2)), as well as assume zero pressure gradient. Agreement between theory and experiment therefore appears impossible to obtain. Zamir (1981) did show, however, that by extrapolating stable experimental results to the limit of zero pressure gradient to obtain the velocity profile in the bisector plane, those of Rubin and Grossman (1971) and Ghia (1975) were the closest.

1.4 The Present Work

It would seem from the conclusions of Zamir (1981) that theoretical streamwise corner flow has limited practical application. To modify the theory by abandoning similarity, one must then deal with three independent variables plus the attending complications. If unsteady flow is associated with the breakdown of similarity in corner flow, then the mathematics are complicated further by the need to introduce time as a fourth independent variable. Obtaining solutions of such equations by computational methods is difficult and costly.

The theoretical work previous to Zamir (1981) is still valuable, however, since one needs to know the structure of similar corner flow. Zamir (1981) has shown that even for small pressure gradients (where measurements are still possible) the boundary layer is steady and similar for flow of Reynolds number less than about 10^4. Any theoretical study of instability, therefore, would use former theoretical results as initial conditions upon which perturbations could be tried.

Particularly important in studying how the corner boundary layer may behave should similarity break down is detailed information concerning secondary flow patterns. The major factor influencing secondary flow patterns even in situations with similarity is the shape of the solid boundary. A streamwise corner boundary has already been specified, but it is not necessary to consider only a

rectangular corner as has been done by most theorists. Corner boundary layer equations for corners of arbitrary angle have been developed in Desai and Mangler (1974) in which one is free to choose the most suitable coordinate system. If the curvilinear coordinate system chosen in Desai and Mangler (1974) is not the most suitable, then one can consider the non-orthogonal Cartesian coordinate system of Barclay and Ridha (1980) because simpler corner boundary layer equations result, and the theoretical results of the flow correspond to those of Ghia (1975) for a rectangular corner.

Another major factor affecting secondary flow patterns is the boundary condition imposed far from the corner, which shall be known as the far-field boundary condition. The reason for the difference between the secondary flow patterns of Desai and Mangler (1974) and Barclay and Ridha (1980), as indicated by the latter authors, is that the flow was assumed to correspond exactly to Blasius flow at infinity in Desai and Mangler (1974). Since the mainstream velocity characteristics within the corner region are predicted more accurately by Ghia (1975) by using the far-field boundary conditions developed by Pal and Rubin (1971), the results of Desai and Mangler (1974) suffer. Barclay and Ridha (1980), on the other hand, used the Pal and Rubin (1971) boundary conditions and reproduced the mainstream velocity profile results of Ghia (1975) for a rectangular corner.

The concern of Desai and Mangler (1974) was to obtain corner boundary layer equations in a general coordinate system and despite the far-field boundary condition this work is valuable. The numerical results of these authors were therefore only meant to be compared with existing theoretical and experimental results, so only corner angles of 90° and 135° were presented.

Including the trivial case of a 180° corner, Barclay and Ridha (1980) obtained results for five different corner angles of two types. The corners of angles 90° and 135° may be termed loosely as concave corners while those of corner angle 225° and 270° are convex corners. With these results the authors noted that the secondary shear layer exhibited an antisymmetric behaviour for angles equidistant from 180°. However, the results comparing boundary layer flow patterns for corners of different angles involve only mainstream and cross-flow velocity magnitudes in the bisector plane, which are graphed as functions of distance from the corner point. Full cross-flow diagrams were presented only for mainstream velocity contours and cross-flow velocity directions, the purpose of which is to compare these quantities for corners equidistant from 180°. The only comment regarding stability was made with reference to the cross-flow velocities adjacent to the corner and flowing toward the corner. Barclay and Ridha (1980) stated that for concave corners a substantial inflow would be a stabilizing mechanism for the boundary layer if present, but no mention of a specific angle was made.

The purpose of the present work is to examine the theoretical boundary layer structure of concave corners, including corner angles less than 90°, with emphasis on the secondary cross-flow structure and keeping in mind the precarious natures of similarity and stability. The formulation of the corner boundary layer equations presented in Chapter 2, Sections 1 and 2, will be patterned after that of Desai and Mangler (1974) in sufficient detail that what may be obscure to some readers of Desai and Mangler (1974) may be made clearer, particularly the fact that the method used by the authors is in fact a singular perturbation expansion. Section 3 of Chapter 2 will deal with the coordinate system to be used. Instead of the overly complicated coordinate system of Desai and Mangler (1974), a form of that used in Barclay and Ridha (1980) will be used here, modified so that the coordinate system covers the entire domain of the corner instead of half. Since only concave corners are of interest here, there is no problem in proceeding in this manner. Boundary conditions and coordinate transforms will then be discussed in the following three sections of Chapter 2. Presented in Chapter 3 is a method of obtaining numerical results which will then be examined and discussed in Chapter 4.

2. GOVERNING EQUATIONS

2.1 Navier-Stokes Equations in Tensor Form

Tensor analysis is used in this section, and the one following, because then one need not consider a specific coordinate system until later. The tensor equations remain valid in any coordinate system. In this work, the tensor notation of Flügge (1972) is used. Explanations of what the various symbols mean will be given as needed, although it is not intended that a treatise of tensor analysis be presented.

The problem is begun by stating the Navier-Stokes and continuity equations for steady, viscous, incompressible laminar flow. With these restrictions, the appropriate equations developed and presented in Flügge (1972) are presented as follows:

$$u^j \, u^i|_j = -\frac{1}{\rho} g^{ij} \, P|_j + \nu u^i|^j_j$$

$$u^j|_j = 0 \, . \qquad (2.1.1)$$

In the above equations, the indices represent the three independent variables ξ^i and therefore take the values one, two and three. The Einstein summation convention is maintained between identical covariant indices and contravariant indices, which are the subindices and superindices respectively. The symbol u^i represents the contravariant components of the velocity vector, and P is the scalar pressure function. The symbols ρ and ν represent respectively the

constants of density and kinematic viscosity. The vertical stroke indicates that the covariant derivative of the preceeding quantity is to be taken. The covariant derivative of u^i can be written as

$$u^i|_j = u^i{}_{,j} + u^k \Gamma^i_{jk} \tag{2.1.2}$$

and that of u_i as

$$u_i|_j = u_{i,j} - u_k \Gamma^k_{ij} \tag{2.1.3}$$

where the comma indicates that the partial derivative is taken (e.g. $u_{i,j} = \frac{\partial u_i}{\partial \xi^j}$) and Γ^k_{ij} is the Christoffel symbol which can be written in terms of the covariant and contravariant metric tensor as

$$\Gamma^k_{ij} = \frac{1}{2} g^{km}(g_{jm,i} + g_{mi,j} - g_{ij,m}) \ . \tag{2.1.4}$$

Lastly, what appears to be a covariant derivative taken with respect to a covariant index and a contravariant index is in fact a short form used to avoid writing the metric tensor; that is:

$$u^i|^j_j = g^{jk}\, u^i|_{jk} = g^{jk}(u^i|_j)|_k \ . \tag{2.1.5}$$

Equations (2.1.1) can be made simpler in form by avoiding the use of the covariant derivative and the attending Christoffel symbols. The continuity equation of (2.1.1) expresses the divergence of the velocity vector being zero. This equation can be simplified (see Appendix I) by writing

the equation as

$$u^j{}_{,j} + u^k \frac{Q_{,k}}{Q} = 0 \qquad (2.1.6)$$

where $$Q = (g)^{\frac{1}{2}} \qquad (2.1.7)$$

Upon multiplying by Q and changing the dummy index k to j and collecting the terms together, the continuity equation becomes

$$(Q\, u^j)_{,j} = 0 \quad . \qquad (2.1.8)$$

For the Navier-Stokes equations of (2.1.1), since the covariant components of the velocity are wanted, one multiplies by g_{li} and changes the index l to i throughout the equations to get

$$u^j\, u_i|_j = -\frac{1}{\rho} P|_i + \nu u_i|^j_j \quad . \qquad (2.1.9)$$

For further simplification, each term will be considered separately. Since the covariant derivative of a scalar is the same as the partial derivative, the pressure term becomes

$$P|_i = P_{,i} \quad . \qquad (2.1.10)$$

The term on the left hand side of (2.1.2) can be shown (see Appendix II) to be given by

$$u^j\, u_i|_j = u^j\, u_{i,j} + \frac{1}{2}(u_j\, u^j{}_{,i} - u^j\, u_{j,i}) \quad . \qquad (2.1.11)$$

The term containing the second-order covariant derivative can be simplified by noting the well-known vector identity written in Gibb's notation as

$$\nabla \times (\nabla \times \bar{u}) = \nabla(\nabla \cdot \bar{u}) - \nabla^2 \bar{u} \quad .$$

If the curl of a vector in tensor notation is represented by

$$\text{Curl } u^i = \varepsilon^{ijk} u_k|_j = \varepsilon^{ijk} u_{k',j} \qquad (2.1.12)$$

where $\varepsilon^{ijk} = \frac{1}{Q} e^{ijk}$

with Q defined above and e^{ijk} is the permutation symbol, and where it is noted that

$$\begin{aligned} \varepsilon^{ijk} u_k|_j &= \varepsilon^{ijk} u_{k',j} - \varepsilon^{ijk} u_m \Gamma^m_{kj} \\ &= \varepsilon^{ijk} u_{k',j} - \frac{u_m}{Q} (e^{ijk} \Gamma^m_{kj}) \\ &= \varepsilon^{ijk} u_{k',j} - \frac{u_m}{Q} (\Gamma^m_{32} - \Gamma^m_{23} + \Gamma^m_{13} - \Gamma^m_{21} - \Gamma^m_{12}) \\ &= \varepsilon^{ijk} u_{k',j} \end{aligned}$$

then the identity can be written in terms of tensor notation as

$$\begin{aligned} & g_{in} \varepsilon^{nrs} (g_{sm} \varepsilon^{mjk} u_{k',j})_{,r} \\ & = (u^j|_j)|_i - u_i|^j_j \quad . \end{aligned} \qquad (2.1.13)$$

Noting the continuity equation of (2.1.1) this becomes

$$u_i|^j_j = - g_{in} \varepsilon^{nrs} (g_{sm} \varepsilon^{mjk} u_{k',j})_{,r} \quad . \qquad (2.1.14)$$

With the relations (2.1.10), (2.1.11) and (2.1.14); equation (2.1.9) can be written as

$$\begin{aligned} & u^j u_{i',j} - \tfrac{1}{2}(u_j u^j{}_{,i} - u^j u_{j,i}) \\ & = \frac{1}{\rho} P_{,i} - \nu g_{in} \varepsilon^{nrs} (g_{sm} \varepsilon^{mjk} u_{k',j})_{,r} \quad . \end{aligned} \qquad (2.1.15)$$

To summarize, the tensor forms of the Navier-Stokes equations and the continuity equation are here presented in forms that do not involve covariant differentiation. The purpose of this section has been to show that the equations used here and in Desai and Mangler (1974) are indeed the correct ones. Therefore the Navier-Stokes and continuity equations of (2.1.1) can be written as

$$u^j u_{i,j} - \frac{1}{2}(u_j u^j{}_{,i} - u^j u_{j,i}) = -\frac{1}{\rho} P_{,i} - \nu g_{in} \varepsilon^{nrs} (g_{sm} \varepsilon^{mjk} u_{k,j})_{,r} \qquad (2.1.16)$$

and $$(Q u^j)_{,j} = 0 \quad .$$

2.2 Boundary Region Equations

The equations of (2.1.16) are still the full Navier-Stokes equations and therefore still too general to be used to obtain solutions for the corner boundary region. A more appropriate set of equations can be derived in the manner previously discussed in Chapter 1. This process of obtaining corner boundary region equations can be summarized in three stages:

1) the independent variables are rescaled according to boundary layer theory;
2) the scaled forms of the dependent variables are deduced by using the forms of the previously obtained potential flow solution; and

3) these expressions for both independent and dependent variables are substituted into the Navier-Stokes equations, and only terms of the lowest order in R_x are retained.

It is desired that the actual coordinate system remains unspecified for the time being in order that the generality of the process may be emphasized. This can be done by continuing to use tensor analysis. It must be noted that the tensor formulations to follow have already been presented in Desai and Mangler (1974), although in a somewhat obscure fashion. They are presented here in order to show that the process leading to the final system of equations is the same as described before despite the perhaps unfamiliar context of tensor notations.

The essence of the boundary layer rescaling of the independent variables is contained in the equations of (1.2.2). The scaled variables X, Y and Z are regarded as functions of other independent variables in the following manner:

$$\begin{aligned} X &= x \\ Y &= Y(\eta,\zeta) \\ Z &= Z(\eta,\zeta) \end{aligned} \qquad (2.2.1)$$

Noting the above and (1.2.2), the transformation tensor t^i_j such that

$$x^i = t^i_j \, \xi^j \qquad (2.2.2)$$

where $x^i = (x,y,z)$

and $\xi^j = (x, \eta, \zeta)$

can be written as

$$t^i_j = \frac{\partial x^i}{\partial \xi^j} = \begin{pmatrix} 1 & 0 & 0 \\ Y\left(\frac{\nu}{2Ux}\right)^{\frac{1}{2}} & Y_\eta\left(\frac{2\nu x}{U}\right)^{\frac{1}{2}} & Y_\zeta\left(\frac{2\nu x}{U}\right)^{\frac{1}{2}} \\ Z\left(\frac{\nu}{2Ux}\right)^{\frac{1}{2}} & Z_\eta\left(\frac{2\nu x}{U}\right)^{\frac{1}{2}} & Z_\zeta\left(\frac{2\nu x}{U}\right)^{\frac{1}{2}} \end{pmatrix} \qquad (2.2.3)$$

with the Jacobean Q of the transformation (i.e. the determinant of t^i_j):

$$Q = \frac{\nu x}{U} 2(Y_\eta Z_\zeta - Y_\zeta Z_\eta) \equiv \frac{\nu x}{U} Q_o \qquad (2.2.4)$$

It is seen in Appendix III that Q represents the same quantity denoted by Q in (2.1.7). With the transformation tensor given above, one can obtain the covariant metric tensor g_{ij} by transforming the Cartesian metric tensor,

$$G_{ij} = \begin{cases} 1 \text{ if } i = j \\ 0 \text{ if } i \neq j \end{cases}$$

as follows (where g_{ij} is symmetric):

$$g_{ij} = t^k_i \, t^m_j \, G_{km}$$

$$= \begin{pmatrix} 1 + \frac{\nu}{Ux}\frac{1}{2}(Y^2 + Z^2) & \frac{\nu}{U}(YY_\eta + ZZ_\eta) & \frac{\nu}{U}(YY_\zeta + ZZ_\zeta) \\ & 2\frac{\nu x}{U}(Y_\eta^2 + Z_\eta^2) & \frac{\nu x}{U} 2(Y_\eta Y_\zeta + Z_\eta Z_\zeta) \\ & & \frac{\nu x}{U} 2(Y_\zeta^2 + Z_\zeta^2) \end{pmatrix}$$

$$= \begin{pmatrix} 1 + \frac{\nu}{Ux} q_{11} & \frac{\nu}{U} q_{12} & \frac{\nu}{U} q_{13} \\ & \frac{\nu x}{U} q_{22} & \frac{\nu x}{U} q_{23} \\ & & \frac{\nu x}{U} q_{33} \end{pmatrix} \qquad (2.2.5)$$

Since the metric tensor is symmetric, only the diagonal and superdiagonal elements are written.

Scaled forms of the dependent variables are needed for both covariant and contravariant cases. A beginning is made by noting the tensor form of (1.2.1):

$$u^i = \varepsilon^{ijk} \Phi_{,j} \Psi_{,k} \qquad (2.2.6)$$

where Φ and Ψ are scalar functions. This expression for u^i can be shown to satisfy the continuity equation (the second equation of (2.1.6)) for any Φ and Ψ. For the present case, proper choice of these functions will ensure proper scaling of the velocities. If the following forms are chosen:

$$\Phi = \nu x \Omega(\eta, \zeta) \quad , \quad \Psi = \Psi(\eta, \zeta) \qquad (2.2.7)$$

then one obtains from (2.2.5) and (2.2.6)

$$u^1 = \frac{U}{Q_o} (\Omega_\eta \Psi_\zeta - \Omega_\zeta \Psi_\eta) \equiv u(\eta, \zeta)\ U$$

$$u^2 = \frac{-\Omega \Psi_\zeta U}{Q_o x} \equiv -\frac{\phi(\eta, \zeta)\ U}{Q_o x}$$

$$u^3 = \frac{\Omega \Psi_\eta U}{Q_o x} \equiv -\frac{\psi(\eta, \zeta)\ U}{Q_o x} \qquad (2.2.8)$$

Since these are the contravariant forms of the velocity vector, it is not readily apparent that these are the scaled forms wanted. Using the transformation tensor (2.2.3) the physically meaningful Cartesian velocity components are found to be

$$
\begin{aligned}
u^{(1)} &= t_i^1 u^i = u(\eta,\zeta)\, U \\
u^{(2)} &= t_i^2 u^i = UR_x^{-\frac{1}{2}} \left(Yu - \frac{2Y_\eta \phi}{Q_o} - \frac{2Y_\zeta \psi}{Q_o}\right) \\
&\equiv v(\eta,\zeta)\, UR_x^{-\frac{1}{2}} \qquad (2.2.9) \\
u^{(3)} &= t_i^3 u^i = UR_x^{-\frac{1}{2}} \left(Zu - \frac{2Z_\eta \phi}{Q_o} - \frac{2Z_\zeta \psi}{Q_o}\right) \\
&\equiv w(\eta,\zeta)\, UR_x^{-\frac{1}{2}}
\end{aligned}
$$

which are exactly like those of (1.3.3), and therefore scaled properly. Covariant velocity components are found by using the metric tensor g_{ij} of (2.2.5) to obtain

$$
\begin{aligned}
u_1 &= g_{1j}\, u^j = uU + \frac{\nu}{x}\left(q_{11}u - \frac{q_{12}}{Q_o}\phi - \frac{q_{13}}{Q_o}\psi\right) \\
&\equiv uU + \frac{\nu}{x} b \\
u_2 &= g_{2j}\, u^j = \nu\left(q_{12}u - \frac{q_{22}}{Q_o}\phi - \frac{q_{23}}{Q_o}\psi\right) \qquad (2.2.10) \\
&\equiv \nu\gamma \\
u_3 &= g_{3j}\, u^j = \nu\left(q_{13}u - \frac{q_{23}}{Q_o}\phi - \frac{q_{33}}{Q_o}\psi\right) \\
&\equiv \nu\delta
\end{aligned}
$$

With the addition of the formulation given next, the above expressions can be substituted into (2.1.16) to obtain a numerically tractable set of equations. The additional formulation is found from the first covariant vorticity component.

$$\omega_1 = g_{1m}\, \epsilon^{mjk}\, u_{k',j}$$

$$= \frac{U}{Q_o x}\,(q_{12}u_{,3} - q_{13}u_{,2} + \delta_{,2} - \gamma_{,3}) + O(\nu) \qquad (2.2.11)$$

$$\equiv -\frac{U}{2x}\, A + O(\nu)$$

where $$A \equiv -\frac{2}{Q_o}\,(q_{12}u_{,3} - q_{13}u_{,2} + \delta_{,2} - \gamma_{,3})$$

or, in terms of u, ϕ and ψ,

$$\frac{Q_o}{2}\, A = (q_{12,3} - q_{13,2})\, u - \frac{q_{22,3} - q_{23,2}}{Q_o}$$

$$+ \frac{q_{33,2} - q_{23,3}}{Q_o}\,\psi - \frac{q_{23}}{Q_o}\,(\phi_{,2} - \psi_{,3}) \qquad (2.2.12)$$

$$- \frac{q_{22}}{Q_o}\,\phi_{,3} - \frac{q_{33}}{Q_o}\,\psi_{,2}$$

The pressure P can be expanded as

$$P = P_o + R_x^{-\frac{1}{2}}\, P_1 + R_x^{-\frac{1}{2}}\, P_2 \ldots \qquad (2.2.13)$$

with $P_o = P_o(x)$, $P_1 \equiv 0$ and $P_2 = P_2(\eta,\zeta)$.

The above expressions can now be substituted into (2.1.16) and, for large Reynolds numbers, retaining only the first-order terms; the following equations result after some tedious algebra:

$$Q_o\, u = \phi_{,2} + \psi_{,3}$$

$$\nabla u + \phi u_{,2} + \psi u_{,3} = 0$$

$$\frac{Q_o}{2} A = (q_{12'3} - q_{13'2})\, u - \frac{q_{22'3} - q_{23'2}}{Q_o}\,\phi + \frac{q_{33'2} - q_{23'3}}{Q_o}\,\psi - \frac{q_{23}}{Q_o}\,(\phi_{,2} - \psi_{,3}) - \frac{q_{22}}{Q_o}\,\phi_{,3} + \frac{q_{33}}{Q_o}\,\psi_{,2} \qquad (2.2.14)$$

$$\frac{Q_o}{2}(\nabla A + \phi A_{,2} + \psi A_{,3} + Q_o uA) + Q_o u(q_{11'2}u_{,3} - q_{11'3}u_{,2}) = 0$$

In the above equations, it was assumed that $P_o(x)$ = Constant. The expressions (2.2.11) and (2.2.12) for A were used to simplify the equations to eliminate γ and δ. The operator ∇, acting on u for example, represents

$$\nabla u = \frac{1}{Q_o}(q_{33}u_{,22} - 2q_{23}u_{,23} + q_{22}u_{,33} + (q_{33'2} - q_{23'3})\, u_{,2} + (q_{22'3} - q_{23'2})\, u_{,3}). \qquad (2.2.15)$$

The pressure term $P_2(\eta,\zeta)$ was eliminated by cross-differentiation.

The set of equations (2.2.14) are the corner boundary region equations referring to a still unspecified coordinate system. These are four equations in the four unknowns: u, A, ϕ and ψ. This set of equations is the final

product of the boundary layer theory approximation which can be used to solve the corner boundary region flow configuration.

2.3 The Coordinate System

It is now necessary to choose a coordinate system to use in specifying and solving the corner boundary region equations. This means that specific choices for $Y(\eta, \zeta)$ and $Z(\eta, \zeta)$ must be made. Certain basic features discussed below must be remembered in order to judge which choice is the most suitable.

The most important feature of the coordinate system is that the physical boundaries of the flow configuration must correspond to coordinate surfaces. Not only does this simplify the assigning of boundary values to specific grid locations but this also makes it easier for these grid locations to remain associated with the physical boundaries should further transformations be needed for computational purposes. Since corners of arbitrary angle are to be considered, the coordinate system will have to change along with the corner angle. Another important feature required is that the coordinate system becomes Cartesian (either orthogonal or non-orthogonal) near the solid boundary far from the corner. As shall be seen below, the flow is of the Blasius type and a Cartesian coordinate system will make it easier to obtain and solve the Blasius-type equations for u, A, ϕ and ψ which are used as boundary conditions far from

the corner. It is also important that no singularities are introduced into the flow field because of the choice of coordinate system.

A less important but still desirable feature of the coordinate system is that it be simple to use, meaning that the resultant form of the equations are as simple as possible. One way that this might be accomplished is to use an orthogonal coordinate system, since there would then be no cross-derivative terms and the metric tensor would have non-zero components only along the diagonal (i.e. $g_{ij} \neq 0$ only if $i = j$). This does not mean, however, that the forms taken by the metric tensor components are simple also. For a corner of angle other than 90°, an orthogonal coordinate system would be curvilinear, which would imply that metric tensor components must be functions of position. Experience has also shown that such a coordinate system is difficult to obtain. Zamir (1970) presented such an orthogonal coordinate system, but it cannot be inverted and it only applies to a right-angled corner.

The simplest coordinate system used for the right-angled corner by Rubin, Ghia and their respective associates is the orthogonal Cartesian system. Not only is it orthogonal, but also the metric tensor components are not functions of position. These two features lead to the most simplified equation forms. That it cannot be used for corners of any other angle is the only drawback. However, it is possible

for a non-orthogonal Cartesian system to represent the corner configuration. Such a coordinate system is used in Barclay and Ridha (1980). The boundary surfaces which the coordinate surfaces parallel are one of the walls and the corner bisector. The only other paper dealing with arbitrarily-angled corners, Desai and Mangler (1974), uses a non-orthogonal coordinate system consisting of a family of lines parallel to the bisector and a family of hyperbolae. The coordinate line of the degenerate hyperbola coincides with the solid boundary comprising the corner. Of these two systems, the non-orthogonal Cartesian coordinate system of Barclay and Ridha (1980) results in simpler forms of the equations since the metric tensor components depend only on the the corner angle and not η and ζ.

For this work, it is decided that a non-orthogonal Cartesian coordinate system similar to that of Barclay and Ridha (1980) will be used. Expressed as a specific form of (1.2.2), this coordinate system is

$$\begin{aligned} x &= X \\ y &= \left(\frac{2\nu x}{U}\right)^{\frac{1}{2}} \eta \sin\alpha \\ z &= \left(\frac{2\nu x}{U}\right)^{\frac{1}{2}} (\eta \cos\alpha + \zeta) \end{aligned} \quad , \qquad (2.3.1)$$

where α is the corner angle. This coordinate system is slightly different from that of Barclay and Ridha (1980) in that each family of coordinate lines parallels a different solid boundary*. Although this coordinate system can not

*see next page.

The Present Work

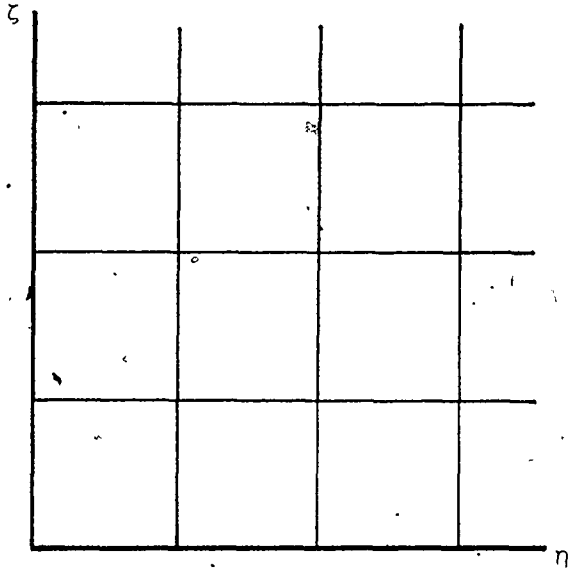

Barclay and Ridha (1980)

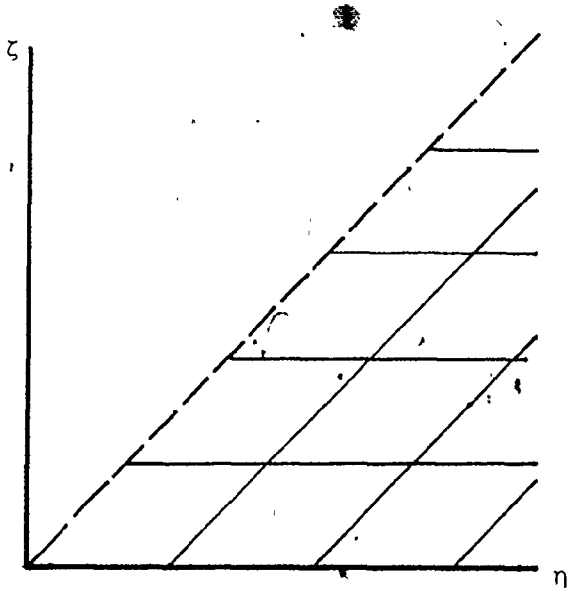

Note: Barclay and Ridha (1980) used a coordinate system in which one family of coordinate lines paralleled the corner bisector. Therefore half of the corner region is considered. Boundary conditions are thus needed on the bisector.

represent corners of angles greater than or equal to 180°, it is adequate for examining concave corners and especially for corners near 90°. For the right-angled corners, the coordinate system becomes orthogonal Cartesian and hence identical to those of Rubin, Ghia and associates. It shall be seen that for this case the equations become identical to those used by these authors. Along with satisfying the important criteria that the coordinate system must satisfy as before discussed, the coordinate system of (2.3.1) is also as simple to use as is possible while still being able to represent corners of arbitrary angle less than 180°.

With the coordinate system specified in (2.3.1), the details of the coordinate variables and the equations can be finalized. The transformation tensor of (2.2.3) becomes

$$t^i_j = \begin{bmatrix} 1 & 0 & 0 \\ \eta \sin\alpha \left(\frac{\nu}{2Ux}\right)^{\frac{1}{2}} & \sin\alpha \left(\frac{2\nu x}{U}\right)^{\frac{1}{2}} & 0 \\ (\eta \cos\alpha + \zeta)\left(\frac{\nu}{2Ux}\right)^{\frac{1}{2}} & \cos\alpha \left(\frac{2\nu x}{U}\right)^{\frac{1}{2}} & \left(\frac{2\nu x}{U}\right)^{\frac{1}{2}} \end{bmatrix}, \quad (2.3.2)$$

the factors q_{ij} of the covariant metric tensor defined in (2.2.5) become (where q_{ij} is symmetric)

$$q_{ij} = \begin{bmatrix} \frac{1}{2}(\eta^2 + 2\eta\zeta \cos\alpha + \zeta^2) & \frac{(\eta + \zeta \cos\alpha)}{2} & \frac{(\eta \cos\alpha + \zeta)}{2 \cos 2} \\ & & \end{bmatrix} \quad \ldots (2.3.3)$$

and the factor in the Jacobean denoted by Q_o in (2.2.4) becomes

$$Q_o = 2 \sin\alpha \quad . \tag{2.3.4}$$

Substituting (2.3.3) and (2.3.4) into the general boundary region equations of (2.2.14), these equations become

$$\begin{aligned}
&u_{\eta\eta} - 2\cos\alpha\, u_{\eta\zeta} + u_{\zeta\zeta} + \sin\alpha\,(\phi u_\eta + \psi u_\zeta) = 0 \quad , \\
&A_{\eta\eta} - 2\cos\alpha\, A_{\eta\zeta} + A_{\zeta\zeta} + \sin\alpha\,(\phi A_\eta + \psi A_\zeta) \\
&\quad + 2\sin\alpha\, uA \\
&\quad + 2u\sin\alpha\,((\eta + \zeta\cos\alpha)u_\eta - (\eta\cos\alpha + \zeta)u_\zeta) = 0 \quad , \\
&2u\sin\alpha = \phi_\eta + \psi_\zeta \quad , \\
&A\sin^2\alpha = \psi_\eta - \phi_\zeta + \cos\alpha\,(\phi_\eta - \psi_\zeta) \quad .
\end{aligned} \tag{2.3.5}$$

For numerical reasons it is easier to solve the above set of equations written as the following second-order partial differential equations by adding, subtracting and simplifying (see Appendix IV):

$$\begin{aligned}
&u_{\eta\eta} - 2\cos\alpha\, u_{\eta\zeta} + u_{\zeta\zeta} + \sin\alpha\,(\phi u_\eta + \psi u_\zeta) = 0 \quad , \\
&A_{\eta\eta} - 2\cos\alpha\, A_{\eta\zeta} + A_{\zeta\zeta} + \sin\alpha\,(\phi A_\eta + \psi A_\zeta) \\
&\quad + 2uA\sin^2\alpha + 2u\sin\alpha\,((\eta + \zeta\cos\alpha)u_\zeta \\
&\quad - (\eta\cos\alpha + \zeta)u_\eta) = 0 \quad , \\
&\phi_{\eta\eta} - 2\cos\alpha\,\phi_{\eta\zeta} + \phi_{\zeta\zeta} + A_\zeta\sin^2\alpha \\
&\quad - 2\sin\alpha\,(u_\eta - u_\zeta\cos\alpha) = 0 \quad , \\
&\psi_{\eta\eta} - 2\cos\alpha\,\psi_{\eta\zeta} + \psi_{\zeta\zeta} - A_\eta\sin^2\alpha \\
&\quad - 2\sin\alpha\,(u_\zeta - u_\eta\cos\alpha) = 0 \quad .
\end{aligned} \tag{2.3.6}$$

For the case of the right-angled corner, the above sets of equations become identical to the equations of the Rubin and Ghia papers, e.g. (2) - (5) of Ghia (1975), (2.15)-(2.19) of Ghia and Davis (1974b), (2.1 a-b) and (2.4 a-b) in Rubin and Grossman (1971).

It is noted that for either set of equations, if the roles of η and ζ are interchanged then the same set of equations result if one lets

$$\begin{aligned} u(\eta,\zeta) &= u(\zeta,\eta) \\ A(\eta,\zeta) &= -A(\zeta,\eta) \\ \phi(\eta,\zeta) &= \psi(\zeta,\eta) \\ \psi(\eta,\zeta) &= \phi(\zeta,\eta) \end{aligned} \qquad (2.3.7)$$

This is a statement of what will be called the "symmetry" conditions. These denote relationships between any two points which are symmetric about the bisector of the corner (i.e. the line $\eta=\zeta$) and especially on the bisector where it is found that:

$$\begin{aligned} A(\eta,\eta) &= -A(\eta,\eta) \quad \text{meaning } A(\eta,\eta) = 0 \\ \phi(\eta,\eta) &= \psi(\eta,\eta) \\ u_\eta(\eta,\eta) &= u_\zeta(\eta,\eta) \end{aligned} \qquad (2.3.8)$$

With either of (2.3.5) or (2.3.6), the boundary region of corner flow is described. Once boundary conditions are found, a unique solution can be found. Boundary conditions are determined in the next two sections beginning with those at $\eta \to \infty$ and $\zeta = \infty$, and then at $\eta = 0$ and $\zeta = 0$. The means by which boundaries at infinity are utilized is then discussed.

2.4 The Far-Field Boundary Condition

For a specific solution of the equations (2.3.5), one needs boundary conditions along the coordinate surfaces given by

$$\eta = 0, \quad \zeta = 0, \quad \eta \to \infty, \quad \zeta \to \infty.$$

The latter two situations are concerned here. For the right-angled corner, asymptotic expressions have already been found by Pal and Rubin (1971). The authors discovered that all quantities behaved algebraically as η, for example, became large. The flow variables for large η were represented by asymptotic series of the forms:

$$\begin{aligned} u(\eta,\zeta) &= \hat{u}_o(\zeta) + \frac{\hat{u}_1(\zeta)}{\eta} + \frac{\hat{u}_2(\zeta)}{\eta^2} + \ldots \\ A(\eta,\zeta) &= \eta A_o(\zeta) + A_1(\zeta) + \frac{A_2(\zeta)}{\eta} + \ldots \\ \phi(\eta,\zeta) &= \eta\phi_o(\zeta) + \phi_1(\zeta) + \frac{\phi_2(\zeta)}{\eta} + \ldots \\ \psi(\eta,\zeta) &= \psi_o(\zeta) + \frac{\psi_1(\zeta)}{\eta} + \frac{\psi_2(\zeta)}{\eta^2} + \ldots . \end{aligned} \tag{2.4.1}$$

If these forms are substituted into the set of equations (2.3.5), then the terms can be collected by various powers of η and the coefficients found by beginning at the first order and neglecting higher orders. In this section, the coefficient functions fr- the top two orders will be considered, for the case of a corner of arbitrary angle, in detail.

In order to substitute the relations of (2.4.1) into the equations of (2.3.5), one must assume that the derivatives can be represented as follows. For u, the derivatives have the forms

$$\begin{aligned}
\hat{u}_\eta &= \frac{-\hat{u}_1(\zeta)}{\eta^2} + 0(\frac{1}{\eta^3}) \\
\hat{u}_\zeta &= \hat{u}'_o(\zeta) + \frac{\hat{u}'_1(\zeta)}{\eta} + 0(\frac{1}{\eta^2}) \\
\hat{u}_{\eta\eta} &= \frac{2\hat{u}_1(\zeta)}{\eta^3} + 0(\frac{1}{\eta^4}) \\
\hat{u}_{\eta\zeta} &= \frac{-\hat{u}'_1(\zeta)}{\eta^2} + 0\ (\frac{1}{\eta^3}) \\
\hat{u}_{\zeta\zeta} &= \hat{u}''_o(\zeta) + \frac{\hat{u}''_1(\zeta)}{\eta} + 0(\frac{1}{\eta^2})
\end{aligned} \tag{2.4.2}$$

where the primes indicate full differentiation with respect to the variable in the brackets. Similar forms are found for the ψ derivatives. For A, the derivatives have the form:

$$\begin{aligned}
A_\eta &= A_o(\zeta) - \frac{A_2(\zeta)}{\eta^2} + 0(\frac{1}{\eta^3}) \\
A_\zeta &= \eta A_o(\zeta) + A'_1(\zeta) + 0(\frac{1}{\eta}) \\
A_{\eta\eta} &= \frac{2A_2(\zeta)}{\eta^3} + 0(\frac{1}{\eta^4}) \\
A_{\eta\zeta} &= A'_o(\zeta) + 0(\frac{1}{\eta^2}) \\
A_{\zeta\zeta} &= \eta A''_o(\zeta) + A''_1(\zeta) + 0(\frac{1}{\eta})
\end{aligned} \tag{2.4.3}$$

and the ϕ derivatives have similar forms. Substituting all these relations into the equations of (2.3.5) obtains the following results. Collecting like terms in η together, the u equation becomes

$$\{\hat{u}_o''(\zeta) + \sin\alpha\ \psi_o\hat{u}_o'(\zeta)\} + \frac{1}{\eta}\{\hat{u}_1''(\zeta) + \sin\alpha\ (\psi_1\hat{u}_o'(\zeta) + \psi_o\hat{u}_o'(\zeta) - \phi_o\hat{u}_1(\zeta))\} \qquad (2.4.4)$$
$$+ \text{higher-order terms} = 0.$$

The A equation becomes

$$\eta\{A_o''(\zeta) + \sin\alpha\ (\phi_o A_o + \psi_o A_o'(\zeta) + 2\hat{u}_o\hat{u}_o(\zeta)) + 2\hat{u}_o A_o \sin^2\alpha\}$$
$$+ \{A_1''(\zeta) - 2A_o'(\zeta)\cos\alpha + \sin\alpha\ (\phi_1 A_o + \psi_o A_1'(\zeta) + \psi_1 A_o'(\zeta) + 2\hat{u}_o\hat{u}_1(\zeta) + \hat{u}_1\hat{u}_o'(\zeta) \qquad (2.4.5)$$
$$+ 2\sin^2\alpha\ (\hat{u}_o A_1 + \hat{u}_1 A_o) + \text{higher-order terms} = 0.$$

The continuity equation becomes

$$\{2\hat{u}_o\sin\alpha - \phi_o - \psi_o'(\zeta)\} + \frac{1}{\eta}\{2\hat{u}_1\sin\alpha - \psi_1'(\zeta)\} \qquad (2.4.6)$$
$$+ \text{higher-order terms} = 0.$$

Lastly, the equation that defines A becomes

$$\eta\{\sin^2\alpha\ A_o + \phi_o'(\zeta)\} + \{\sin^2\alpha\ A_1 + \phi_1'(\zeta) \qquad (2.4.7)$$
$$- \cos\alpha\ (\phi_o - \psi_o'(\zeta)) + \text{higher-order terms} = 0.$$

The boundary conditions for these problems can be discovered by examining the "symmetry" relations of (2.3.8) and applying (2.4.1). It is noted that

$$u(\eta,0) = 0 \text{ implies } \hat{u}_o(0) = 0,\ \hat{u}_1(0) = 0,\ \ldots$$
$$\phi(\eta,0) = 0 \text{ implies } \phi_o(0) = 0,\ \phi_1(0) = 0,\ \ldots \qquad (2.4.8)$$
$$\psi(\eta,0) = 0 \text{ implies } \psi_o(0) = 0,\ \psi_1(0) = 0,\ \ldots$$

and

$u(\eta,\zeta) \to 1$ as $\zeta \to \infty$ for large η implies

$\hat{u}_o \to 1$, $\hat{u}_1 \to 0$, ... as $\zeta \to \infty$;

$A(\eta,\zeta) \to 0$ as $\zeta \to \infty$ for large η implies

$A_o \to 0$, $A_1 \to 0$, ... as $\zeta \to \infty$.

For large η, all the terms except the top orders can be neglected in equations (2.4.4) to (2.4.7) to obtain

$$\hat{u}_o''(\zeta) + \sin\alpha\ \psi_o \hat{u}_o'(\zeta) = 0 \quad , \tag{2.4.9a}$$

$$A_o''(\zeta) + \sin\alpha\ (\phi_o A_o + \psi_o A_o'(\zeta) + 2\hat{u}_o \hat{u}_o'(\zeta)) + 2\hat{u}_o A_o \sin^2\alpha = 0 \quad , \tag{2.4.9b}$$

$$2\hat{u}_o \sin\alpha = \phi_o + \psi_o'(\zeta) \quad , \tag{2.4.9c}$$

$$\sin^2\alpha\ A_o = -\phi_o'(\zeta) \quad . \tag{2.4.9d}$$

The search for a solution is begun by letting

$$\phi_o(\zeta) = B'(\zeta) \quad \text{and} \quad \psi_o(\zeta) = B(\zeta) \quad , \tag{2.4.10}$$

where B is some function yet to be determined. Using these, one substitutes into (2.4.9c) to obtain

$$\hat{u}_o(\zeta) = \frac{B'(\zeta)}{\sin\alpha} \quad , \tag{2.4.11}$$

and into (2.4.9d) to obtain

$$A_o(\zeta) = -\frac{B''(\zeta)}{\sin^2\alpha} \quad . \tag{2.4.12}$$

Substituting (2.4.10) and (2.4.11) into (2.4.9a) results in

$$B'''(\zeta) + \sin\alpha\ BB''(\zeta) = 0 \quad . \tag{2.4.13}$$

Lastly, substituting (2.4.10) to (2.4.12) into (2.4.9b) results in

$$B''''(\zeta) + \sin\alpha\ (B'''(\zeta) + B'(\zeta)\ B''(\zeta)) = 0$$

or $(B'''(\zeta) + \sin\alpha\, BB''(\zeta))' = 0$,

which is satisfied by (2.4.13). The boundary conditions for $B(\zeta)$ can be found by examining the condition given in (2.4.8) and using (2.4.10) to (2.4.12) to find that

$u_o(0) = 0$ and $\phi_o(0) = 0$ imply $B'(0) = 0$,

$\psi_o(0) = 0$ implies $B(0) = 0$, and

$\hat{u}_o \to 1$ as $\zeta \to \infty$ implies $B' \to \sin\alpha$ as $\zeta \to \infty$.

Therefore, in summary, the first-order quantities are found by using (2.4.10) to (2.4.12) where

$$B'''(\zeta) + \sin\alpha\, BB''(\zeta) = 0$$

with $B = B' = 0$ at $\zeta = 0$ (2.4.14)

and $B' \to \sin\alpha$ as $\zeta \to \infty$.

If (2.4.14) looks familiar, it can be seen that if one transforms the independent variable ζ by using

$$\xi = \zeta \sin\alpha$$

so that $B'(\zeta) = \sin\alpha\, B'(\xi)$,

$B''(\zeta) = \sin^2\alpha\, B''(\xi)$ (2.4.15)

and $B'''(\zeta) = \sin^3\alpha\, B'''(\xi)$;

then (2.4.14) becomes

$$B'''(\xi) + BB''(\xi) = 0$$

with $B(0) = B'(0) = 0$ (2.4.16)

and $B'(\xi) \to 1$ as $\xi \to \infty$.

Since this is the Blasius equation in a Cartesian coordinate system, (2.4.14) is then the Blasius equation in a non-orthogonal Cartesian system. Two properties of the Blasius function $B(\xi)$ will be needed later in this section. It is

well known that (cf. James and Watson (1963)):

$$B'' = 0.4696 \text{ at } \xi = 0 \tag{2.4.17}$$

and $$B \sim \xi - 1.21678 \text{ for large } \xi.$$

In terms of ζ, these conditions become

$$B'' = 0.4696 \sin^2\alpha \text{ at } \zeta = 0 \tag{2.4.18}$$

and $$B \sim \zeta \sin\alpha - 1.21678 \text{ for large } \zeta.$$

It is also noted that $B(\zeta)$ varies exponentially as ζ increases, and therefore approaches its limit faster than does an algebraically behaved quantity.

With the first-order solutions found, it is now possible to consider the second-order problem. Substituting the equations of set (2.4.9) and (2.4.10) to (2.4.13) into (2.4.4) to (2.4.7) and neglecting all but the top order terms, one obtains

$$\hat{u}_1''(\zeta) + \psi_1 B''(\zeta) + \sin\alpha\,(B\hat{u}_1'(\zeta) - \hat{u}_1 B'(\zeta)) = 0 \tag{2.4.19a}$$

$$\begin{aligned} A_1''(\zeta) + \frac{2\cos\alpha}{\sin^2\alpha} - BA_1'(\zeta)\sin\alpha - \frac{\phi_1 B''(\zeta)}{\sin\alpha} \\ - \frac{\psi_1 B'''(\zeta)}{\sin\alpha} + 2\hat{u}_1'(\zeta)\,B'(\zeta) + \hat{u}_1 B''(\zeta) \\ + \zeta\frac{\cos\alpha}{\sin\alpha} B'(\zeta)\,B''(\zeta) + 2\sin\alpha\, A_1 B'(\zeta) \\ - 2\hat{u}_1 B''(\zeta) \end{aligned} \tag{2.4.19b}$$

$$2\hat{u}_1 \sin\alpha = \psi_1'(\zeta) \tag{2.4.19c}$$

$$A_1 \sin^2\alpha = -\phi_1'(\zeta) \tag{2.4.19d}$$

Substituting (2.4.19c) into (2.4.19a) results in

$$\psi_1'''(\zeta) + \sin\alpha\,(B\psi_1''(\zeta) - B'(\zeta)\,\psi_1'(\zeta) + 2B''(\alpha)\,\psi_1 = 0 \qquad (2.4.20)$$

with boundary conditions (from (2.4.8)):

$\psi_1 = 0$ at $\zeta = 0$

$\hat{u}_1 = 0$ implying $\psi_1' = 0$ at $\zeta = 0$

$\hat{u}_1 \to 0$ implying $\psi_1' \to 0$ as $\zeta \to \infty$.

Using the transformations of (2.4.15), the above problem becomes

$$\psi_1'''(\xi) + B\psi_1''(\xi) - B'(\xi)\,\psi_1'(\xi) + 2B''(\xi)\,\psi_1 = 0$$

with $\psi_1 = \psi_1' = 0$ at $\xi = 0$ (2.4.21)

and $\psi_1' \to 0$ as $\xi \to \infty$.

The only solution to this problem is (see Libbey and Fox (1963)):

$$\psi_1 \equiv 0 \text{ implying } \hat{u}_1 \equiv 0. \qquad (2.4.22)$$

Substituting (2.4.19d) into (2.4.19b) and noting (2.4.8) and (2.4.22) produces the following:

$$\phi_1'''(\zeta) + \sin\alpha\,(B\phi_1''(\zeta) + 2B'(\zeta)\,\phi_1'(\zeta) + B''(\zeta)\,\phi_1) = 2\cos\alpha\,(B'''(\zeta) + \zeta\sin\alpha\,B'(\zeta)\,B''(\zeta)) \qquad (2.4.23)$$

with $\phi_1 = 0$ at $\zeta = 0$

and $A_1 \to 0$ implying $\phi_1' \to 0$ as $\zeta \to \infty$.

The solution for the above problem can be found by splitting the solution into a particular and homogeneous part. A particular solution to (2.4.23) is

$$\phi_p = \cos\alpha\ (\zeta B'(\zeta) - B) \qquad (2.4.24)$$

which satisfies the main equation of (2.4.23). The associated homogeneous equation is

$$\phi_h''(\zeta) + \sin\alpha\ (B\phi_h''(\zeta) + 2B'(\zeta)\ \phi_h'(\zeta) + B''(\zeta)\ \phi_h) = 0 \qquad (2.4.25)$$

which can be written as

$$(\phi_h'(\zeta) + \sin\alpha\ B\phi_h)'' = 0 \qquad (2.4.26)$$

and integrated twice to get

$$\phi_h'(\zeta) + \sin\alpha\ B\phi_h = C\zeta + D \qquad (2.4.27)$$

where C and D are constants of integration, which will be determined by boundary conditions. From the theory of first-order ordinary differential equations, the general solution to (2.4.27) is

$$\phi_h(\zeta) = A\ e^{-\sin\alpha \int_0^\zeta B\ dt} + e^{-\sin\alpha \int_0^\zeta B\ dt} \int_0^\zeta (C\tau + D)\ e^{+\sin\alpha \int_0^\tau B\cdot dt}\ d\tau \qquad (2.4.28)$$

where A is another constant to be determined. Noting (2.4.14), the exponential can be written as

$$e^{-\sin\alpha \int_0^\zeta B\cdot dt} = e^{+\int_0^\zeta \frac{B''(t)}{B''(t)}\ dt}$$

$$= e^{(\ln(B''(\zeta)) + C')}$$

$$= KB''(\zeta)$$

where K is a constant. The general solution (2.4.28) now becomes

$$\phi_h(\zeta) = AKB''(\zeta) + B''(\zeta) \int_0^\zeta \frac{C\tau + D}{B''(\tau)}\ d\tau \qquad (2.4.29)$$

From the first boundary condition of (2.4.23), which is

$$\phi_1(0) = 0,$$

it can be seen that since

$$\phi_p(0) = 0,$$

therefore $\phi_h(0) = 0,$

which implies that

$$A = 0.$$

The other boundary condition of (2.4.23) can be interpreted as follows:

$$\phi \to \lambda \quad \text{as} \quad \zeta \to \infty \tag{2.4.32}$$

where λ is a constant. If one writes

$$\phi_1 = \phi_p + \phi_h = \cos\alpha\,(\zeta B'(\zeta) - B) + \phi_h \tag{2.4.33}$$

and notes that for large ζ, one can write

$$\zeta B'(\zeta) - B \simeq \zeta \sin\alpha - \zeta \sin\alpha + 1.21678$$
$$\simeq 1.21678 \tag{2.4.34}$$

from (2.4.18), then (2.4.32) can be written as

$$\phi_h \to \lambda - \cos\alpha\,(1.21678) \quad \text{as} \quad \zeta \to \infty. \tag{2.4.35}$$

Equation (2.4.27) for large ζ can be written as

$$\phi_h'(\zeta) + \sin\alpha\,(\zeta \sin\alpha - 1.21678)$$
$$= C\zeta + D \tag{2.4.36}$$

where, by equating the coefficients of like powers of ζ, it is found that

$$C = \zeta \sin^2\alpha\, \phi_h$$
$$D = -1.21678 \sin\alpha\, \phi_h + \phi_h'(\zeta) \tag{2.4.37}$$

for which, as $\zeta \to \infty$, one obtains

$$C = \zeta \sin^2\alpha \ (\lambda - 1.21678 \cos\alpha)$$
$$D = \phi_h'(\zeta) - 1.21678 \sin\alpha \ \phi_h \ . \qquad (2.4.38)$$

The problem (2.4.23) is now determined except for the constant λ. This is not unexpected since (2.4.23) specified only two boundary conditions. The third condition needed to determine λ must be found elsewhere. From (2.3.8), one recalls that

$$\phi(\eta,\eta) = \psi(\eta,\eta). \qquad (2.3.12b)$$

Upon substituting in the asymptotic forms of (2.4.1), the above expression becomes

$$\eta\phi_o(\zeta) + \phi_1(\zeta) = \psi_o(\zeta) + O(\tfrac{1}{\eta}) \quad \text{where } \eta = \zeta,$$

or, from (2.4.10) and $\eta = \zeta$;

$$\zeta B'(\zeta) + \phi_1(\zeta) = B(\zeta) + O(\tfrac{1}{\zeta}) \qquad (2.4.40)$$

and for $\zeta \to \infty$ noting (2.4.18) this becomes

$$\phi_1 \to -1.21678 \text{ as } \zeta \to \infty. \qquad (2.4.41)$$

Comparing this expression with that of (2.4.32), one concludes that

$$\lambda = -1.21678. \qquad (2.4.42)$$

Noting (2.4.38), the solution of (2.4.32) can be stated as

$$\phi_1(\zeta) = \cos\alpha \ (\zeta B'(\zeta) - B) + \phi_h(\zeta)$$

where ϕ_h is the solution of

$$\phi_h'(\zeta) + \sin\alpha \ B\phi_h = -1.21678 \sin\alpha \ (1 + \cos\alpha)(\zeta \sin\alpha - 1.21678) \qquad (2.4.43)$$

with $\phi_1(0) = 0$,

or in other words, by noting (2.4.28) and (2.4.31) as well

as (2.4.42),

$$\phi_1(\zeta) = \cos\alpha\ (\zeta B'(\zeta) - B) - \lambda \sin\alpha\ (1 + \cos\alpha)\ B''(\zeta) \int_0^{\zeta} \frac{t \sin\alpha - \lambda}{B''(t)}\, dt \tag{2.4.44}$$

which, when $\alpha = 90^{\circ}$, is the same expression as found in Pal and Rubin (1971).

With the top two orders now known as follows:

$$\begin{aligned} u(\eta,\zeta) &\sim \frac{B'(\zeta)}{\sin\alpha} + O(\frac{1}{\eta^2}) \\ A(\eta,\zeta) &\sim \frac{\eta B''(\zeta)}{\sin^2\alpha} - \frac{\phi_1'(\zeta)}{\sin\alpha} + O(\frac{1}{\eta}) \\ \phi(\eta,\zeta) &\sim \eta B'(\zeta) + \phi_1(\zeta) + O(\frac{1}{\eta}) \\ \psi(\eta,\zeta) &\sim B(\zeta) + O(\frac{1}{\eta^2}) \ , \end{aligned} \tag{2.4.45}$$

no higher orders will be needed, as shall be seen. The asymptotic expressions for large ζ start with

$$\begin{aligned} u(\eta,\zeta) &= \tilde{u}_o(\eta) + \frac{\tilde{u}_1(\eta)}{\zeta} + \ldots \\ A(\eta,\zeta) &= \zeta\tilde{A}_o(\eta) + \tilde{A}_1(\eta) + \ldots \\ \phi(\eta,\zeta) &= \tilde{\phi}_o(\eta) + \frac{\tilde{\phi}_1(\eta)}{\zeta} + \ldots \\ \psi(\eta,\zeta) &= \zeta\tilde{\psi}_o(\eta) + \tilde{\psi}_1(\eta) + \ldots \end{aligned} \tag{2.4.46}$$

and by following the same proceedure to obtain

$$u(\eta,\zeta) \sim \frac{B'(\eta)}{\sin\alpha} + O(\frac{1}{\zeta^2}) \tag{2.4.47a}$$

$$A(\eta,\zeta) \sim \frac{\zeta B''(\eta)}{\sin^2\alpha} + \frac{\phi_1'(\eta)}{\sin\alpha} + O(\frac{1}{\zeta}) \tag{2.4.47b}$$

$$\phi(\eta,\zeta) \sim B(\eta) + O(\frac{1}{\zeta^2}) \qquad (2.4.47c)$$

$$\psi(\eta,\zeta) \sim \zeta B'(\eta) + \phi_1(\eta) + O(\frac{1}{\zeta}) \qquad (2.4.47d)$$

where $B(\eta)$ and $\phi_1(\eta)$ are the same functions as before with the independent variables renamed.

In (2.4.45) and (2.4.47), all quantities except $u(\eta,\zeta)$ are unbounded as either η or ζ approaches infinity. In order to obtain bounded dependent variables, the unbounded terms in (2.4.45) and (2.4.47) must be removed. The transformed variables are given by

$$\begin{aligned} \bar{u}(\eta,\zeta) &= u(\eta,\zeta) \\ \bar{A}(\eta,\zeta) &= A(\eta,\zeta) + \frac{\eta u_\zeta(\infty,\zeta)}{\sin\alpha} - \frac{\zeta u_\eta(\eta,\infty)}{\sin\alpha} \\ \bar{\phi}(\eta,\zeta) &= \phi(\eta,\zeta) - \eta u(\infty,\zeta)\ \sin\alpha \\ \bar{\psi}(\eta,\zeta) &= \psi(\eta,\zeta) - \zeta u(\eta,\infty)\ \sin\alpha \end{aligned} \qquad (2.4.48)$$

where, as η is allowed to approach infinity in (2.4.45), one obtains

$$u(\infty,\zeta) = \frac{B'(\zeta)}{\sin\alpha}$$

so that $$B'(\zeta) = \sin\alpha\ u(\infty,\zeta) \qquad (2.4.49a)$$

and, from (2.4.42) in a similar manner,

$$B'(\eta) = \sin\alpha\ u(\eta,\infty)\ . \qquad (2.4.49b)$$

The far-field boundary conditions can now be found for the $\eta \to \infty$ boundary, say, by substituting (2.4.45) and (2.4.49) into (2.4.48) and letting η become infinite to get.

$$\bar{u}(\infty,\zeta) = u(\infty,\zeta) \qquad (2.4.50a)$$

$$\bar{A}(\infty,\zeta) = -\frac{\phi_1'(\zeta)}{\sin^2\alpha} \qquad (2.4.50b)$$

$$\bar{\phi}(\infty,\zeta) = \phi_1(\zeta) \qquad (2.4.50c)$$

$$\bar{\psi}(\infty,\zeta) = B(\zeta) - \zeta \sin\alpha \qquad (2.4.50d)$$

and at the $\zeta \to \infty$ boundary, by substituting (2.4.47) and (2.4.49) into (2.4.48), one obtains

$$\begin{aligned} \bar{u}(\eta,\infty) &= u(\eta,\infty) \\ \bar{A}(\eta,\infty) &= \frac{\phi_1'(\eta)}{\sin^2\alpha} \\ \bar{\phi}(\eta,\infty) &= B(\eta) - \eta \sin\alpha \\ \bar{\psi}(\eta,\infty) &= \phi_1(\eta) \ . \end{aligned} \qquad (2.4.51)$$

In both cases, when the remaining independent variable becomes infinite, the barred values of (2.4.50) and (2.4.51) become

$$\begin{aligned} \bar{u}(\infty,\infty) &= 1 \\ \bar{A}(\infty,\infty) &= 0 \\ \bar{\phi}(\infty,\infty) &= -\lambda \\ \bar{\psi}(\infty,\infty) &= -\lambda \ , \end{aligned} \qquad (2.4.52)$$

thus demonstrating boundedness.

As a final note to this section, the main set of equations, last presented in (2.3.6), can now be written in terms of the bounded quantities to obtain ,

$$\bar{u}_{\eta\eta} - 2\cos\alpha\ \bar{u}_{\eta\zeta} + \bar{u}_{\zeta\zeta} + \sin\alpha\ ((\bar{\phi} + \eta \sin\alpha\ \bar{u}(\infty,\zeta))\bar{u}_{\eta}$$

$$+ (\bar{\psi} + \zeta \sin\alpha\ \bar{u}(\eta,\infty)]\bar{u}_{\zeta}) = 0 \qquad (2.4.53a)$$

$$\bar{A}_{\eta\eta} - 2\cos\alpha\,\bar{A}_{\eta\zeta} + \bar{A}_{\zeta\zeta} + \sin\alpha\,((\bar{\phi} + \eta\sin\alpha\,\bar{u}(\infty,\zeta))\bar{A}_{\eta}$$

$$+ (\bar{\psi} + \zeta\sin\alpha\,\bar{u}(\eta,\infty))\bar{A}_{\zeta}) + 2\bar{u}\bar{A}\sin^2\alpha$$

$$- 2\cot\alpha\,(\bar{u}_{\eta\eta}(\eta,\infty) - \bar{u}_{\zeta\zeta}(\infty,\zeta)) - \bar{\phi}\bar{u}_{\zeta}(\infty,\zeta) + \bar{\psi}\bar{u}_{\eta}(\eta,\infty)$$

$$+ \zeta\{\bar{u}_{\eta\eta}(\eta,\infty)\,(\bar{\phi} - \bar{\phi}(\eta,\infty) + \eta\sin\alpha\,(\bar{u}(\infty,\zeta) - 1))$$

$$+ 2\bar{u}\sin\alpha\,(\bar{u}_{\eta}(\eta,\infty) - \bar{u}_{\eta} + \bar{u}_{\zeta}\cos\alpha)\}$$

$$- \eta\{\bar{u}_{\zeta\zeta}(\infty,\zeta)\,(\bar{\psi} - \bar{\psi}(\infty,\zeta) + \zeta\sin\alpha\,(\bar{u}(\eta,\infty) - 1))$$

$$+ 2\bar{u}\sin\alpha\,(\bar{u}_{\zeta}(\infty,\zeta) - \bar{u}_{\zeta} + \bar{u}_{\eta}\cos\alpha)\} = 0 \qquad (2.4.53b)$$

$$\bar{\phi}_{\eta\eta} - 2\cos\alpha\,\bar{\phi}_{\eta\zeta} + \bar{\phi}_{\zeta\zeta} + \bar{A}_{\zeta}\sin^2\alpha \qquad (2.4.53c)$$

$$- 2\sin\alpha\,(\bar{u}_{\eta} - \tfrac{1}{2}\bar{u}_{\eta}(\eta,\infty) - \cos\alpha\,(\bar{u}_{\zeta} - \bar{u}_{\zeta}(\infty,\zeta)) = 0$$

$$\bar{\psi}_{\eta\eta} - 2\cos\alpha\,\bar{\psi}_{\eta\zeta} + \bar{\psi}_{\zeta\zeta} - \bar{A}_{\eta}\sin^2\alpha \qquad (2.4.53d)$$

$$- 2\sin\alpha\,(\bar{u}_{\zeta} - \tfrac{1}{2}\bar{u}_{\zeta}(\infty,\zeta) - \cos\alpha\,(\bar{u}_{\eta} - \bar{u}_{\eta}(\eta,\infty)) = 0\ .$$

These equations, along with the boundary conditions given by (2.4.50) and (2.4.51), specify the corner boundary region problem completely.

2.5 The Wall Boundary Conditions

Most of the boundary conditions for the flow quantities at the wall have already been deduced from the no-slip condition. Noting (2.4.8), these boundary conditions are

$$\bar{u} = \bar{\phi} = \bar{\psi} = 0 \quad \text{at} \quad \eta = 0 \text{ or } \zeta = 0 \ . \tag{2.5.1}$$

The wall condition for $\bar{A}$, however, is not so easily obtained. To do so, one begins by considering the two first-order equations of (2.3.5), which are written in terms of bounded quantities as

$$\bar{A} \sin^2\alpha = \bar{\psi}_\eta - \bar{\phi}_\zeta + \cos\alpha \, (\bar{\phi}_\eta - \bar{\psi}_\zeta) + \sin\alpha \cos\alpha \, (\bar{u}(\infty,\zeta) - \bar{u}(\eta,\infty)) \ , \tag{2.5.2a}$$

$$2\bar{u} \sin\alpha = \bar{\phi}_\eta + \bar{\psi}_\zeta + \sin\alpha \, (\bar{u}(\infty,\zeta) + \bar{u}(\eta,\infty)) \ . \tag{2.5.2b}$$

At the boundary $\eta = 0$, where all quantities (except $\bar{A}$) and their derivatives in ζ are zero, (2.5.2a) and (2.5.2b) are

$$\bar{A}(0,\zeta) \sin^2\alpha = \bar{\psi}_\eta(0,\zeta) + \cos\alpha \, \bar{\phi}_\eta(0,\zeta) + \sin\alpha \cos\alpha \, \bar{u}(\infty,\zeta) \ , \tag{2.5.3a}$$

$$0 = \bar{\phi}_\eta(0,\zeta) + \sin\alpha \, \bar{u}(\infty,\zeta) \ . \tag{2.5.3b}$$

By substituting for $\bar{\phi}_\eta(0,\zeta)$ in (2.5.3a) using (2.5.3b), the wall condition for $\bar{A}(0,\zeta)$ is found to be

$$\bar{A}(0,\zeta) = \frac{\bar{\psi}_\eta(0,\zeta)}{\sin^2\alpha} \ . \tag{2.5.4}$$

A similar argument for the boundary $\zeta = 0$ is used to obtain

$$\bar{A}(\eta,0) = -\frac{\bar{\phi}_\zeta(\eta,0)}{\sin^2\alpha} \quad . \tag{2.5.5}$$

With the above information in hand, and with the far-field boundary condition known, the boundary conditions of the main equations are completely specified if one assumes that the right hand sides of (2.5.4) and (2.5.5) are known in advance of solving the $\bar{A}$-equation. In practical terms, this means that equations (2.5.4) and (2.5.5) are iterated upon to obtain the correct wall conditions of $\bar{A}$.

2.6 Application of the Far-Field Conditions

Up to this point, it has been assumed that the domain of the equations of the flow variables in the cross-stream plane of the streamwise corner flow problem is infinite. For practical purposes, however, the far-field conditions need to be applied at a specific coordinate surface. Until Ghia (1975) presented another approach, what was done was to choose some large yet finite value at which to apply the asymptotic expressions, where enough terms were used to represent quantities accurately. Since a large number of terms may be needed, and since obtaining these terms may be difficult, a simpler approach would be to transform the independent variables of the equations so that true infinity is mapped onto a given finite value. With this

approach, only the first two terms of the asymptotic expressions are needed to represent the far-field conditions accurately. Thus, the far-field conditions denoted by (2.4.50) and (2.4.51) are applied at true infinity. If the same variable transform is used for each coordinate, the infinite domain is now mapped onto a square domain with the flow quantities available along the whole periphery.

Some transforms that can be used for this purpose are presented in Sills (1969). The two that are to be considered here are those denoted by Sills (1969) as transformation I:

$$\eta = \frac{n}{\beta(1 - n)} \quad \text{or} \quad n = \frac{\beta\eta}{\beta\eta + 1} \ , \tag{2.6.1}$$

and transformation II:

$$\eta = -\frac{1}{\beta} \ln(1 - n) \quad \text{or} \quad n = 1 - e^{-\beta\eta} \ , \tag{2.6.2}$$

where β is a parameter in both cases.

Both transformations have similar properties. Both map the interval $(0,\infty)$ in η onto the interval $(0,1)$ in n. Regularly-spaced subintervals in n correspond to increasingly larger intervals with increasing η. The parameter β can be chosen in such a way as to control how much larger successive η-subintervals become. One of the above transforms can be used to transform the domain (η,ζ), where η and ζ range from zero to infinity, onto the domain (n,s), where n and s range from zero to unity. For numerical purposes, discrete points regularly spaced in the domain (n,s) can be mapped onto points in (η,ζ), which are concentrated near the corner

of the solid boundary. One can therefore choose β to obtain the desired concentration of data points in the corner.

One can develop formulae relating the derivatives with either of the above transforms. For transformation I, equations (2.6.1) are used to find for some function $Q(\eta,\zeta)$:

$$Q_\eta = Q_n \frac{\partial n}{\partial \eta} = Q_n \frac{\beta(\beta\eta + 1) - \beta^2\eta}{(\beta\eta + 1)^2} = Q_n \frac{\beta}{(\beta\eta + 1)^2}$$
$$= Q_n \beta(1 - n)^2 , \tag{2.6.3}$$

and similarly in ζ, one finds

$$Q_\zeta = Q_s \beta(1 - s)^2 .$$

Higher derivatives sre found by using (2.6.3) repeatedly. The results sre summarized as follows:

$$\begin{aligned} Q_\eta &= \beta(1 - n)^2 Q_n , \quad Q_\zeta = \beta(1 - s)^2 Q_s , \\ Q_{\eta\eta} &= \beta^2(1 - n)^4 Q_{nn} - 2\beta^2(1 - n)^3 Q_n , \\ Q_{\eta\zeta} &= \beta^2(1 - n)^2(1 - s)^2 Q_{ns} , \\ Q_{\zeta\zeta} &= \beta^2(1 - s)^4 Q_{ss} - 2\beta^2(1 - s)^3 Q_s . \end{aligned} \tag{2.6.4}$$

Formulae for transformation II are found in a similar fashion starting with (2.6.2) to obtain

$$\begin{aligned} Q_\eta &= \beta(1 - n) Q_n , \quad Q_\zeta = \beta(1 - s) Q_s , \\ Q_{\eta\eta} &= \beta^2(1 - n)^2 Q_{nn} - \beta^2(1 - n) Q_n , \\ Q_{\eta\zeta} &= \beta^2(1 - n)(1 - s) Q_{ns} , \\ Q_{\zeta\zeta} &= \beta^2(1 - s)^2 Q_{ss} - \beta^2(1 - s) Q_s . \end{aligned} \tag{2.6.5}$$

The difference between transformations I and II is that the η-subintervals corresponding to equal n-subintervals increase algebraically for transformation I and exponentially for transformation II as n increases. It was shown by Pal and Rubin (1971) that the flow quantities behave algebraically as they approach the far-field boundary. It is no doubt for this reason that Ghia (1975) chose transformation I for his equations. This reason can be illustrated with the following argument.

For large η (and similarly for large ζ), all of the barred quantities can be represented by the now-familiar asymptotic expression

$$\bar{Q} = a(\zeta) + \frac{1}{\eta} b(\zeta) + \frac{1}{\eta^2} c(\zeta) + \ldots \quad . \tag{2.6.6}$$

Using transformation I, this expression and some of its n-derivatives can be written as

$$\bar{Q} = a(s) + \beta b(s) \frac{1 - n}{n} + \ldots \quad ,$$

$$\bar{Q}_n = - \beta b(s) \frac{1}{n^2} + \ldots \quad , \tag{2.6.7}$$

$$\bar{Q}_{nn} = 2\beta b(s) \frac{1}{n^3} + \ldots$$

where it can be seen that as n approaches unity, all the n-derivatives remain finite. Using transformation II, however, results in

$$\bar{Q} = a(s) - \frac{\beta b(s)}{\ln(1-n)} + \dots ,$$

$$\bar{Q}_n = -\beta b(s) \frac{(1-n)^{-1}}{(\ln(1-n))^2} + \dots ,$$

$$\bar{Q}_{nn} = -\beta b(s) \left\{ \frac{(1-n)^{-2}}{(\ln(1-n))^2} + \frac{2(1-n)^{-2}}{(\ln(1-n))^3} \right\} + \dots , \qquad (2.6.8)$$

where one can use L'Hopital's Rule to find:

$$1) \quad \lim_{n\to 1} \frac{(1-n)^{-1}}{(\ln(1-n))^2} = \lim_{n\to 1} \frac{(1-n)^{-2}}{-2\ln(1-n)\ (1-n)^{-1}}$$

$$= \lim_{n\to 1} \frac{(1-n)^{-1}}{-2\ln(1-n)}$$

$$= \lim_{n\to 1} \frac{-(1-n)^{-2}}{2\ (1-n)^{-1}}$$

$$= \lim_{n\to 1} \frac{-1}{2(1-n)} \qquad (2.6.9)$$

$$2) \quad \lim_{n\to 1} \frac{(1-n)^{-2}}{(\ln(1-n))^2} = \dots = \lim_{n\to 1} \frac{2}{(1-n)^2}$$

$$3) \quad \lim_{n\to 1} \frac{2(1-n)^{-2}}{(\ln(1-n))^3} = \dots = \lim_{n\to 1} \frac{-8/3}{(1-n)^2}$$

and thus as n approaches unity, all the limits are unbounded so all the derivatives of (2.6.8) can be unbounded as well. Also, while the n-derivatives are unbounded, the derivatives with respect to the physical coordinate η are bounded. One can demonstrate this either by finding η-derivatives of (2.6.6) or by using the η-relations of (2.6.5) in (2.6.8) while noting (2.6.9).

If one objects to this unboundedness as described above, then transformation I must be used to map the η or ζ interval from 0 to ∞ onto the interval 0 to 1 so that one has a finite region over which to apply the Dirichlet boundary conditions mentioned above. It will be seen in a later section, however, that transformation I presents other problems when trying to solve the system of equations numerically. To summarize this section, the equations resulting from both transformations will be noted here for refrence. The equations (2.4.53) once acted upon by transformation I become

$$\beta^2(1-n)^2((1-n)^2\bar{u}_n)_n - 2\cos\alpha\,\beta^2(1-n)^2(1-s)^2\bar{u}_{ns} + \beta^2(1-s)^2((1-s)^2\bar{u}_s)_s + \sin\alpha\,((\bar{\phi} + \eta\sin\alpha\,\bar{u}(1,s))\,\beta(1-n)^2\bar{u}_n + (\bar{\psi} + \zeta\sin\alpha\,\bar{u}(n,1))\,\beta(1-s)^2\bar{u}_s) = 0 \qquad (2.6.10a)$$

$$\beta^2(1-n)^2((1-n)^2\bar{A}_n)_n - 2\cos\alpha\,\beta^2(1-n)^2(1-s)^2\bar{A}_{ns}$$
$$+\beta^2(1-s)^2((1-s)^2\bar{A}_s)_s + \sin\alpha\{(\bar{\phi}+\eta\sin\alpha\,\bar{u}(1,s))$$
$$\beta(1-n)^2\bar{A}_n + (\bar{\psi}+\zeta\sin\alpha\,\bar{u}(n,1))\,\beta(1-s)^2\bar{A}_s\}$$
$$+2\bar{u}\bar{A}\sin^2\alpha - 2\cot\alpha\,(\bar{u}_{\eta\eta}(n,1) - \bar{u}_{\zeta\zeta}(1,s)) - \bar{\phi}\bar{u}_\eta(n,1)$$
$$+\bar{\psi}\bar{u}_\zeta(1,s) + \zeta\{\bar{u}_{\eta\eta}(n,1)\,(\bar{\phi}-\bar{\phi}(n,1)+\eta\sin\alpha\,(\bar{u}(1,s)-1))$$
$$+2\bar{u}\cos\alpha\,(\bar{u}_\eta(n,1) - \beta(1-n)^2\bar{u}_n + \cos\alpha\,\beta(1-s)^2\bar{u}_s)\}$$
$$-\eta\{\bar{u}_{\zeta\zeta}(1,s)\,(\bar{\psi}-\bar{\psi}(1,s)+\zeta\sin\alpha\,(\bar{u}(n,1)-1))$$
$$+2\bar{u}\sin\alpha\,(\bar{u}_\zeta(1,s) - \beta(1-s)^2\bar{u}_s + \cos\alpha\,\beta(1-n)^2\bar{u}_n)\}$$
$$= 0 \qquad (2.6.10b)$$

$$\beta^2(1-n)^2((1-n)^2\bar{\phi}_n)_n - \cos\alpha\,\beta^2(1-n)^2(1-s)^2\bar{\phi}_{ns}$$
$$+\beta^2(1-s)^2((1-s)^2\bar{\phi}_s)_s + \sin^2\alpha\,\beta(1-s)^2\bar{A}_s$$
$$-2\sin\alpha\{\beta(1-n)^2\bar{u}_n - \tfrac{1}{2}\bar{u}_\eta(n,1) - \cos\alpha\,(\beta(1-s)^2\bar{u}_s$$
$$-\bar{u}_\zeta(1,s)\} = 0 \qquad (2.6.10c)$$

$$\beta^2(1-n)^2((1-n)^2\bar{\psi}_n)_n - 2\cos\alpha\,\beta^2(1-n)^2(1-s)^2\bar{\psi}_{ns}$$
$$+\beta^2(1-s)^2((1-s)^2\bar{\psi}_s)_s - \sin^2\alpha\,\beta(1-n)^2\bar{A}_n$$
$$-2\sin\alpha\{\beta(1-s)^2\bar{u}_s - \tfrac{1}{2}\bar{u}_\zeta(1,s) - \cos\alpha\,(\beta(1-n)^2\bar{u}_n$$
$$-\bar{u}_\eta(n,1))\} = 0 \qquad (2.6.10d)$$

where $\eta = \dfrac{n}{\beta(1-n)}$ and $\zeta = \dfrac{s}{\beta(1-s)}$. (2.6.11)

The same set of equations acted upon by transformation II become

$$\beta^2(1-n)\,((1-n)\,\bar{u}_n)_n - 2\cos\alpha\,\beta^2(1-n)(1-s)\,\bar{u}_{ns} + \beta^2(1-s)\,((1-s)\,\bar{u}_s)_s + \sin\alpha\,\{(\bar{\phi} \pm \eta\sin\alpha\,\bar{u}(1,s))\,\beta(1-n)\,\bar{u}_n + (\bar{\psi} + \zeta\sin\alpha\,\bar{u}(n,1))\,\beta(1-s)\,\bar{u}_s\} = 0 \qquad (2.6.12a)$$

$$\beta^2(1-n)\,((1-n)\,\bar{A}_n)_n - 2\cos\alpha\,\beta^2(1-n)(1-s)\,\bar{A}_{ns} + \beta^2(1-s)\,((1-s)\,\bar{A}_s)_s + \sin\alpha\,\{(\bar{\phi} + \eta\sin\alpha\,\bar{u}(1,s))\,\beta(1-n)\,\bar{A}_n + (\bar{\psi} + \zeta\sin\alpha\,\bar{u}(1,n))\,\beta(1-s)\,\bar{A}_s\} + 2\bar{u}\bar{A}\sin^2\alpha - 2\cot\alpha\,(\bar{u}_{\eta\eta}(n,1) - \bar{u}_{\zeta\zeta}(1,s)) - \bar{\phi}\bar{u}_\eta(n,1) + \bar{\psi}\bar{u}_\zeta(1,s) + \zeta\,\{\bar{u}_{\eta\eta}(n,1)\,(\bar{\phi} - \bar{\phi}(n,1)) + \eta\sin\alpha\,(\bar{u}(1,s) - 1)) + 2\bar{u}\sin\alpha\,(\bar{u}_\eta(n,1) - \beta(1-n)\,\bar{u}_n + \cos\alpha\,\beta(1-s)\,\bar{u}_s)\} - \eta\,\{\bar{u}_{\zeta\zeta}(1,s)\,(\bar{\psi} - \bar{\psi}(1,s)) + \zeta\sin\alpha\,(\bar{u}(n,1) - 1)) + 2\bar{u}\sin\alpha\,(\bar{u}_\zeta(1,s) - \beta(1-s)\,\bar{u}_s + \cos\alpha\,\beta(1-n)\,\bar{u}_n)\} = 0 \qquad (2.6.12b)$$

$$\beta^2(1-n)\,((1-n)\,\bar{\phi}_n)_n - 2\cos\alpha\,\beta^2(1-n)(1-s)\,\bar{\phi}_{ns} + \beta^2(1-s)\,((1-s)\,\bar{\phi}_s)_s - \sin^2\alpha\,\beta(1-s)\,\bar{A}_s - 2\sin\alpha\,\{\beta(1-n)\,\bar{u}_n - \tfrac{1}{2}\bar{u}_\eta(n,1) - \cos\alpha\,(\beta(1-s)\,\bar{u}_s - \bar{u}_\zeta(1,s))\} = 0 \qquad (2.6.12c)$$

$$\beta^2(1-n)\,((1-n)\,\bar{\psi}_n)_n - 2\cos\alpha\,\beta^2(1-n)(1-s)\,\bar{\psi}_{ns} + \beta^2(1-s)\,((1-s)\,\bar{\psi}_s)_s - \sin^2\alpha\,\beta(1-n)\,\bar{A}_n - 2\sin\alpha\,\{\beta(1-s)\,\bar{u}_s - \tfrac{1}{2}\bar{u}_\zeta(1,s) - \cos\alpha\,(\beta(1-n)\,\bar{u}_n - \bar{u}_\eta(n,1))\} = 0 \qquad (2.6.12d)$$

where $\eta = -\frac{1}{\beta}\ln(1-n)$ and $\zeta = -\frac{1}{\beta}\ln(1-s)$. (2.6.13)

3. SOLUTION OF THE EQUATIONS

3.1 Introduction

This chapter describes the various steps taken to find the numerical solution of the governing equations. The far-field conditions are dealt with first, the wall boundary conditions second, and the equations of the main system last.

In order that this chapter can be applied to either of the two transforms discussed earlier, the following notations are used. Equations (2.6.3) can be written as

$$Q_\zeta = \frac{\partial s}{\partial \zeta}\frac{\partial Q}{\partial s} \equiv S_\zeta Q_s \qquad (3.1.1)$$

$$Q_{\zeta\zeta} = \left(\frac{\partial s}{\partial \zeta}\right)^2 \frac{\partial^2 Q}{\partial s^2} + \frac{\partial^2 s}{\partial \zeta^2}\frac{\partial Q}{\partial s}$$

$$\equiv (S_\zeta)^2 Q_{ss} + S_{\zeta\zeta} Q_s \qquad (3.1.2)$$

and similarly for η-derivatives (e.g. $Q_\eta = N_\eta Q_n$). The forms taken by S_ζ and so on depend on which transformation is used, as can be seen in (2.6.4) and (2.6.5). For reference, the third-order derivative is

$$Q_{\zeta\zeta\zeta} = (S_\zeta)^3 Q_{sss} + 3(S_\zeta)^2 S_{\zeta\zeta} Q_{ss} + S_{\zeta\zeta\zeta} Q_s \qquad (3.1.3)$$

Therefore,

$$Q_{\zeta\zeta\zeta} \equiv \beta^3 (1 - s)^6 Q_{sss} - 6\beta^3 (1 - s)^5 Q_{ss} + 6\beta^3 (1 - s)^4 Q_s \qquad (3.1.4)$$

in terms of transformation I and

$$Q_{\zeta\zeta\zeta} = \beta^3(1-s)^3 Q_{sss} - 3\beta^3(1-s)^2 Q_{ss} + \beta^3(1-s) Q_s \qquad (3.1.5)$$

in terms of transformation II.

3.2 The Far-Field Equations

Because of symmetry, only one of s or n need be treated as variables. In the following discussion, s is the variable and n is held constant at unity. Using the transformations of the previous section and noting the ζ and s derivatives are full derivatives, (2.4.14) becomes

$$(S')^3 B''' + (S')^2 S'' B'' + S''' B' + \sin\left((S')^2 B'' + S'' S' B'\right) B = 0 \qquad (3.2.1)$$

with $$B(0) = B'(0) = 0 , \qquad (3.2.2)$$

and instead of $B' \to \sin\alpha$ as $S \to 1$, one uses (2.4.18), which is

$$B''(0) = \frac{0.4696 \sin^2\alpha}{\beta^2} , \qquad (3.2.3)$$

where the primes of B represent full s-derivatives of B and primes of S are functions that can be written in terms of s. At the same time, (2.4.42) becomes

$$\phi_1(s) = \cos\alpha \left(\zeta(s) S' B' - B\right) + \phi_h(s) \qquad (3.2.4)$$

where $\phi_h(s)$ is the solution of

$$S' \phi_h' + \sin\alpha \, B\phi_h = \mp \lambda \sin\alpha \, (1 + \cos\alpha) \, (\zeta(s) \sin\alpha + \lambda) \tag{3.2.5}$$

where $$\phi_h(0) = 0 \tag{3.2.6}$$

and the constant λ is from (2.4.42). The equations and initial conditions (3.2.1), (3.2.2), (3.2.3); and (3.2.5), (3.2.6), (3.2.7) comprise a set of two initial-value problems, one of third order and the other of first order. This set of equations would be more easily solved if they were written in terms of first-order initial-value equations only. Letting

$$y_1 = B(s), \; y_2 = B'(s), \; y_3 = B''(s) \text{ and } y_4 = \phi_h(s); \tag{3.2.7}$$

the set of equations becomes

$$y_1'(s) \equiv y_2(s) \quad \text{with} \quad y_1(0) = 0 , \tag{3.2.8}$$

$$y_2'(s) = y_3(s) \quad \text{with} \quad y_2(0) = 0 , \tag{3.2.9}$$

$$y_3'(s) = \frac{-(S')^2 S' y_3 - S' S''' y_2 - y_1 \sin\alpha \, ((S')^2 y_3 - S' S'' y_2)}{(S')^3} \tag{3.2.10}$$

with $$y_3(0) = \frac{0.4696 \sin^2\alpha}{\beta^2}$$

and

$$y_4'(s) = \frac{\lambda \sin\alpha \, (1 + \cos\alpha) \, (\zeta(s) \sin\alpha + \lambda) - y_1 y_4 \sin\alpha}{S'}$$

with $$y_4(0) = 0 . \tag{3.2.11}$$

The set of equations given by (3.2.8) to (3.2.11) can be solved using a Runge-Kutta routine. The routine is halted when y_1 to y_4 approach constant values. Once solutions are obtained, the outer boundary conditions of (2.4.50) are

$$\bar{u}(1,s) = S'\, y_2(s)/\sin\alpha$$

$$\bar{u}_\zeta(1,s) = ((S')^2 y_3 + S'S'' y_2)/\sin\alpha$$

$$\bar{u}_{\zeta\zeta}(1,s) = -y_1((S')^2 y_3 - S'S'' y_2)$$

$$\bar{A}(1,s) = (y_1 y_4 - \lambda(1+\cos\alpha)(\zeta(s)\sin\alpha + \lambda))/\sin\alpha$$
$$- \cos\alpha\, \zeta(s)\, ((S')^2 y_3 + S'S'' y_2)/\sin^2\alpha \qquad (3.2.12)$$

$$\bar{\phi}(1,s) = y_4 + \cos\alpha\, (\zeta(s)\, S' y_2 - y_1)$$

$$\bar{\psi}(1,s) = y_1 - \zeta(s)\sin\alpha$$

and the other boundary conditions of (2.4.51), by "symmetry", are

$$\bar{u}(n,1) = N'\, y_2/\sin\alpha$$

$$\bar{u}_\eta(n,1) = ((N')^2 y_3 + N'N'' y_2)/\sin\alpha$$

$$\bar{u}_{\eta\eta}(n,1) = -y_1((N')^2 y_3 + N'N'' y_2)$$

$$\bar{A}(n,1) = (y_1 y_4 + \lambda(1+\cos\alpha)(\eta(n)\sin\alpha + \lambda))/\sin\alpha$$
$$+ \cos\alpha\, \eta(n)\, ((N')^2 y_3 + N'N'' y_2)/\sin^2\alpha \qquad (3.2.13)$$

$$\bar{\phi}(n,1) = y_1 - \eta(n)\sin\alpha$$

$$\bar{\psi}(n,1) = y_4 + \cos\alpha\, (\eta(n)\, N' y_2 - y_1)$$

3.3 The Wall Boundary Value of $\bar{A}$

Along with the wall boundary conditions given by (2.5.1) and transformed, which are

$$\bar{u} = \bar{\phi} = \bar{\psi} = 0 \quad \text{on} \quad n = 0 \text{ or } s = 0, \tag{3.3.1}$$

the wall conditions of $\bar{A}$ given by (2.5.4) and (2.5.5) after either transformation is applied become

$$\begin{aligned} \bar{A}(0,s) &= \beta\bar{\psi}_n(0,s)/\sin^2\alpha \\ \bar{A}(n,0) &= -\beta\bar{\phi}_s(n,0)/\sin^2\alpha \end{aligned} \tag{3.3.2}$$

These boundary conditions need to be updated whenever new values of $\bar{\phi}$ or $\bar{\psi}$ are available. From (2.3.11), it is noted that once $\bar{A}(0,s)$, say, has been updated, then one can use

$$\bar{A}(n,0) = \bar{A}(0,s) \tag{3.3.3}$$

for the other wall boundary. Thus, only one of $\bar{\phi}$ or $\bar{\psi}$ need be available before the $\bar{A}$-equation is solved.

In order to obtain the $\bar{A}$ wall conditions, one must use foreward difference approximations to obtain estimates of $\bar{\psi}_n(0,s)$ or $\bar{\phi}_s(n,0)$. With all parts of

$$\bar{A}(0,1) = \beta\bar{\psi}_n(0,1)/\sin^2\alpha \tag{3.3.4}$$

already known from the far-field boundary conditions, this could be used to test the accuracy of various foreward difference schemes. A five-point foreward difference formula was found to be much more accurate than a two-point or three-point scheme.

3.4 Solution of the Main Equations

The main equations, given by (2.6.10) or (2.6.12), consist of four second-order elliptic linear partial differential equations of the form

$$a(av_n)_n + 2bv_{ns} + c(cv_s)_s + dv_n + ev_s + fv + g = 0 \tag{3.4.1}$$

where v represents one of the dependent variables $\bar{u}$, $\bar{A}$, $\bar{\phi}$, or $\bar{\psi}$; and the letters a to g represent coefficients, which may depend upon dependent variables other than that represented by v as well as the independent variables n and s. Since the main equations are so complex, they must be solved numerically. The illustration of the numerical procedure, which is described in this section, can be simplified by using (3.4.1) instead of an equation of (2.6.10) or (2.6.12).

The introduction of a fictitious time-derivative will be useful in presenting the solution procedure. The equation (3.4.1) then becomes

$$v_t = a(av_n)_n + 2bv_{ns} + c(cv_s)_s + dv_n + ev_s + fv + g \,. \tag{3.4.2}$$

In general, the dependent variables besides that represented by v are not known beforehand, meaning that the coefficients may also be unknown. In practice, one approximates the unknowns and iterates to obtain more accurate approximations. When this iteration process has converged, or when the difference between successive iterations is less than some value, the value of v_t is zero to this degree of accuracy.

Thus, the time-derivative disappears and the numerical solution is of the desired equations. Since one is interested only in the converged results, the intermediate results at smaller "times" are ignored.

When one proceeds to solve the equations of the system numerically, the coefficients and v are represented in a discrete form with derivatives approximated by appropriate difference formulae.

3.5 Numerical Considerations of Coordinate Transforms

It was mentioned in Section 6 of Chapter 2 that numerical problems would arise depending on which of transformations I or II was used. These problems occur at or near the outer boundary where the far-field conditions are applied. If there are only second-order derivatives in an equation (i.e. if d and e of (3.4.1) or (3.4.2) are zero, as is the case with the $\bar{\phi}$ and $\bar{\psi}$-equations), using transformation II results in the second-order derivative being

$$\beta^2(1-n)\,((1-n)v_n)_n = \beta^2(1-n)^2 v_{nn} - \beta^2(1-n)v_n \,. \qquad (3.5.1)$$

Using three-point central differences to approximate the derivatives, one has (where h is the numerical grid spacing in both the n and s-directions) the following:

$$\beta^2(1-n)^2\,\frac{V_{i+1,j}-2V_{i,j}+V_{i-1,j}}{h^2} - \beta^2(1-n)\,\frac{V_{i+1,j}-V_{i-1,j}}{2h}+O(h^2) \tag{3.5.2}$$

where $V_{i,j} = v(n,s)$ where $n = ih$, $s = jh$ and h is the grid spacing. Considering a point next to the outer boundary where $V_{i+1,j}$ is known (i.e. $n = 1 - h$), the coefficient of $V_{i+1,j}$ is

$$\frac{\beta^2h^2}{h^2} - \frac{\beta^2h}{2h} = \frac{\beta^2}{2}\,. \tag{3.5.3}$$

If instead transformation I is used so that the second-order derivative is

$$\beta^2(1-n)^2((1-n)^2v_n)_n = \beta^2(1-n)^4v_{nn} - 2\beta^2(1-n)^3v_n\,, \tag{3.5.4}$$

then the coefficient of the known $V_{i+1,j}$ on the boundary, found in a similar manner, is

$$\frac{\beta^2h^4}{2} - \frac{2\beta^2h^3}{2h} = \beta^2h^2 - \beta^2h^2 = 0. \tag{3.5.5}$$

This means that the information at the outer boundary does not enter into the numerical solution procedure. Even if the initial estimate of the solution satisfies the outer boundary conditions, any error accumulated during the numerical proceedure would destroy this agreement.

One can deal with this problem simply by using a different approximation for the derivatives. Suppose (3.5.4) were written as

$$- \beta^2(1 - n)^2 \left((1 - n)^2 v_n\right)_n$$

$$= \beta^2(1 - n)^2 \left\{\left((1 - n)^2\right)_n v_n + (1 - n)^2 v_{nn}\right\} , \qquad (3.5.6)$$

and the following approximations were used:

$$\left((1 - n)^2\right)_n = \frac{(1 - (n + \frac{1}{2}h))^2 - (1 - (n - \frac{1}{2}h))^2}{h}$$

$$(1 - n)^2 = \frac{(1 - (n + \frac{1}{2}h))^2 + (1 - (n - \frac{1}{2}h))^2}{2} . \qquad (3.5.7)$$

Using normal central differences for the derivatives of v, (3.5.6) with (3.5.7) can be approximated by

$$\frac{\beta^2(1 - n)^2}{h^2}\left[(1 - (n + \tfrac{1}{2}h))^2 V_{i+1,j} - \{(1 - (n + \tfrac{1}{2}h))^2 + (1 - (n - \tfrac{1}{2}h))^2\}V_{i,j} + (1 - (n - \tfrac{1}{2}h))^2 V_{i-1,j}\right] . \qquad (3.5.8)$$

The coefficient of $V_{i+1,j}$, when $n = 1 - h$, is

$$\frac{\beta^2 h^2}{h^2}\left(\frac{h}{2}\right)^2 = \left(\frac{\beta h}{2}\right)^2 , \qquad (3.5.9)$$

which is not equal to zero. The information at the outer boundary is therefore available for computation.

A more serious problem that arises from using transformation I involves the magnitude of error introduced by using difference formulae of given accuracy to approximate derivatives. Consider those terms containing spatial

derivatives of v (except the cross-derivative) of (3.4.2):

$$a^2 v_{nn} + c^2 v_{ss} + (d + aa_n) v_n + (e + cc_s) v_s \qquad (3.5.10)$$

where, for transformation I,

$$a = \beta(1 - n)^2 \quad , \quad c = \beta(1 - s)^2 \quad . \qquad (3.5.11)$$

If three-point differences are used such that

$$v_n = \frac{1}{2h} D_n V + O(h^2) \quad , \qquad (3.5.12)$$

then (3.5.10) is approximated by

$$\frac{\beta^2(1 - n)^4}{h^2} D_n^2 V + \frac{\beta^2(1 - s)^4}{h^2} D_s^2 V$$

$$+ \frac{d - 2\beta^2(1 - n)^3}{2h} D_n V \qquad (3.5.13)$$

$$+ \frac{e - 2\beta^2(1 - s)^3}{2h} D_s V + O(h^2) \quad .$$

For a grid point near a corner formed by a wall and a far-field boundary, where

$$n = 1 - h \quad \text{and} \quad s = h \quad , \qquad (3.5.14)$$

(3.5.13) becomes

$$\beta^2 h^2 D_n^2 V + \frac{\beta^2(1 - h)^4}{h^2} D_s^2 V + \frac{d - 2\beta^2 h^3}{2h} D_n V$$

$$+ \frac{e - 2\beta^2(1 - h)^3}{2h} D_s V + O(h^2) \quad . \qquad (3.5.15)$$

It is noted that the first and third term (assuming d = 0) are of the same order of magnitude as the error term, which in turn could dominate that region of the corner. Once the solution procedure is described, an illustration of this

problem will be presented. Recalling (3.5.9), the error term could also dominate the information contained in the far-field boundary condition even though the coefficient is non-zero.

This problem could be remedied by using higher-order difference formulae to approximate the derivatives. Five-point difference formulae (represented below by D^*) would lead to the following result, which corresponds to (3.5.15):

$$\frac{\beta^2 h^2}{12} D^{*2}_n V + \frac{\beta^2 (1-h)^4}{12h^2} D^{*2}_s V + \frac{d - 2\beta^2 h^3}{24h} D^*_n V + \frac{e - 2\beta^2 (1-h)^3}{24h} D^*_s V + O(h^3) \qquad (3.5.16)$$

where the error term is an order of h smaller than any of the difference terms. There is also no problem at the outer boundary, since the coefficient of $V_{i+1,j}$, with $n = 1 - h$, is

$$11 \frac{\beta^2 h^4}{12h^2} - 6 \frac{2\beta^2 h^3}{24h} = \frac{5}{12} \beta^2 h^2 \neq 0 , \qquad (3.5.17)$$

which is about the same size as the corresponding expression (3.5.9). The penalty for using higher-order difference approximations is, of course, that the difference equations become more complicated and require more computer time and storage to solve numerically.

All of the problems discussed have been consequences of using transformation I. If instead transformation II is used, the problems are absent.

Noting that for transformation II

$$a = \beta(1 - n) \quad \text{and} \quad c = \beta(1 - s) \; , \tag{3.5.18}$$

expression (3.5.10) becomes

$$\beta^2(1 - n)^2 v_{nn} + \beta^2(1 - s)^2 v_{ss} + (d - \beta^2(1 - n)) v_n + (e - \beta^2(1 - s)) v_s \; . \tag{3.5.19}$$

Ordinary three-point differences can be used to approximate the derivatives so that (3.5.19) at $n = 1 - h$ and $s = h$ becomes

$$\beta^2 D_n^2 V + \frac{\beta^2(1 - h)^2}{h^2} D_s^2 V + \frac{d - \beta^2 h}{2h} D_n V + \frac{e - \beta^2(1 - h)}{2h} D_s V + O(h^2) \tag{3.5.20}$$

where the error term is two orders of h smaller than the difference terms. Assuming d and e are zero, the far-field boundary coefficient of $V_{i+1,j}$ corresponding to (3.5.5) and (3.5.9) is

$$\beta^2 - \frac{\beta^2}{2} = \frac{\beta^2}{2} \; , \tag{3.5.21}$$

which is larger than any coefficient examined using transformation I with any difference scheme. However, since the error term $O(h^2)$ contains expressions involving

$$h^2 v_{sss} \quad \text{and} \quad h^2 v_{ssss} \tag{3.5.22}$$

for three-point difference approximations for first and second-order derivatives, these third and fourth-order derivatives, in this same problem area, may be large enough

to cause the error term to dominate nevertheless. As in the discussion of (2.6.8), if these derivatives are included, one gets

$$\bar{Q}_{sss} = -\beta b(n)\left\{\frac{2(1-s)^{-3}}{(\ln(1-s))^2} + \frac{6(1-s)^{-3}}{(\ln(1-s))^3} + \frac{6(1-s)^{-3}}{(\ln(1-s))^4}\right\} + \ldots$$

$$\bar{Q}_{ssss} = -\beta b(n)\left\{\frac{6(1-s)^{-4}}{(\ln(1-s))^2} + \frac{24(1-s)^{-4}}{(\ln(1-s))^3} + \frac{36(1-s)^{-4}}{(\ln(1-s))^4} + \frac{24(1-s)^{-4}}{(\ln(1-s))^5}\right\} + \ldots \qquad (3.5.23)$$

and one notes that if $b(n)$ is non-zero, then the derivatives become unbounded as s approaches unity by considering the limits of the s-terms as has been done.

These numerical problems will be examined again after the method used to solve the partial differential equations has been introduced.

3.6 The Numerical Method

One can begin by considering either (3.4.1) or (3.4.2) with the difference approximations substituted whenever derivatives appear. Three or five-point central differences are used for approximating the spatial derivatives and a two-point forward-difference approximation is substituted for the fictitious time-derivative. If $V_{i,j}$ is the discrete

approximation of $v(n,6)$, then the difference equation, for (3.4.2) say, is

$$\frac{V^*_{i,j} - V_{i,j}}{\rho} = (a^2)_{i,j}(V_{nn})_{i,j} + 2b_{i,j}(V_{ns})_{i,j} + (c^2)_{i,j}(V_{ss})_{i,j} + ((aa_n)_{i,j} + d_{i,j})(V_n)_{i,j} + ((cc_s)_{i,j} + e_{i,j})(V_s)_{i,j} + f_{i,j}V_{i,j} + g_{i,j} \tag{3.6.1}$$

or

$$V^*_{i,j} = V_{i,j} + \rho\{(a^2)_{i,j}(V_{nn})_{i,j} + 2b_{i,j}(V_{ns})_{i,j} + (c^2)_{i,j}(V_{ss})_{i,j} + ((aa_n)_{i,j} + d_{i,j})(V_n)_{i,j} + ((cc_s)_{i,j} + e_{i,j})(V_s)_{i,j} + f_{i,j}V_{i,j} + g_{i,j}\} \tag{3.6.2}$$

where $V^*_{i,j}$ is the new value of $V_{i,j}$ at a later "time", ρ is the time-step, $(V_{nn})_{i,j}$ etc. are the central difference approximations used, and the coefficients of (3.6.2) are discretized forms of those of (3.4.2).

If updated values are used as soon as they become available, then (3.6.2) describes a point Gauss-Seidel method of integration where the time-step parameter ρ can be chosen to be large and still maintain computational stability. This was the basic method used, with some modifications described below, to solve the system of equations. The

main modification was to postulate a spatially-dependent time-step parameter of the form

$$\rho \equiv \frac{\omega}{f_{i,j} + q_{i,j}} \tag{3.6.3}$$

where $q_{i,j}$ is the sum of the coefficients of $V_{i,j}$ (as opposed to $V_{i+1,j}$ for example) arising from the central difference approximations, and ω is a relaxation parameter. With (3.6.3), the difference equation (3.6.2) becomes an S O R type of iteration algorithm. For the interior points of the iteration scheme with three-point approximations,

$$q_{i,j} = -\frac{2}{h^2}\{(a^2)_{i,j} + (c^2)_{i,j}\} \tag{3.6.4}$$

was used. With five-point approximations,

$$q_{i,j} = -\frac{5}{12h^2}\{(a^2)_{i,j} + (c^2)_{i,j}\} \tag{3.6.5}$$

was used. This scheme is valid provided

$$f_{i,j} + q_{i,j} \neq 0 \tag{3.6.6}$$

for any n or s within the interval (0,1), which is not the case for the $\bar{A}$-equation. For the $\bar{u}$-equation, the parameter ω must be very small in order for the computation to remain stable. Use of (3.6.3) was therefore abandoned in favor of constant ρ for the $\bar{u}$ and $\bar{A}$-equations. In the $\bar{\phi}$ and $\bar{\psi}$ equations, however, the scheme works well.

The numerical process is begun from an initial estimate of the solutions obtained in a manner suggested by Ghia and Davis (1974b) from the known boundary conditions

$$\bar{u}_{i,j} = \bar{u}_{i,m}\,\bar{u}_{m,j}$$

$$\bar{\phi}_{i,j} = \bar{\phi}_{i,m}\,\bar{\phi}_{m,j}\,\{1 - e^{-15(n_i + s_j)^2}\}/\bar{\phi}_{m,m}$$

$$\bar{\psi}_{i,j} = \bar{\psi}_{i,m}\,\bar{\psi}_{m,j}\,\{1 - e^{-15(n_i + s_j)^2}\}/\bar{\psi}_{m,m}$$

$$\bar{A}_{i,j} = (a)_{i,j}(\bar{n})_{i,j} - (c)_{i,j}(\bar{s})_{i,j} \qquad (3.6.7)$$

$$+ \cos\alpha\,\{(a)_{i,j}(\bar{\phi}_n)_{i,j} - (c)_{i,j}(\bar{\psi}_s)_{i,j}\}$$

$$+ \sin\alpha\,\cos\alpha\,(\bar{u}_{m,j} - \bar{u}_{i,m})$$

where $i,j = 2, 3, \ldots, m - 1$

and m^2 is the total number of grid points per dependent variable. The exponential factor within the curly brackets represents an attempt to have an initial estimate nearer the expected final solution as presented in Ghia (1975) for the case of the rectangular corner. The last relation of (3.6.7) is a numerical form of the defining equation of $\bar{A}$ as found in (2.3.5). It was found that for $\alpha = 90^\circ$; $\rho = 0.004$ for $\bar{u}$ and $\bar{A}$-equations and $\omega = 1.87$ for $\bar{\phi}$ and $\bar{\psi}$-equations, so these values were used in the computation.

Another device used to accelerate the computational process was to note that by using the "symmetry" relations of (3.3.11), as soon as $V^*_{i,j}$ is found at a grid point (i,j), a new value at (j,i) is found also. Values at two places can be updated for each use of (3.6.2).

3.7 Summary

The following sequence summarizes the general proceedure used to obtain numerical solutions:

1) Boundary conditions are input and initial estimates are obtained using (3.6.7);
2) The $\bar{u}$-equation is iterated upon via (3.6.2) once for all points followed by the $\bar{\phi}$-equation;
3) Boundary conditions of $\bar{A}$ along the walls are updated using a five-point foreward difference formula as described in Chapter 3, Section 2;
4) The $\bar{A}$-equation followed by the $\bar{\psi}$-equation are iterated upon in the same manner as for those of step 2 above;
5) The stopping criterion (described below) is tested, and if it fails then program control goes to step 2, but if the test succeds, then control goes to the next step;
6) The converged solution approximations are processed, printed and filed.

In practice, steps 2 to 4 are repeated a fixed number of times before entering step 5.

Two different types of stopping criteria can be used in step 5. The more conventional criterion is to examine the largest difference between grid points of successive iterations. When the largest difference falls below a given value, the solution is accepted as converged. For reference this shall be called the normal criterion. Since the largest difference may not decrease steadily because of the iterative

behavior of all four system equations, one must be careful that the value chosen to halt the computation process is small enough so that subsequent fluctuations will be insignificantly small.

Another criterion involves examining certain features of the solution. The profiles of $\bar{u}(s,s)$ and $\bar{A}(0,s)$ were chosen, and when $\bar{A}(0,s)$ was found to be much more sensitive to the number of iterations than $\bar{u}(s,s)$, the latter was dropped. If the largest difference between points of successive iterations was to fall below a certain value related to the resolution of a graph, then the scheme can be considered as converged with the understanding that the next few iterations are not going to make significant changes in the solution. This will be called the resolution criterion.

4. RESULTS

4.1 Data Reduction

Quantities of major interest are the physical components of velocity, which are given in terms of u, ϕ and ψ by

$$\begin{aligned} u^{(1)} &= t_i^1 u^i = uU \\ u^{(2)} &= UR^{-\frac{1}{2}}(\eta u \sin\alpha - \phi) = vUR^{-\frac{1}{2}} \\ u^{(3)} &= UR^{-\frac{1}{2}}((\eta \cos\alpha + \zeta)u - \phi \cot\alpha \\ &\quad - \psi \csc\alpha) \\ &= wUR^{-\frac{1}{2}} \end{aligned} \tag{4.1.1}$$

or, in terms of the bounded quantities, by

$$\begin{aligned} u^{(1)} &= \bar{u}U \\ u^{(2)} &= UR^{-\frac{1}{2}}(\eta \sin\alpha\,(\bar{u} - \bar{u}(\infty,\zeta)) - \bar{\phi}) \\ &= vUR^{-\frac{1}{2}} \\ u^{(3)} &= UR^{-\frac{1}{2}}(\eta \cos\alpha\,(\bar{u} - \bar{u}(\infty,\zeta)) \\ &\quad + \zeta\,(\bar{u} - \bar{u}(\eta,\infty)) - \bar{\phi}\cot\alpha - \bar{\psi}\csc\alpha) \\ &= wUR^{-\frac{1}{2}} . \end{aligned} \tag{4.1.2}$$

With the cross-flow velocity components v and w thus obtained, the magnitude r and direction angle θ (measured counterclockwise from the z-axis) of the cross-flow velocity are

$$r = (v^2 + w^2)^{\frac{1}{2}} \tag{4.1.3}$$

and

$$\theta = \tan^{-1}\left(\frac{v}{w}\right) .$$

Since the data to be processed are still in terms of n and s, it is desirable to transform the velocity components so that they can be expressed in terms of the more physically meaningful coordinates η and ζ. This is easy to do by using the inverse transformation I of (2.6.1), but to obtain regularly-spaced data points in η and ζ it is necessary to interpolate. To do this, a bicubic spline interpolation routine was used. With this done, it was then possible to produce graphs or tables of the quantities of interest in terms of regular intervals of η and ζ. For square regions, contour plots of the quantities with respect to either (n,s) or (η,ζ) were made using a standard computer routine. For smooth graphs, more points could be found by using a cubic spline interpolation routine. These standard computer routines are listed at the end of the thesis.

4.2 The Right-Angled Corner

Results for the right-angled corner shall be used as a test for the computation and reduction procedures by comparison with the results of other authors. In particular, these results are used to decide which of transformation I and II is preferable and, given the transformation, should a three-point or a five-point difference estimate be used for the derivatives.

The first case tried was that using transformation I and three-point difference approximations. It has already

been noted that problems may arise near the corners where one independent variable has the value zero and the other unity. The quantity $\bar{A}$, evaluated at various values of s along the wall n = 0, is shown in Figure 2 for the present case. The ten curves shown represent the function $\bar{A}(0,s)$ evaluated at intervals of the solution process a fixed number of iterations apart. Curve number 1 represents the initial approximation of $\bar{A}(0,s)$. Note the irregularity near s = 1 that appears almost immediately and the deviations that increase as the computer precedure continues as indicated by successively numbered curves.

The next case tried was that using transformation I and five-point difference approximations. Figures 3 and 4 illustrate the behavior of $\bar{A}(0,s)$ with continuing computer processing as did Figure 2 described above. The value of $\bar{A}(0,s)$ of Figure 3 seems to converge as the process iterates from the initial estimate of $\bar{A}(0,s)$ labelled 1 through to curve 5, where the process was halted using the normal criterion. When a smaller halting criterion parameter was used, however, the curves of $\bar{A}(0,s)$ labelled 6 through 10 illustrate that when the iteration process continued, the error of that region of the corner still caused fluctuations. Despite this, the results obtained at the point where the computer program was halted at curve 5 compared well with results presented by other authors. Figure 5 compares the mainstream velocity profiles of different authors. The contour Figures 6, 7 and 8 compare very closely with those

presented by Ghia (1975) in the (n,s) coordinates.

So far, it seems that it would be optimum to use five-point differences with transformation I for reasons of improved accuracy although more computing time is needed than with three-point differences. However, both schemes have the problem of not being computationally stable. If the tolerance used in the normal criterion for stopping the procedure had been too small, the computation would not have halted when the solution approximation was available. This reason, along with increased computing time, provided the motivation to try transformation II. The final case tried, therefore, was that using transformation II and three-point difference approximations. Convergence was achieved more surely than with transformation I. The contour Figures 9, 10 and 11 represent the flow quantities for transformation II. They differ from those of transformation I only because of the different transformations used, which can be detected by noting that the features of Figures 9 to 11 appear larger than those of Figures 6 to 8. If one transforms both sets of information from (n,s) coordinates of transformations I and II to (η,ζ) coordinates using the appropriate inverse transformations as given in (2.6.1) or (2.6.2), then the solutions using different transformations compare so closely that it becomes difficult to tell them apart. This is especially true of the contours of the various quantities that lie within the boundary region, which can be defined to be at and within the mainstream velocity contour $\bar{u} = 0.9$.

In addition to the convergence and solution characteristics, the three-point transformation II scheme is faster than the five-point transformation I scheme since there are fewer point values that need to be processed in one iteration. It is also possible to use the aforementioned resolution criterion for halting the computer program.

To summarize, it is first of all noted that the equations and boundary conditions presented here and specified for the right-angled corner with transformation I become identical to those used by Ghia (1975). The results presented in that paper compare very well with those presented here. This means that the computational scheme, while different from that described by Ghia (1975), leads to the same results. It is next noted that differences between solutions obtained by using transformation I or II are nearly non-existant when viewed with respect to (η,ζ) coordinates. Figures 12, 13 and 14 display results, in terms of (η,ζ) coordinates, of mainstream velocity, cross-flow velocity magnitude and modified mainstream vorticity respectively. The smaller insets to these figures are plots of the corresponding results available from Rubin and Grossman (1971). The results of Barclay and Ridha (1980) for the right-angled corner agree well with those of Ghia (1975) and therefore with the present results also. With these conclutions and excellent comparisons, one can use the solution scheme presented in this work to examine corners of different corner angles with confidence in the results.

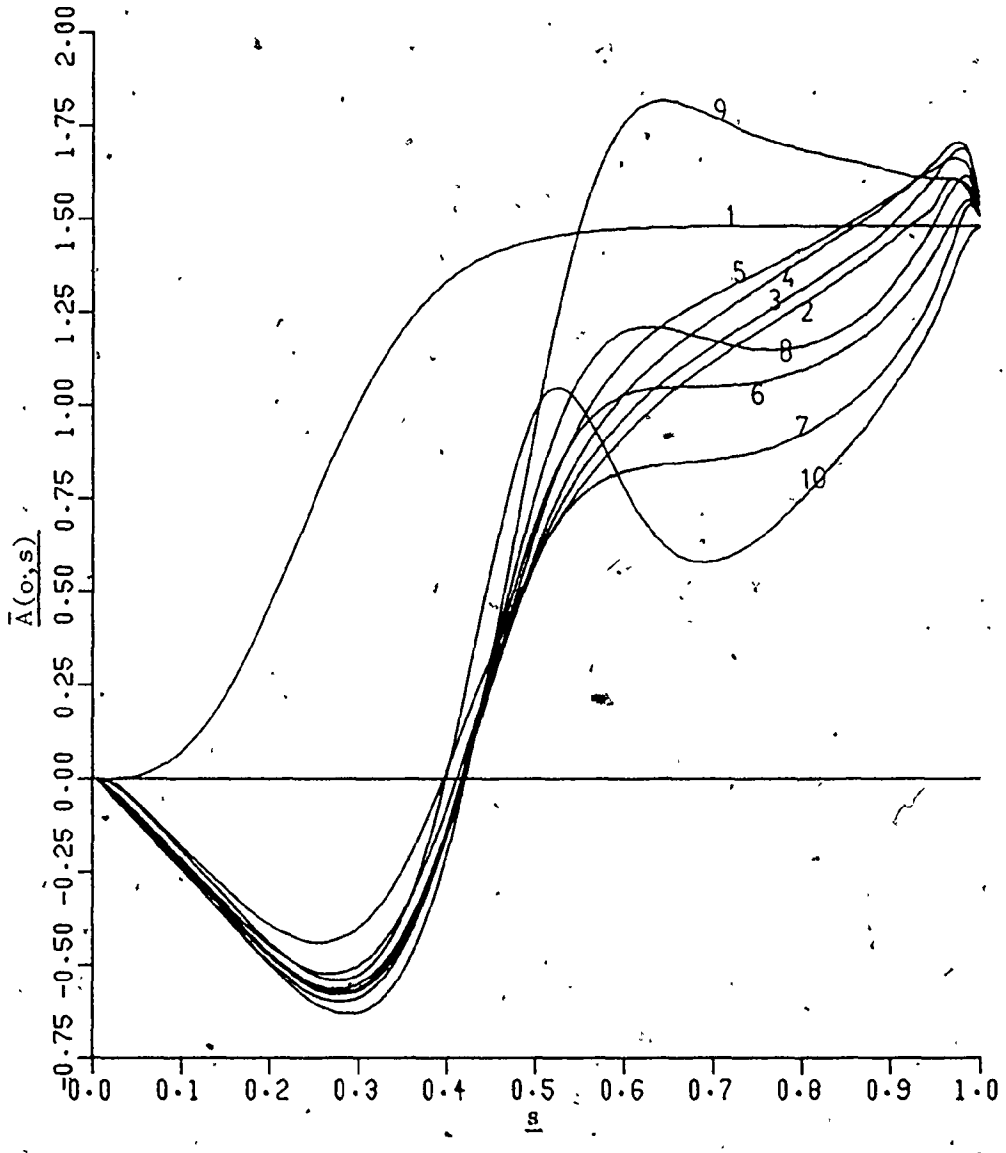

Figure 2

Sequence of modified vorticity curves along a wall for a transformation I 3-point scheme.

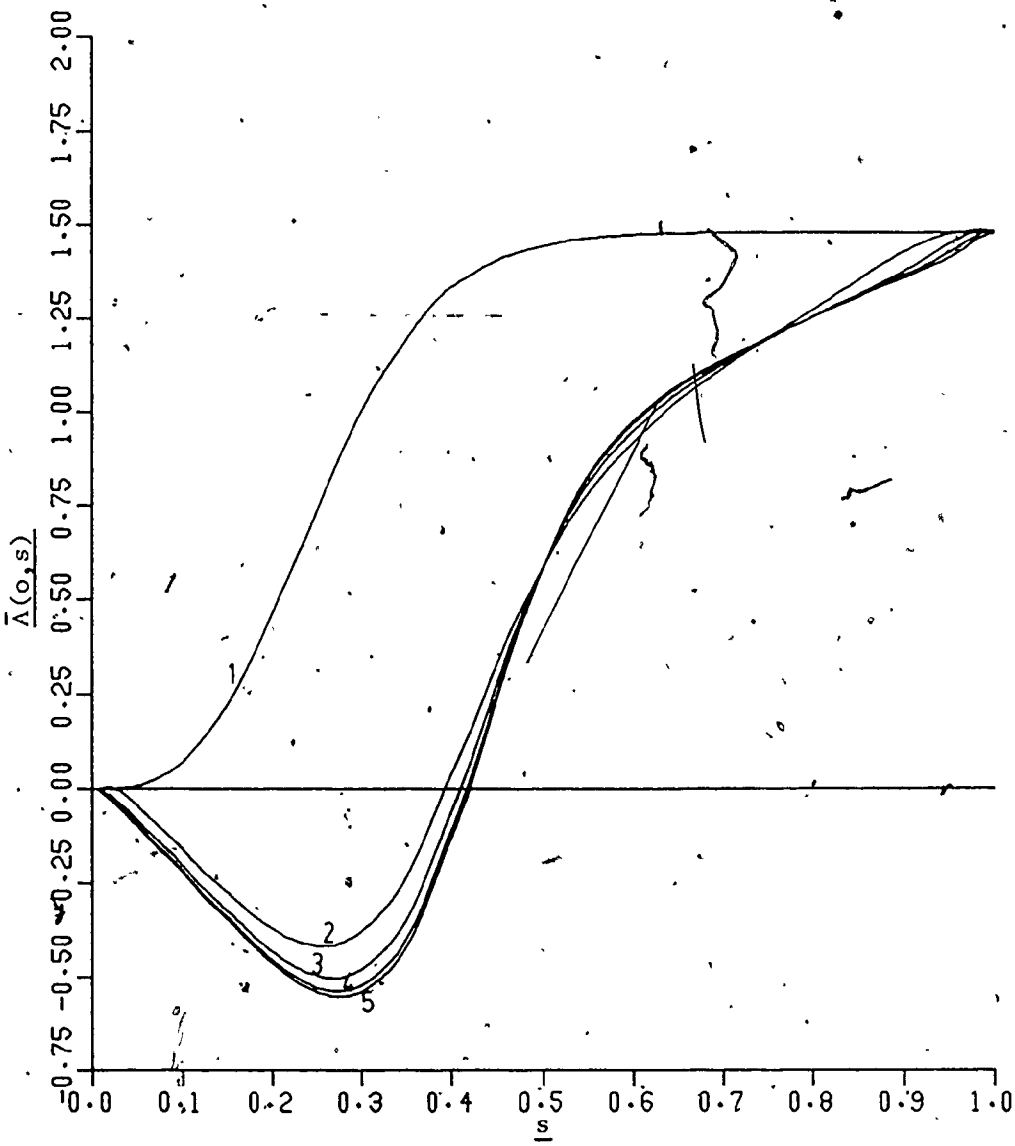

Figure 3

First part of sequence of modified vorticity curves along a wall for a transformation I 5-point scheme.

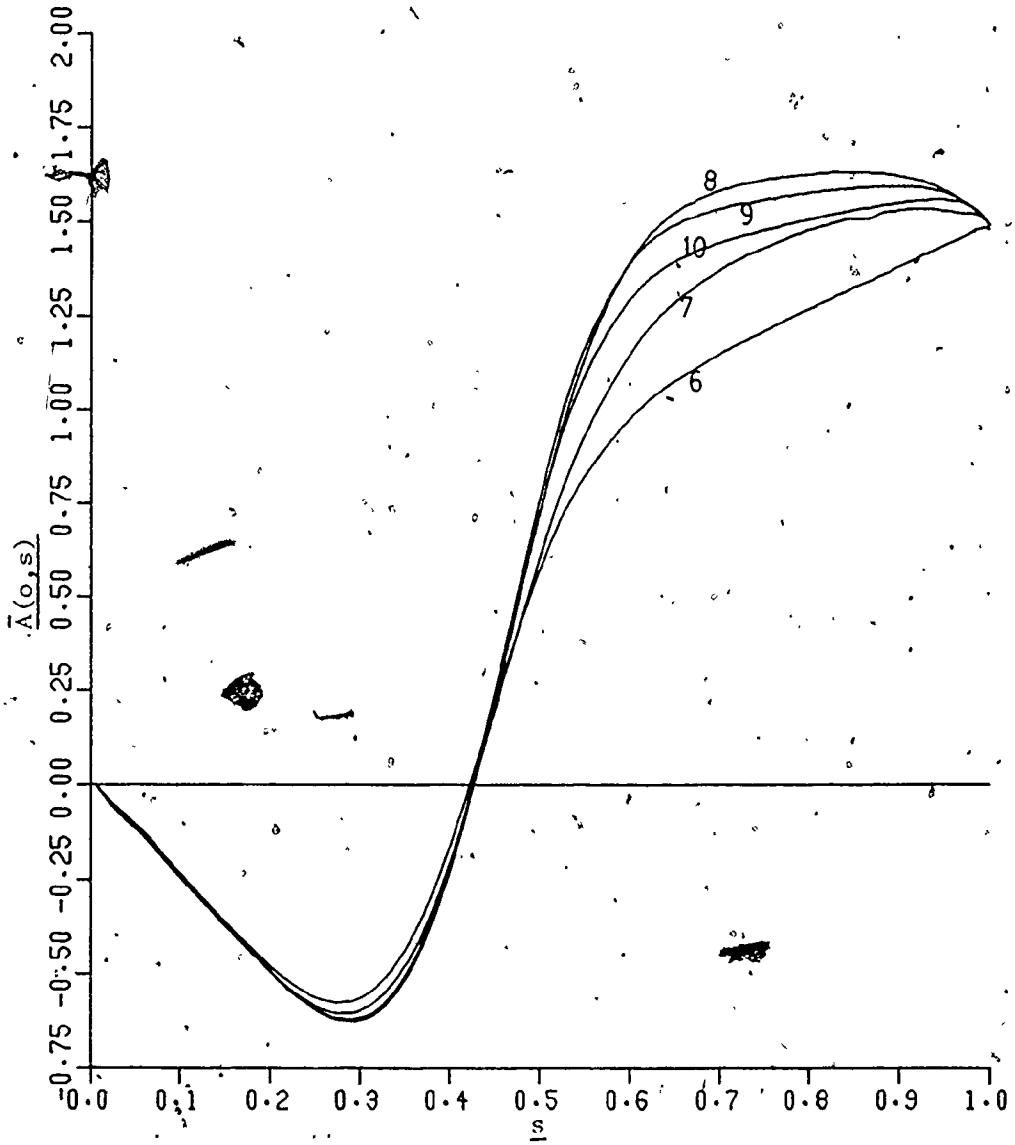

Figure 4

Last part of sequence of modified vorticity curves along a wall for a transformation I 5-point scheme.

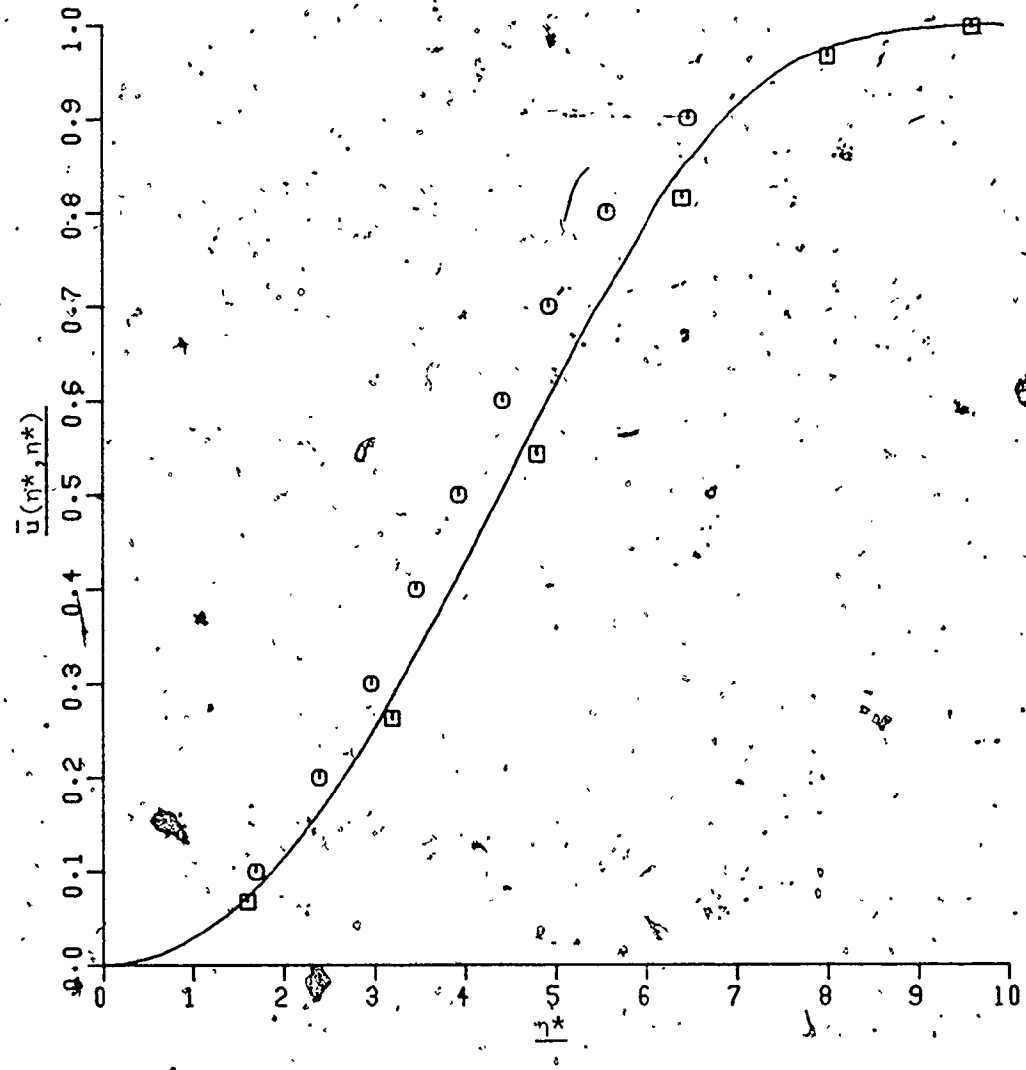

Figure 5

Mainstream Velocity Profile

⊙ : Desai & Mangler (1974)

⊡ : Rubin & Grossman (1971), Ghia (1975)

/ : Present results

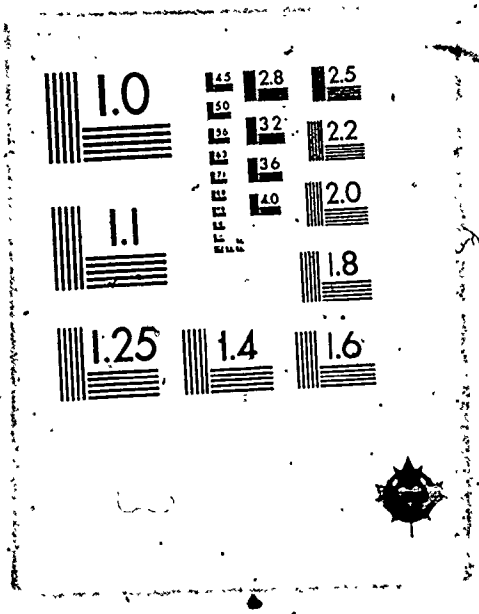

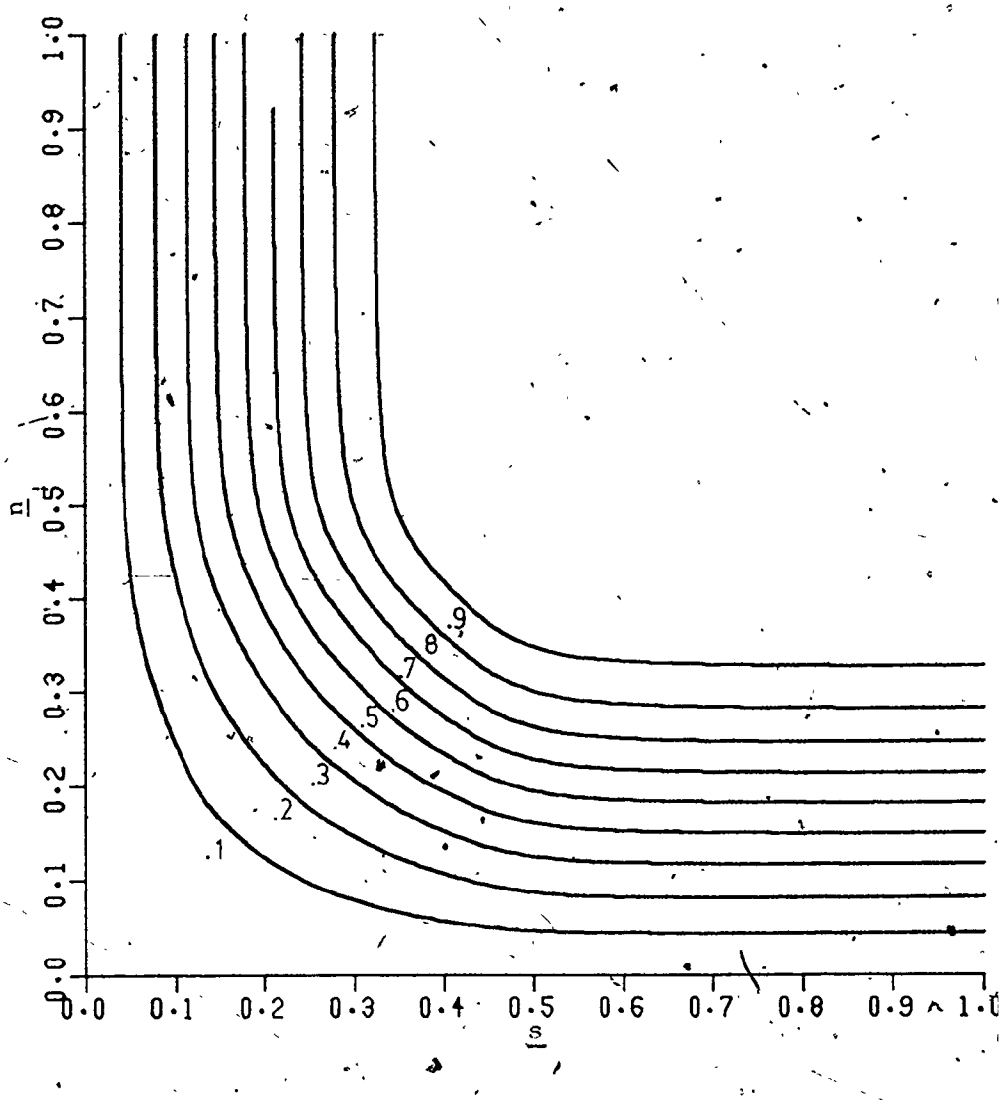

Figure 6

Mainstream Velocity Contours $\bar{u}(n,s)$

Transformation I with 5-Point Differences

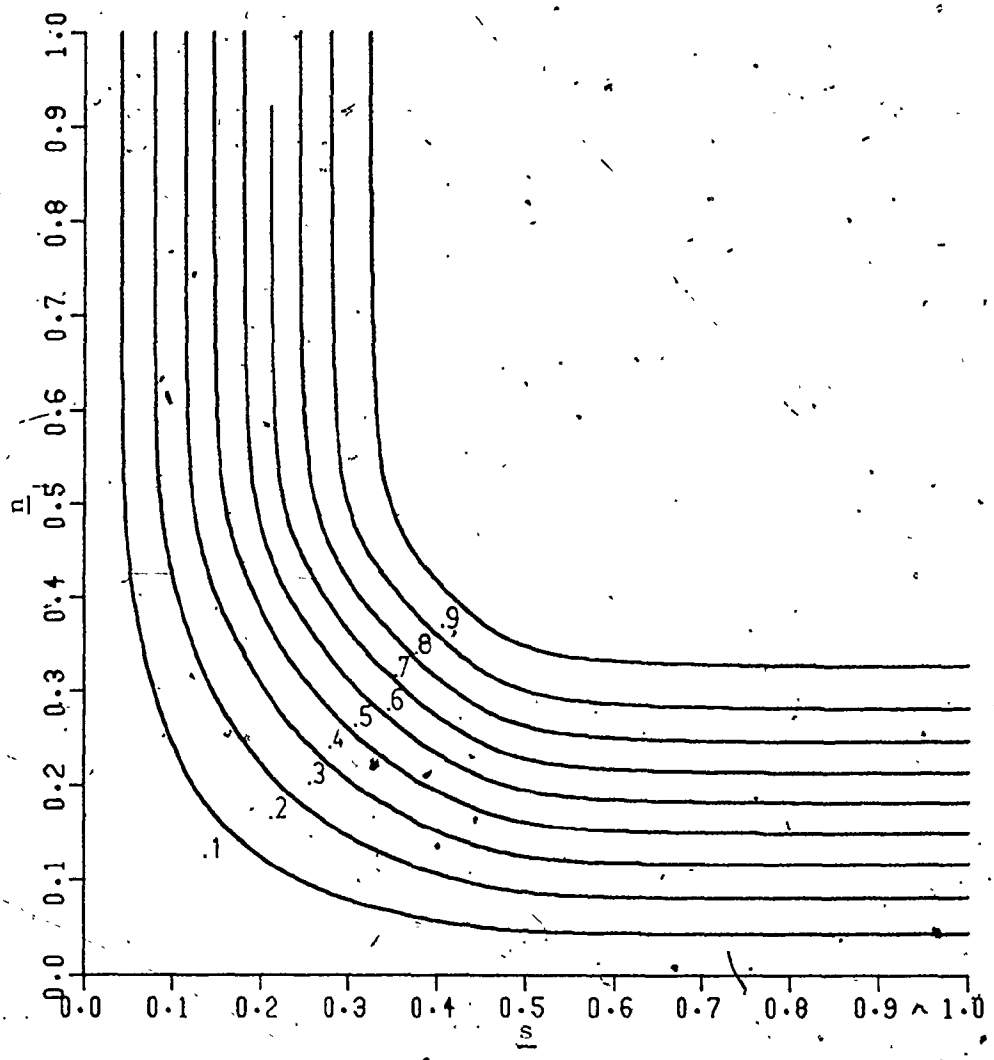

Figure 6

Mainstream Velocity Contours $\bar{u}(n,s)$

Transformation I with 5-Point Differences

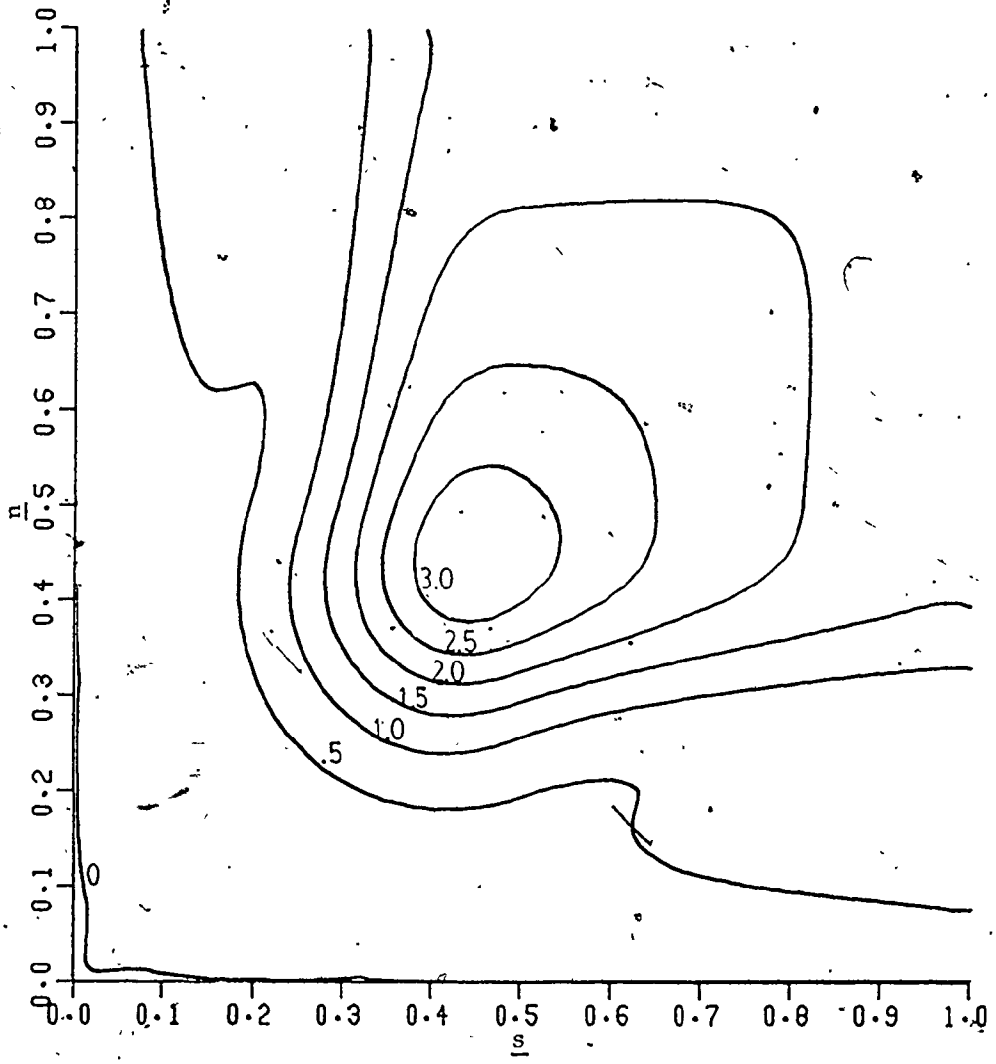

Figure 7

Cross-Flow Velocity Magnitudes

$r = (v^2 + w^2)^{1/2}$

Transformation I with Five-Point Differences

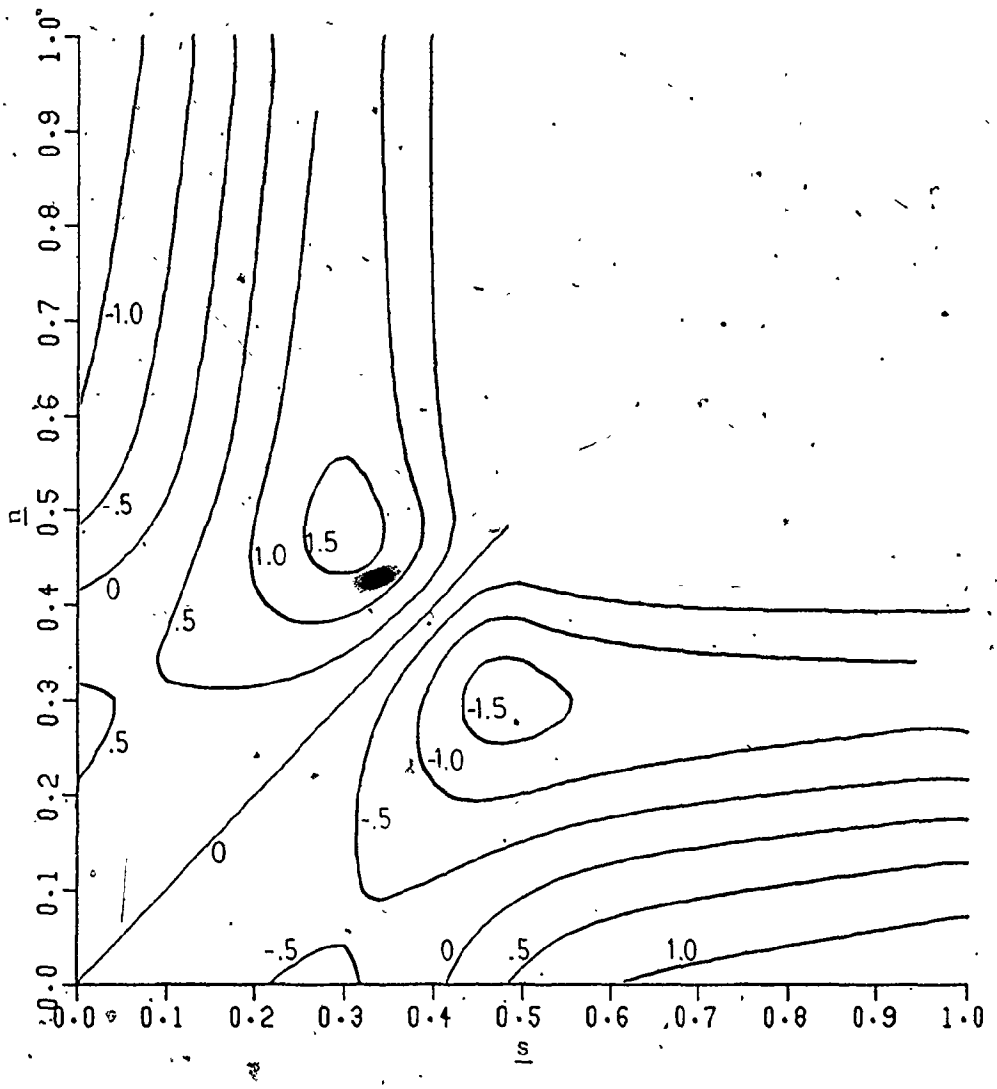

Figure 8
Mainstream Vorticity $\bar{A}(n, s)$
Transformation I with 5-Point Differences

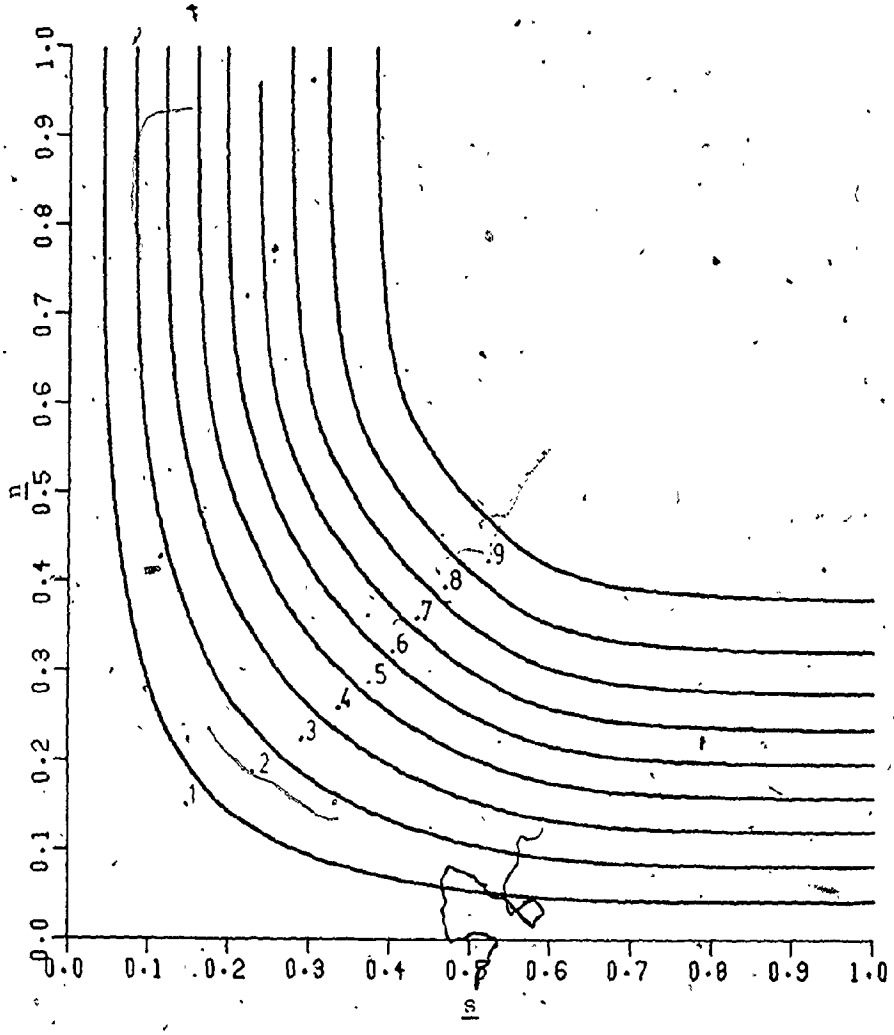

Figure 9
Contour graph of the mainstream velocity $\bar{u}(n,s)$ obtained using the 3-point transformation II scheme

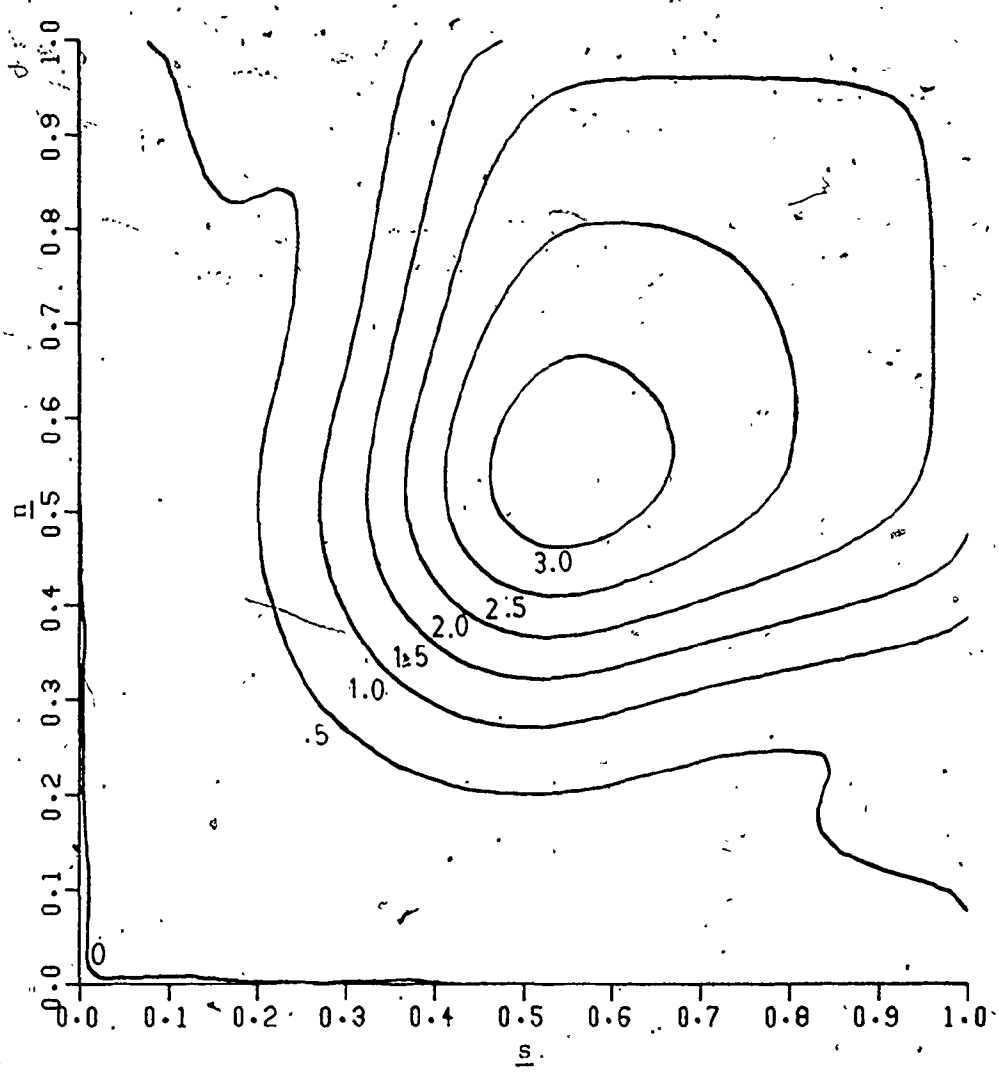

Figure 10

Contour graph of secondary flow velocity given by

$$r = (v^2 + w^2)^{\frac{1}{2}}$$

obtained with the 3-point transformation II scheme

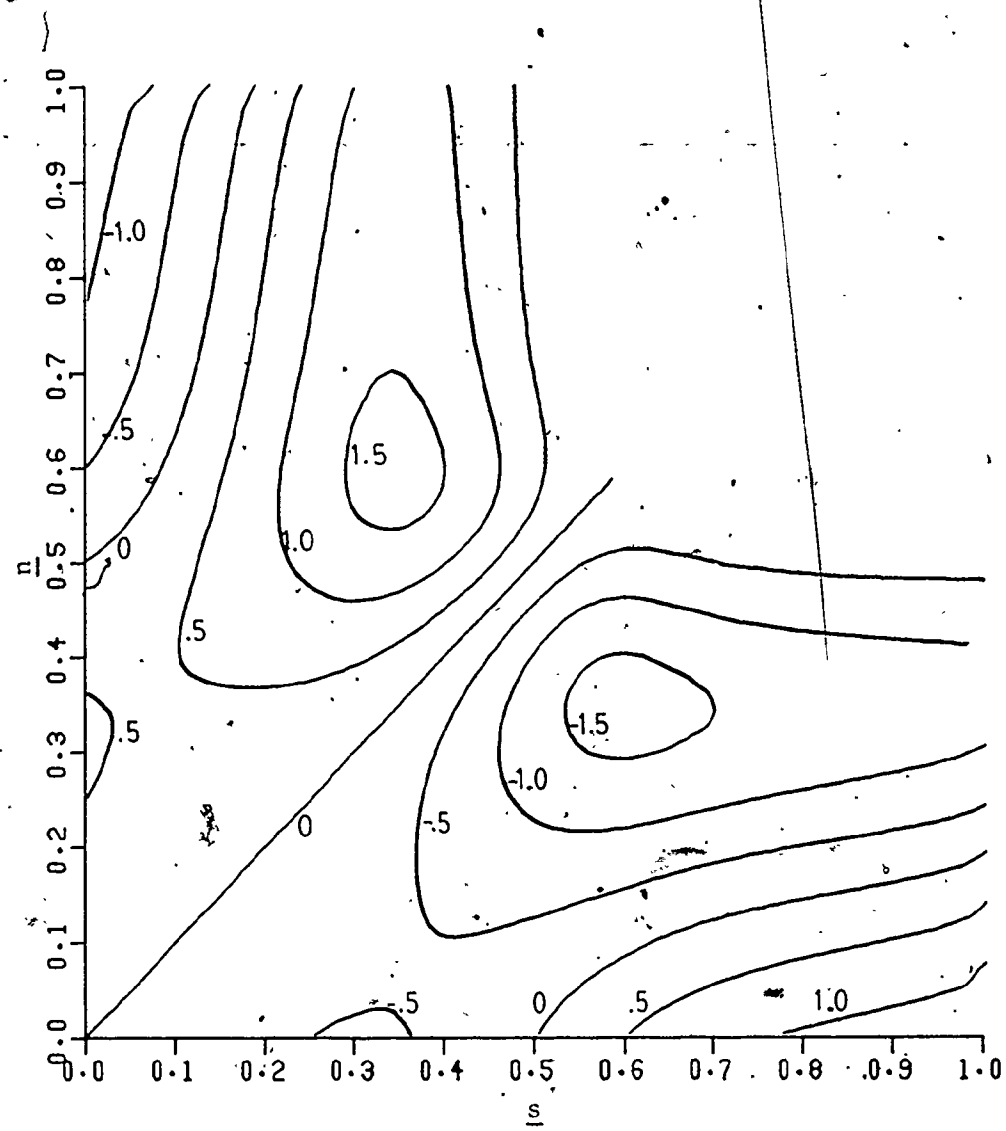

Figure 11

Contour graph of the modified vorticity function $\bar{A}(n,s)$ obtained with the 3-point transformation II scheme

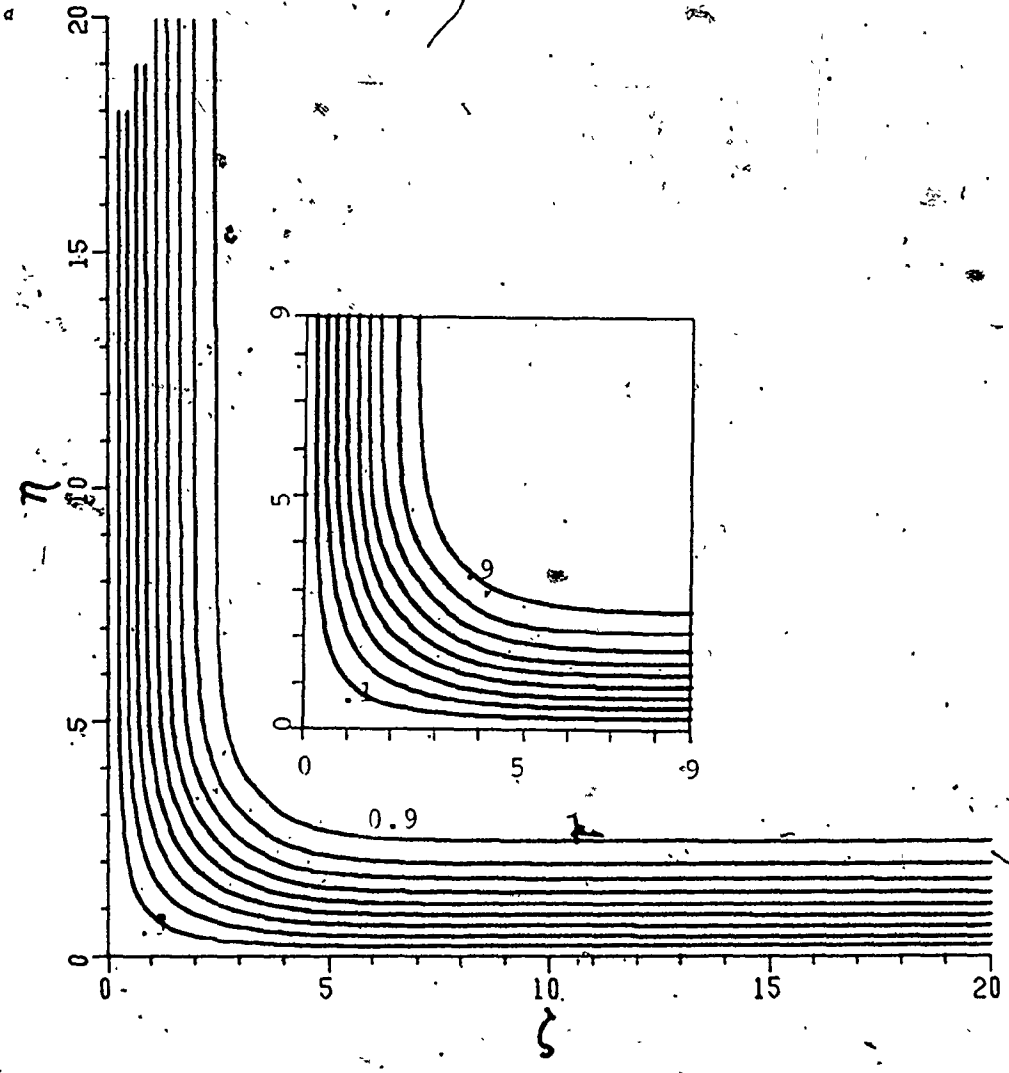

Figure 12

Mainstream velocity $\bar{u}(\eta, \zeta)$.
The smaller plot shows the results of Rubin & Grossman (1971).

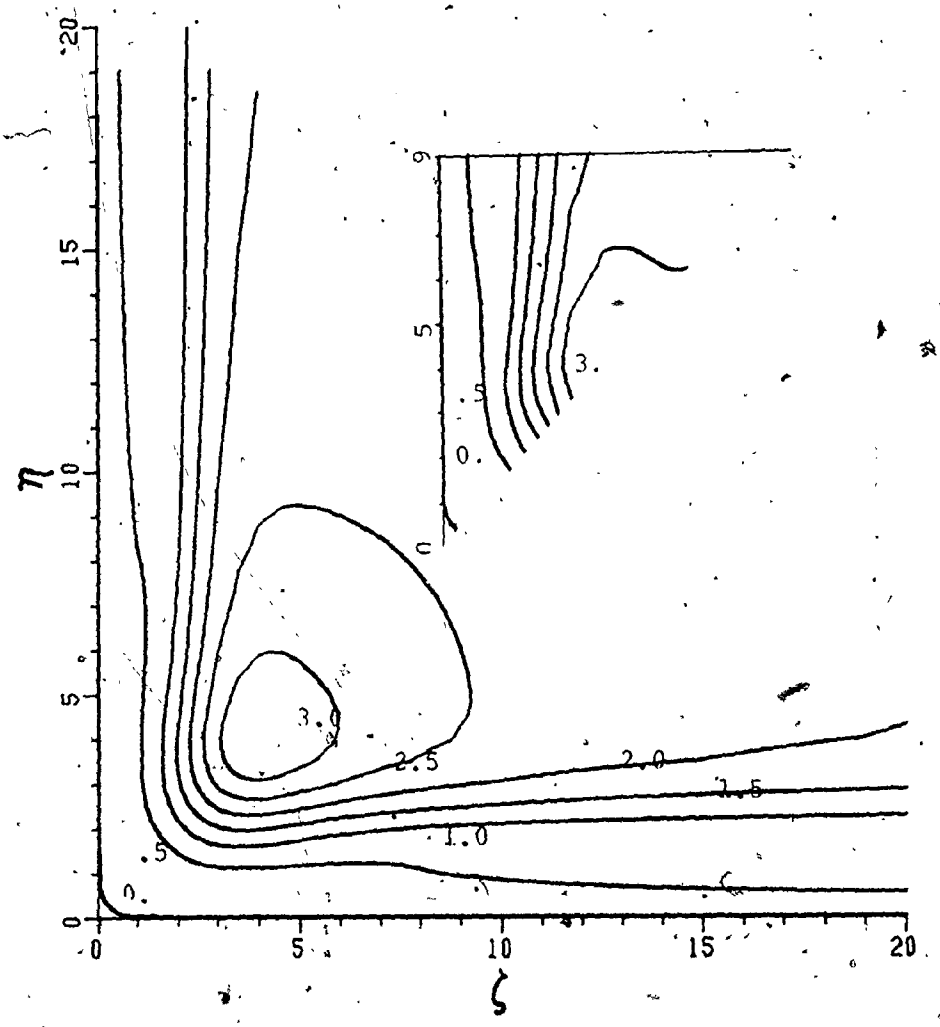

Figure 13

Cross-Flow Velocity Magnitude

$$r(\eta,\zeta) = (v^2 + w^2)^{\frac{1}{2}}$$

The smaller plot shows the results of Rubin and Grossman (1971) with symmetry assumed.

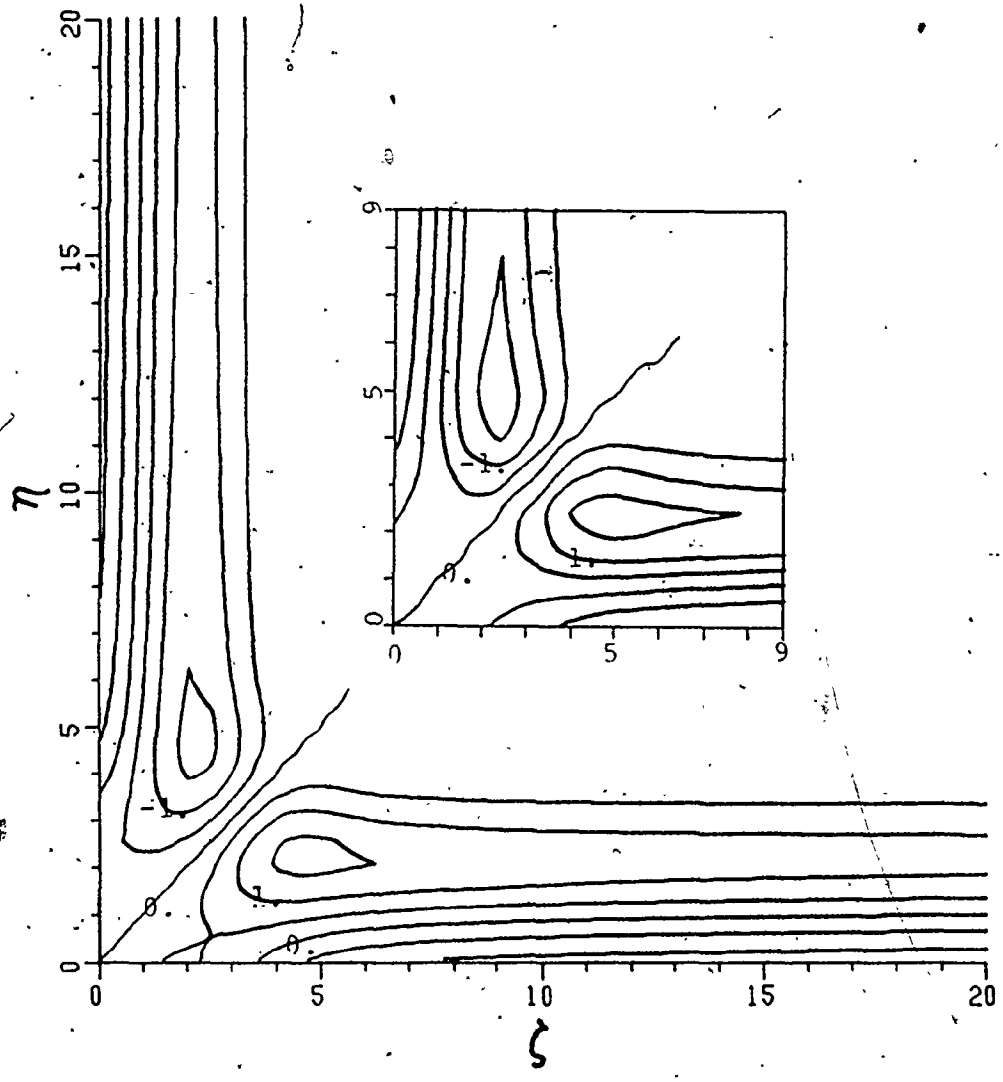

Figure 14

Modified mainstream vorticity $\bar{A}(\eta, \zeta)$.

The smaller plot shows the results of Rubin & Grossman (1971).

4.3 Corners of Different Angles

Four other sets of results were obtained besides that of the right-angled corner. Taken together, the results for the following five corner angles:

$$\alpha = 30^{\circ},\ 60^{\circ},\ 90^{\circ},\ 120^{\circ} \text{ and } 150^{\circ}; \qquad (4.3.1)$$

can be examined to note how changes in the corner angle produce differences in various flow quantities. These results will be presented graphically in terms of the "physical" variables η and ζ.

The mainstream velocity profiles in the bisector plane, shown in Figure 15, consists of the mainstream velocity profile $\bar{u}(\eta_z, \eta_z)$ where

$$\eta_z = \frac{S}{x}\left(\frac{Ux}{\nu}\right)^{\frac{1}{2}} = 2\eta\ (1 + \cos\alpha)^{\frac{1}{2}} \qquad (4.3.2)$$

is independent of corner angle α. Figure 16 displays the skin friction versus η_z for all five angles. Similar figures are given in Barclay and Ridha (1980) for the angles 90°, 135°, 180°, 225° and 270°*. In both cases, the velocity profiles for the concave corners are of the S-type, which characterize velocity profiles that may lead to boundary layer separation. As the corner angle becomes smaller, the profiles deviate more radically from Blasius profiles. The point at which the mainstream velocity profile $\bar{u}(\eta_z, \eta_z)$ approaches unity occurs at successively larger values of η_z, indicating that the corner boundary region is thickening.

* Comparisons with Barclay and Ridha (1980) are not possible because of the different angles considered (except 90 degrees, which is the same as Rubin & Grossman (1971) and Ghia (1975)).

Also, in both cases, the skin friction for angles less than 180° indicates a deficit at the corner, but increases to the Blasius value away from the corner. Again as the corner angle decreases, the skin friction approaches the Blasius value at progressively larger distances from the corner.

One way to examine the secondary flow in directions perpendicular to the mainstream direction is to examine magnitudes and directions at various points. This flow is called secondary because it is of the order of $R_x^{-\frac{1}{2}}$ in magnitude, compared to order unity for the mainstream velocity. The directions at various points are indicated by the arrows in Figures 17 to 21. These plots were drawn so that the axes correspond to the walls, the different corner angles are apparent, and the resulting flow field appears as it would naturally. The coordinates η and ζ of these figures measure along coordinate lines of the non-orthogonal Cartesian coordinate system, which are parallel to each axis.

From these diagrams, it is possible to distinguish three separate regions in general. All three, however, may not be present in a particular case. Beginning with the 150° corner of Figure 17, one notes that in the outer region the flow is toward the corner along the walls. Before the corner is reached, the cross-flow directions turn outward so that they eventually point away from the corner in a direction parallel to the bisector. From the detail of the

figure, the cross-flow behavior right at the corner is evident. This, denoted as the inner region, appears to flow into the corner. As the corner angle decreases through 120° to 90° (Figures 18 and 19), one notices the emergence of a middle region, which is characterized by flow moving outward from the corner. This flow region meets the incoming flow of the outer region at which point both are deflected away from the walls to form the outward-moving flow parallel to the bisector. As the corner angle continues to decrease to 60° (Figure 20), the middle region becomes larger while the inner region decreases. For the 30° corner (Figure 21), the inner region is no longer evident and the middle region completely dominates the interior flow field.

Figures 22 to 26 are contour graphs representing the cross-flow velocity magnitudes. The number of contour lines (spaced 0.5 units apart in all cases) increase with decreasing corner angle. In all cases, the point of highest cross-flow velocity occurs at some point on the bisector and decreases in magnitude quickly as one moves from this point towards any point on the solid boundary near the corner. By comparing figures of series 17 - 21 and 22 - 26 of corresponding corner angle, the region of highest cross-flow velocity is directed outward from the corner and parallel to the bisector. It is also noted that as the corner angle decreases and the middle region of the cross-flow becomes larger, regions of local maxima or ridges form

near the walls and far from the corner. The valley regions between the ridge and the central maximum correspond to areas where the outgoing flow of the middle region collides with the incoming flow of the outer region. The ridges themselves indicate that the flow of the outer region is affected by the middle region flow so that the penetration of the outer region toward the corner is halted. In all cases, there is a large gap between the solid boundary near the corner and the first contour ($r = 0.5$), indicating low cross-flow velocity gradients near the corner.

The contours of Figures 27 to 31 denote values of the modified vorticity function $\bar{A}(\eta,\zeta)$. Once again, contour lines become more closely spaced with decreasing corner angle. There exists a region along the bisector where the modified vorticity contour lines are closely spaced, indicating a region where gradients are large. This region coincides not with the maximum cross-flow velocity region, but with the region adjacent and closer to the corner along the bisector where the cross-flow velocity is being accelerated. Since the flow direction is generally outward along the bisector, acceleration implies increasing flow speed. Other regions containing large gradients of $\bar{A}(\eta,\zeta)$ are located along each wall and far from the corner. These regions correspond to the ridges of the cross-flow velocity magnitude diagrams where they appear in the smaller angles. These regions denote areas where again the cross-flow is

being accelerated, but in this instance acceleration implies rapidly changing velocity directions rather than changes of speed. At the corner, gradients of $\bar{A}(\eta,\zeta)$ are small and become smaller as the corner angle increases. For the 120° and 150° corners (Figures 28 and 27 respectively), there is a region where $\bar{A}(\eta,\zeta)$ is zero right at the corner. This region corresponds to the previously mentioned inner region which disappears with decreasing corner angle.

The presence of the inner region, where the cross-flow is directed towards the corner, was first noted by Ghia (1975). After checking that these velocity directions were independent of the initial approximation, the author suggested that these inflow velocities may indicate the presence of viscous eddies of the Stokes slow-flow region suggested by Tokuda (1972). This feature of the inner region is not detected in other numerical solutions, including the concave corners of Barclay and Ridha (1980) where a less-fine grid was used. Even with the fine grid used by Ghia (1975), only a few grid points appear to lie within the inner region. In the present treatment, a few more grid points occupy the inner region, but not enough to show eddy currents. According to Tokuda (1972), a finite difference method would never probe the inner region fully, but other features besides eddy currents were predicted by the same author. The flow structure is also characterized by a separating flow profile. Although in practice separation would not

take place were it not for slight fluctuations in the mainstream flow, leading edge effects or other destabilizing influences as shown by Zamir (1981). Tokuda (1972) also predicted an almost inviscid flow region with low shear flow existing along the corner bisector and boundary layer type viscous flow far from the solid boundary or away from the bisector, and cited the bulge in the isovels of Zamir and Young (1970) as evidence of a low shear flow region surrounded by a high shear flow region. The present work indicates a low shear flow region at the corner since the skin friction coefficient based on the mainstream velocity u (see Figure 16) is zero. At least for the larger angles, $\bar{A}(\eta,\zeta)$ is zero at the corner, denoting a region of irrotational and hence inviscid flow. From the preceeding figures, it is seen that the low shear region at the corner broadens as the corner angle decreases while the irrotational region becomes smaller. This would seem to indicate, at least theoretically, that these combined effects are maximized for a concave corner of a certain angle.

Barclay and Vidha (1980) remarked that for concave corners, a substantial inflow near the corner along the bisector would be a stabilizing mechanism for the boundary layer. Although the velocity magnitudes of the inner region are not very substantial, the disappearance of the inner region with decreasing corner angle would seem to indicate a loss of stability based on this remark.

The characteristics of the outer flow region were proposed from the experiments of Zamir and Young (1970) and are the dominant feature of the numerical solutions of Rubin and Grossman (1971) and Ghia (1975). The secondary flow of this region is directed toward the corner when near the walls. Before the corner is reached, however, the flow is directed away from the walls and turned to point outward in a region near the corner bisector. For the corners of angles 120° and 150°, the entire flow field consists of the inner and outer regions only. It appears from Figures 17 and 18 that the flow nearest the walls flows inward right into the corner.

For the 90° corner of Figure 19, there exists a middle region in which the secondary flow is directed strictly outward from the corner, even along the walls. This flow region collides with the incoming flow of the outer region near the walls so that the flow is directed away from the wall and into the outward-flowing region around the bisector. As the corner angle becomes smaller, the middle region becomes more prominent (see Figure 20). The point along the wall where the middle and outer regions collide occurs farther away from the corner. At the same time, the inner region receeds farther into the corner until it vanishes from view (Figure 21).

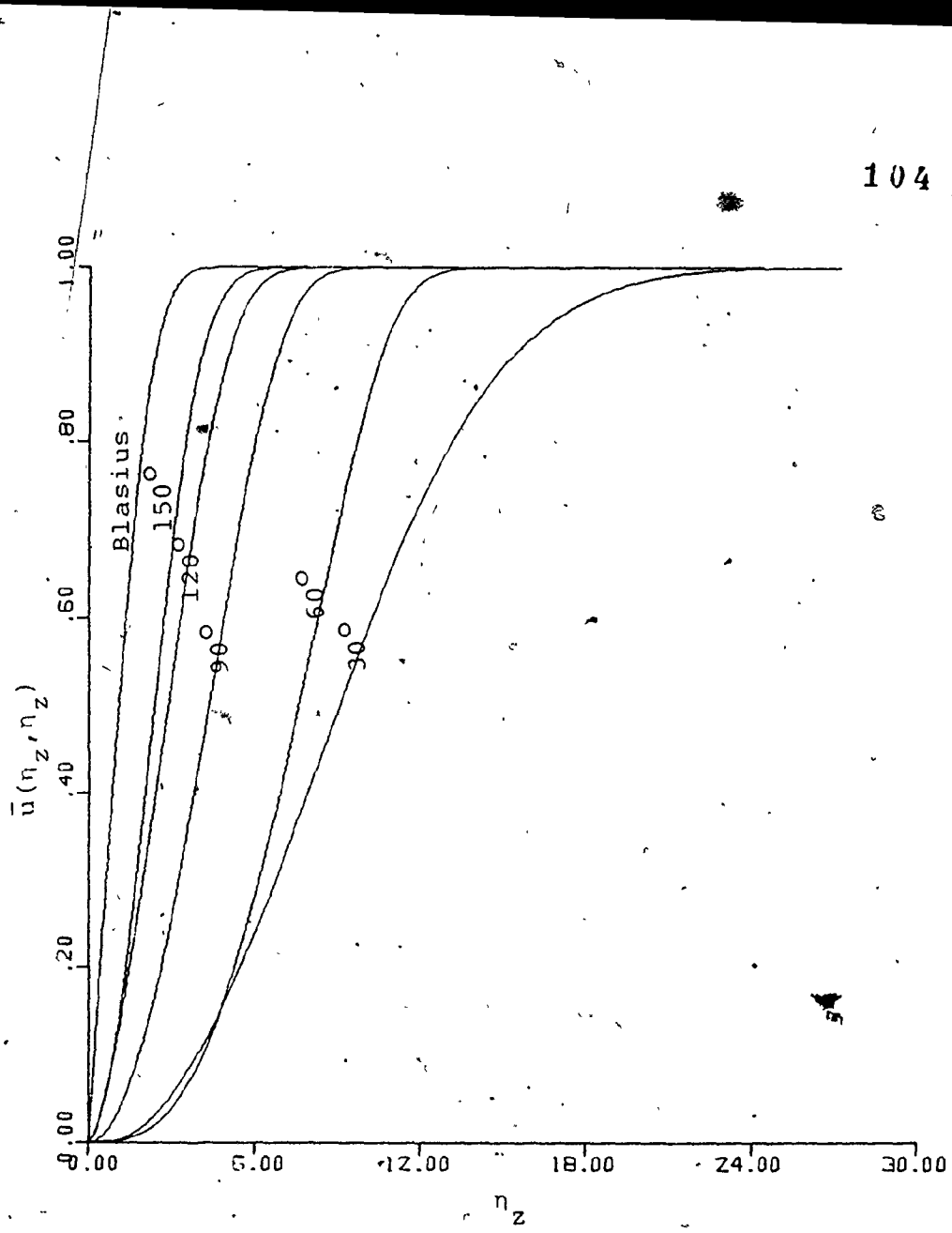

Figure 15

Mainstream Velocity $\bar{u}$ in the Bisector Plane $\eta_z = \eta_z$ (where η_z is independent of α).

Note: The overlapping of the 30° and 60° curves is due to the absence and presence respectively of the Inner Region, of secondary cross-flow.

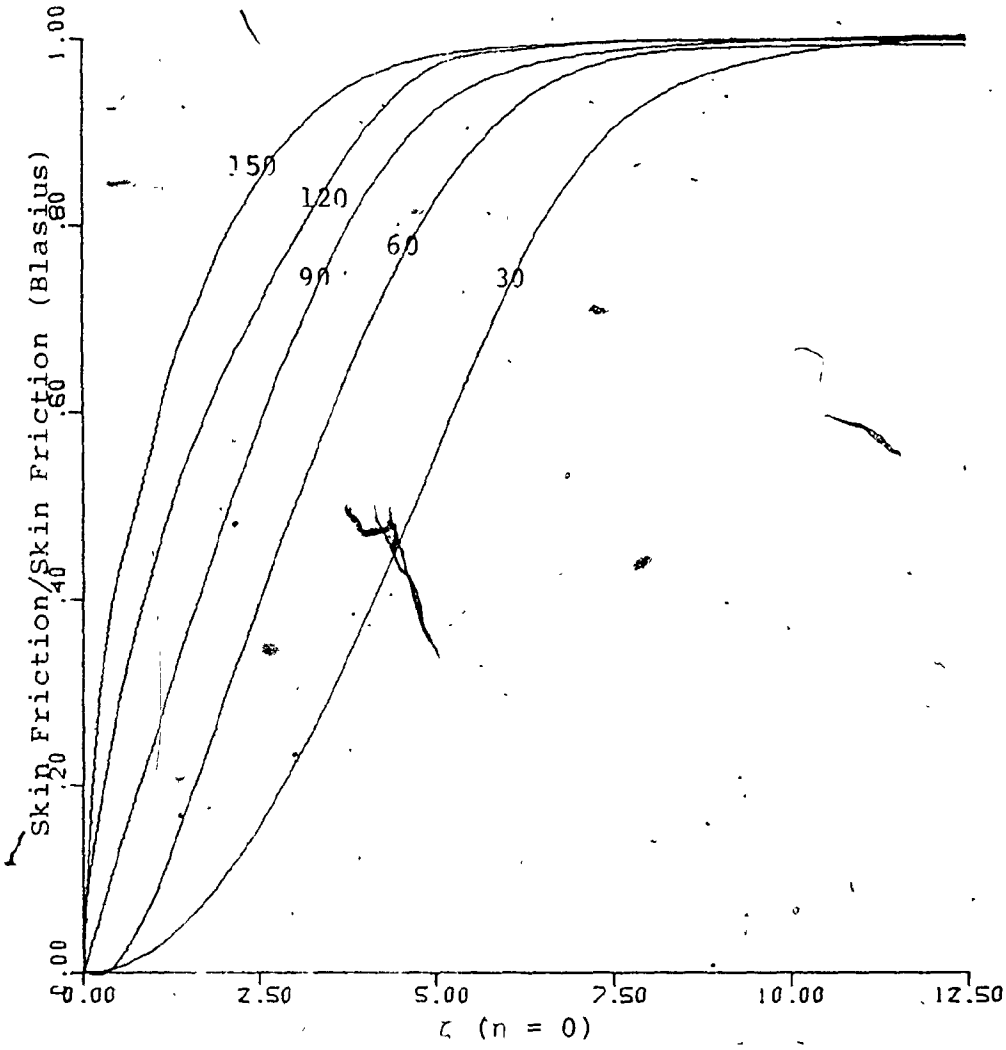

Figure 16

Skin Friction Behavior Along a Wall
for Various Corner Angles
Note: ζ with $\eta = 0$ is independent of α.

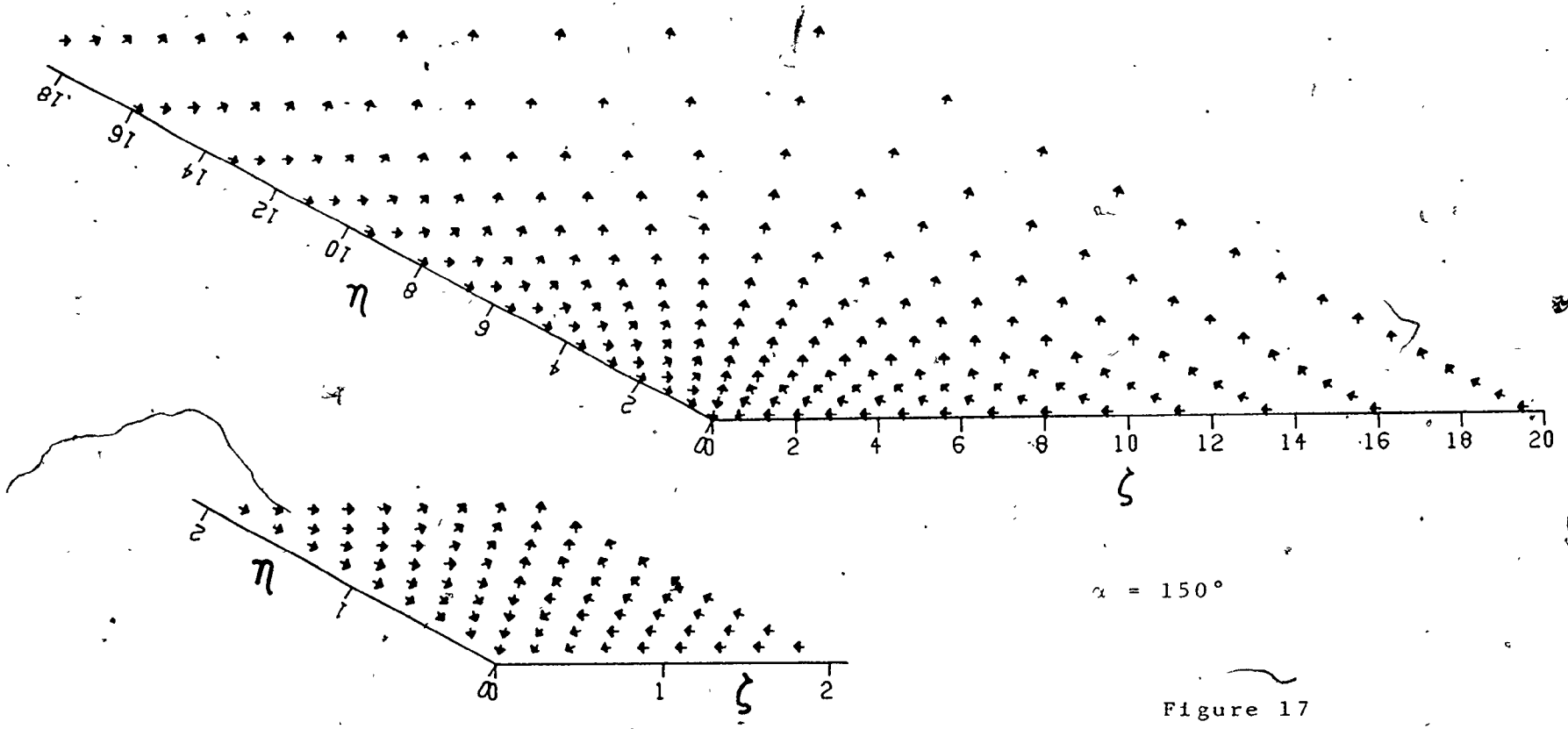

$\alpha = 150°$

Figure 17
Secondary Cross-Flow directions

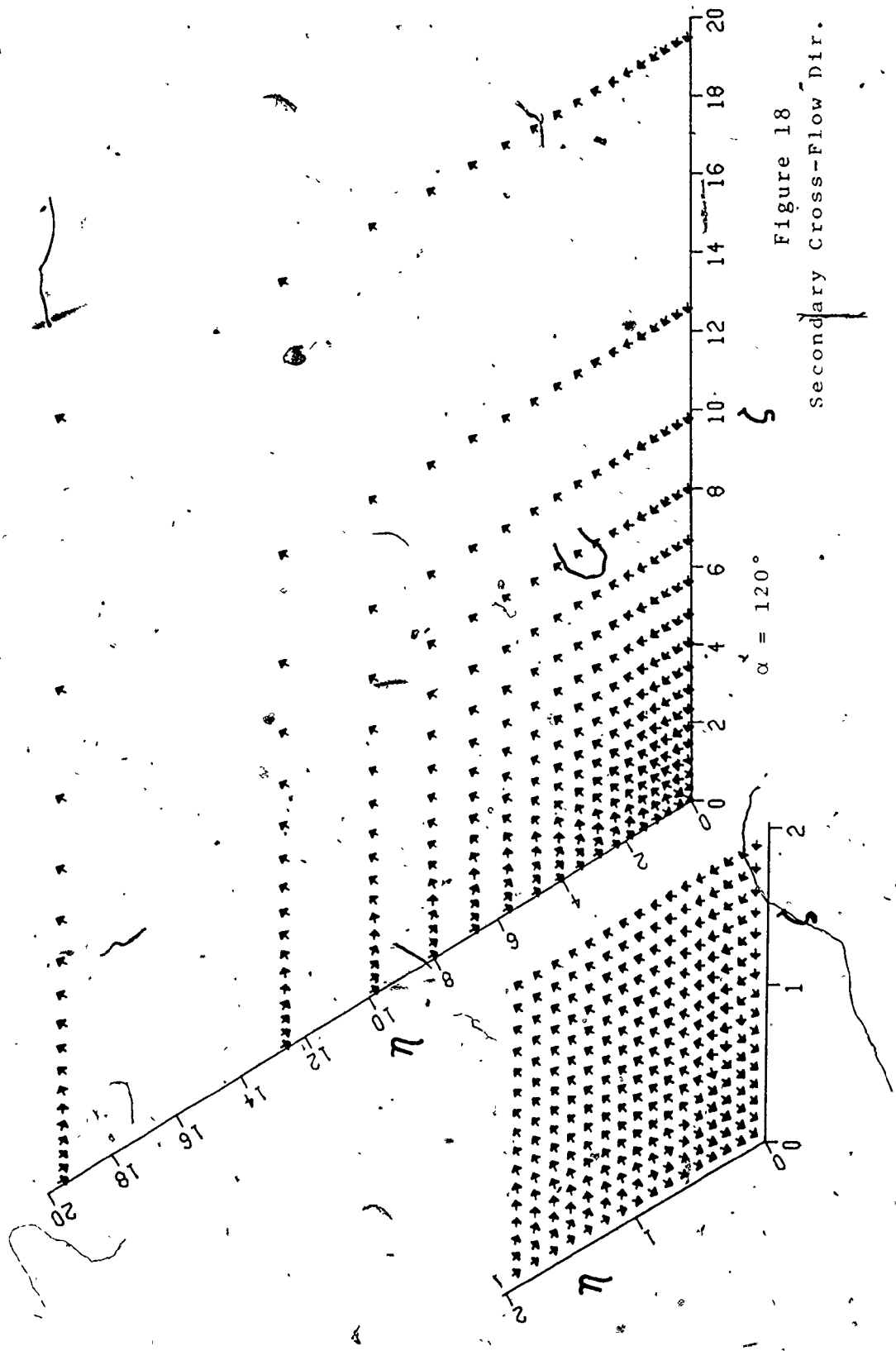

Figure 18
Secondary Cross-Flow Dir.

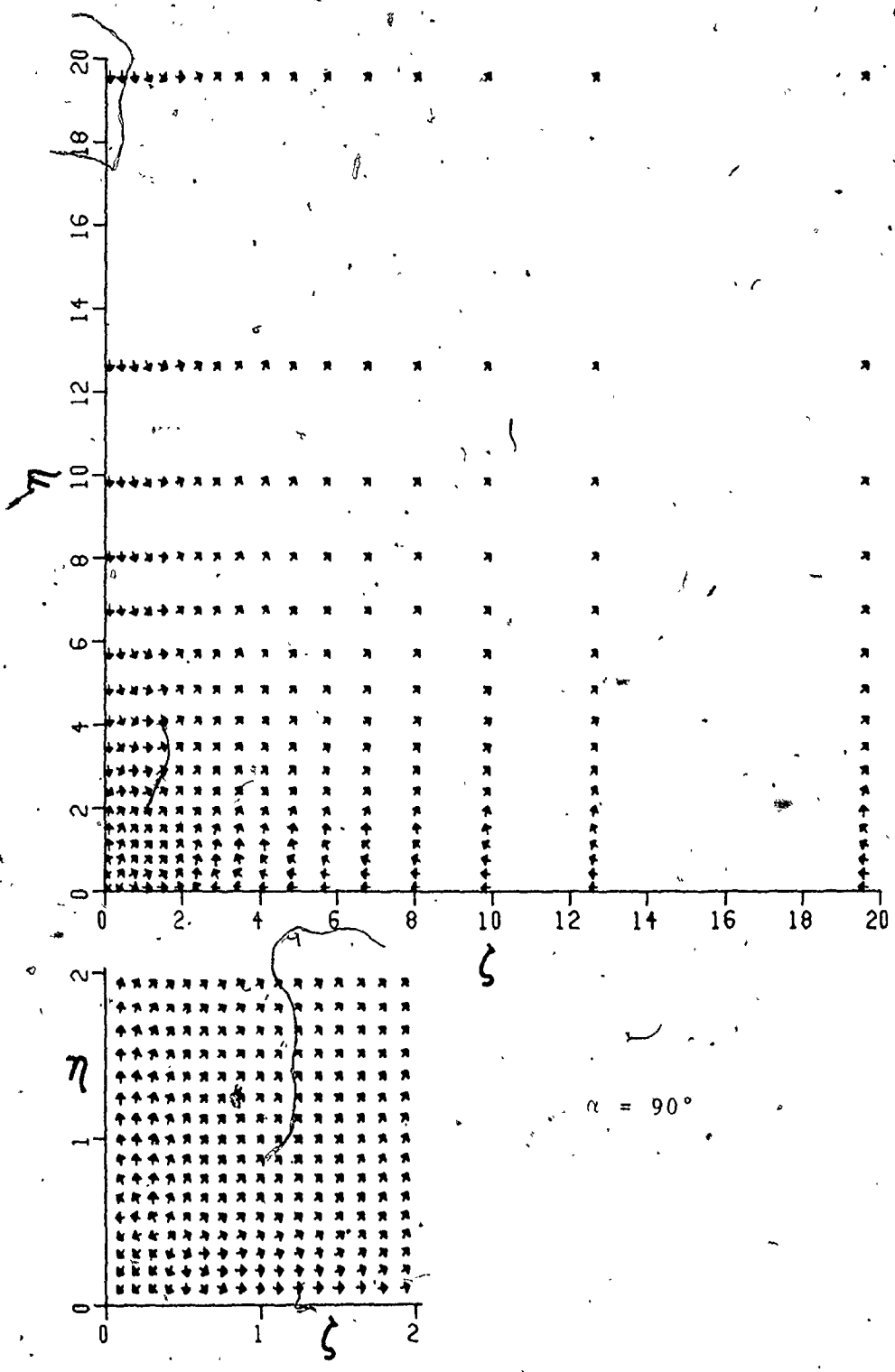

$\alpha = 90°$

Figure 19

Secondary Cross-flow Dir.

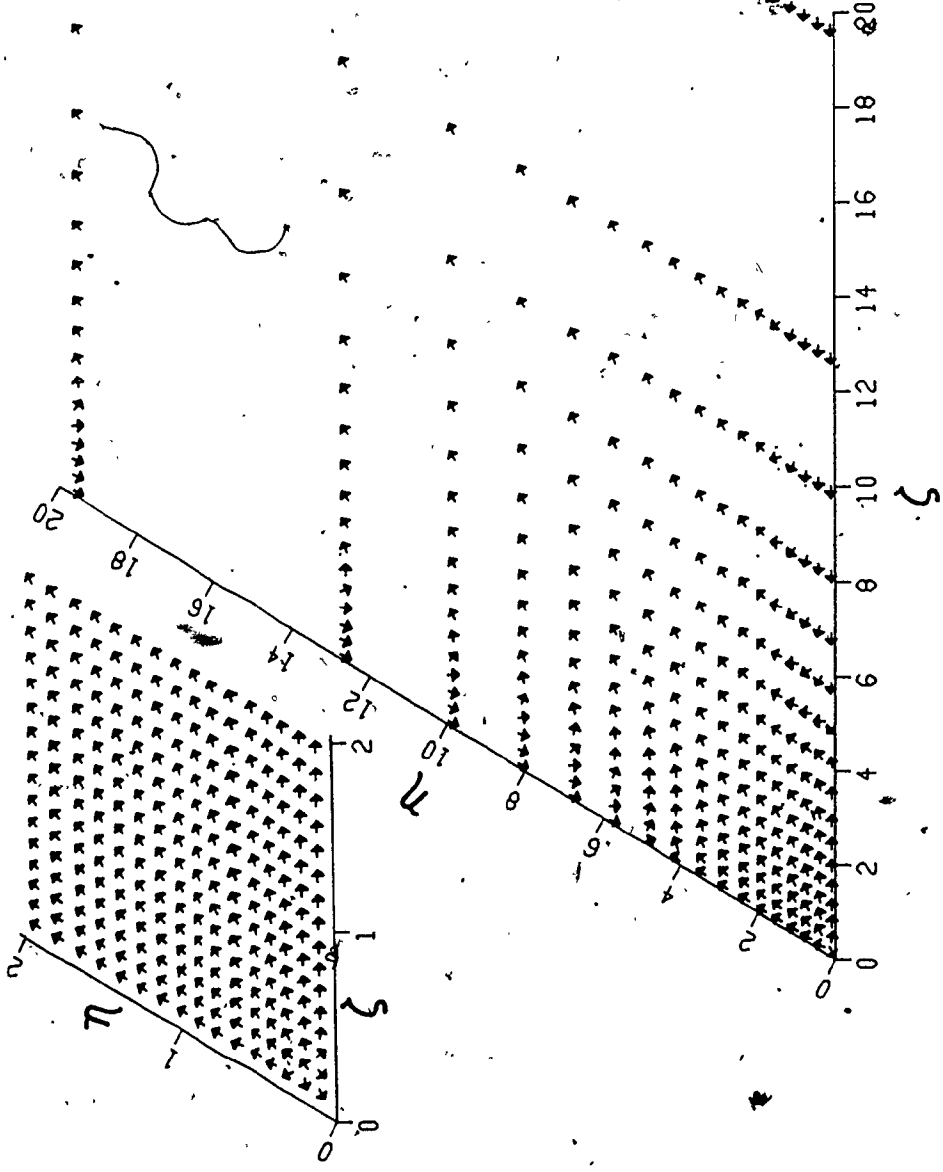

Figure 20
Secondary Cross-Flow Directions

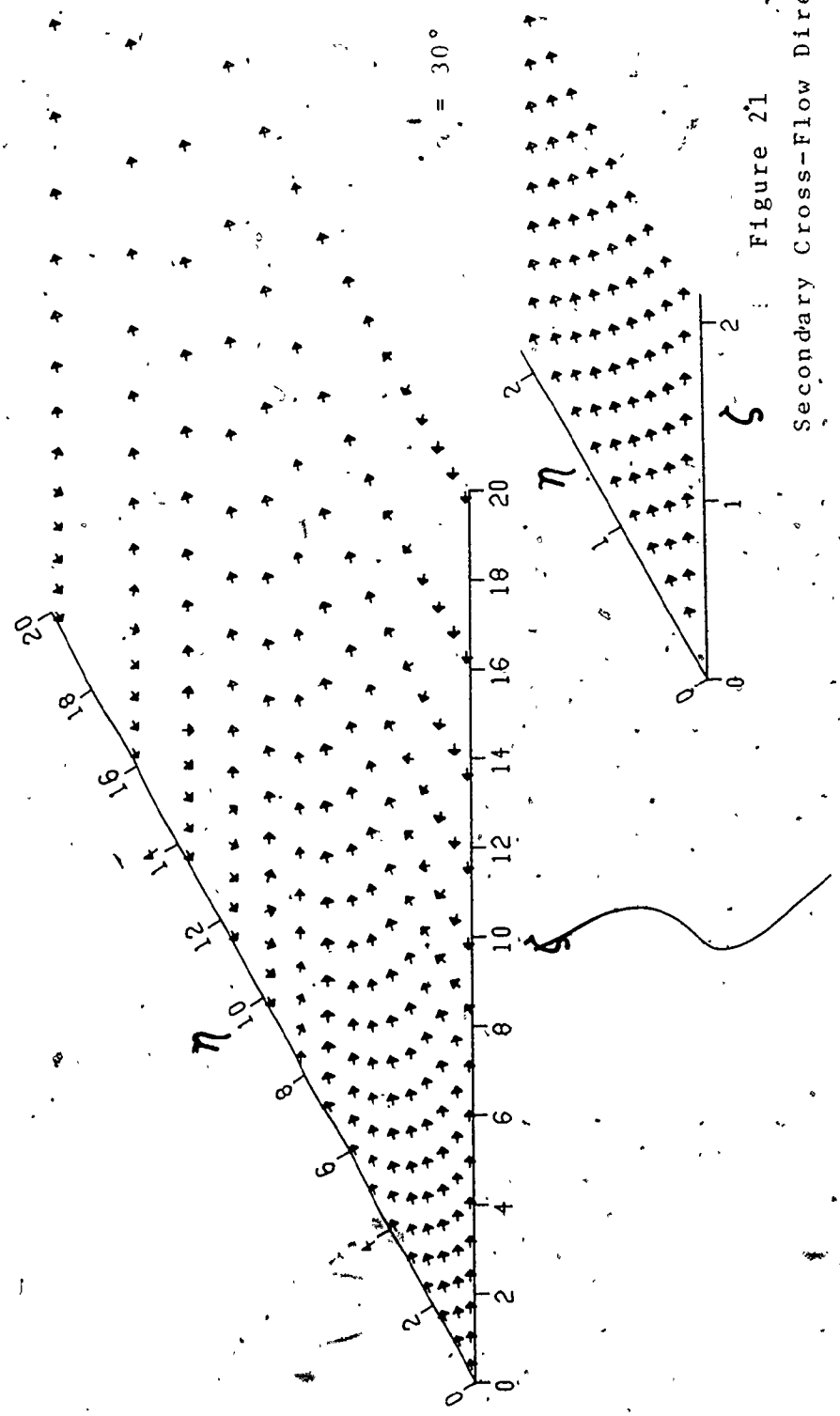

Figure 21 Secondary Cross-Flow Directions

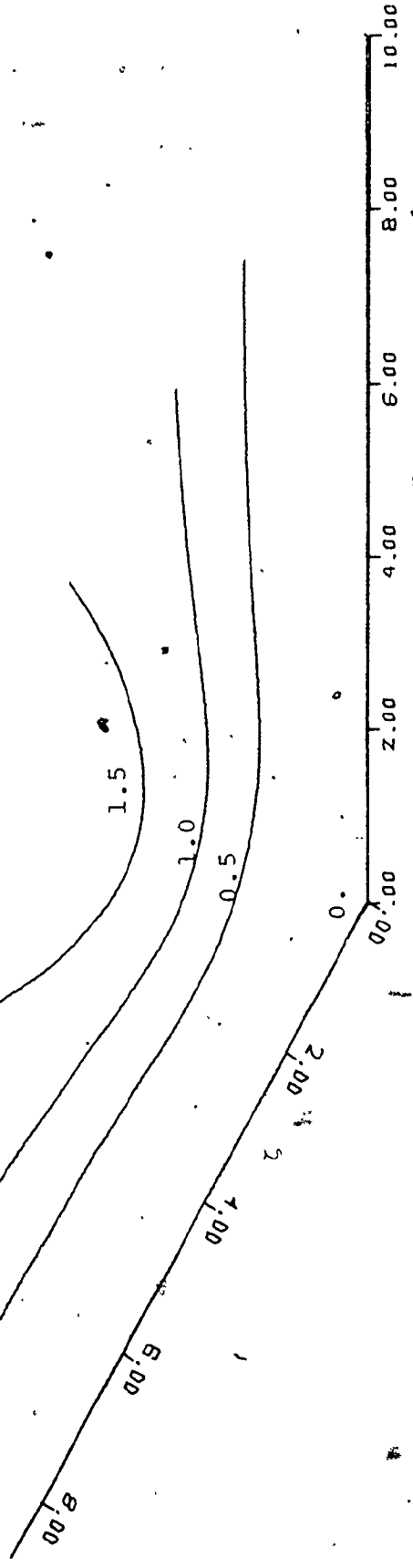

Figure 22 Contours of $r(\eta,\zeta)$ for $\alpha = 150^{\circ}$

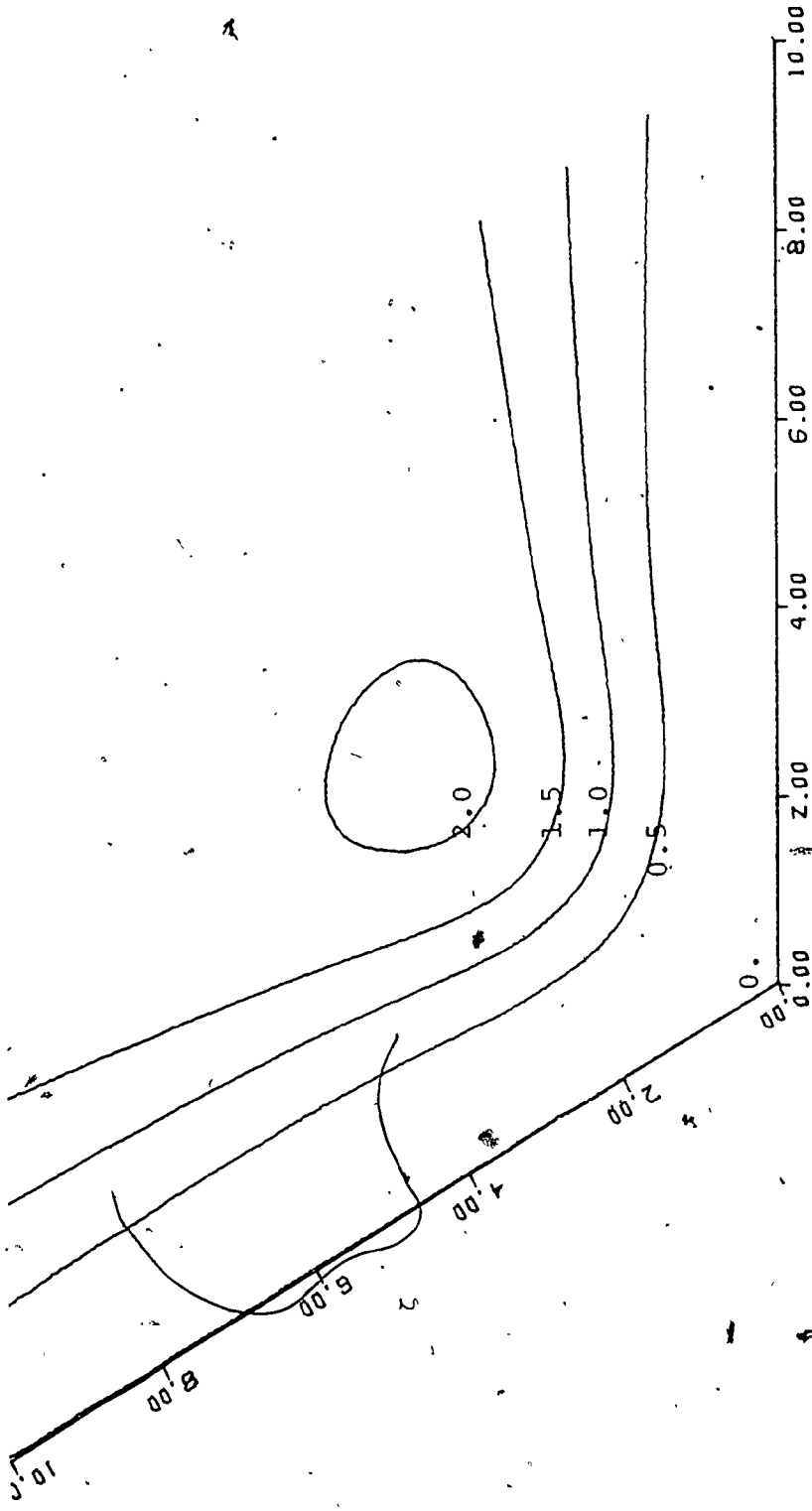

Figure 23 Contours of $r(\eta,\zeta)$ for $\alpha = 120^{\circ}$

Figure 24

Contours of $r(\eta,\zeta)$ for $\alpha = 90^{\circ}$

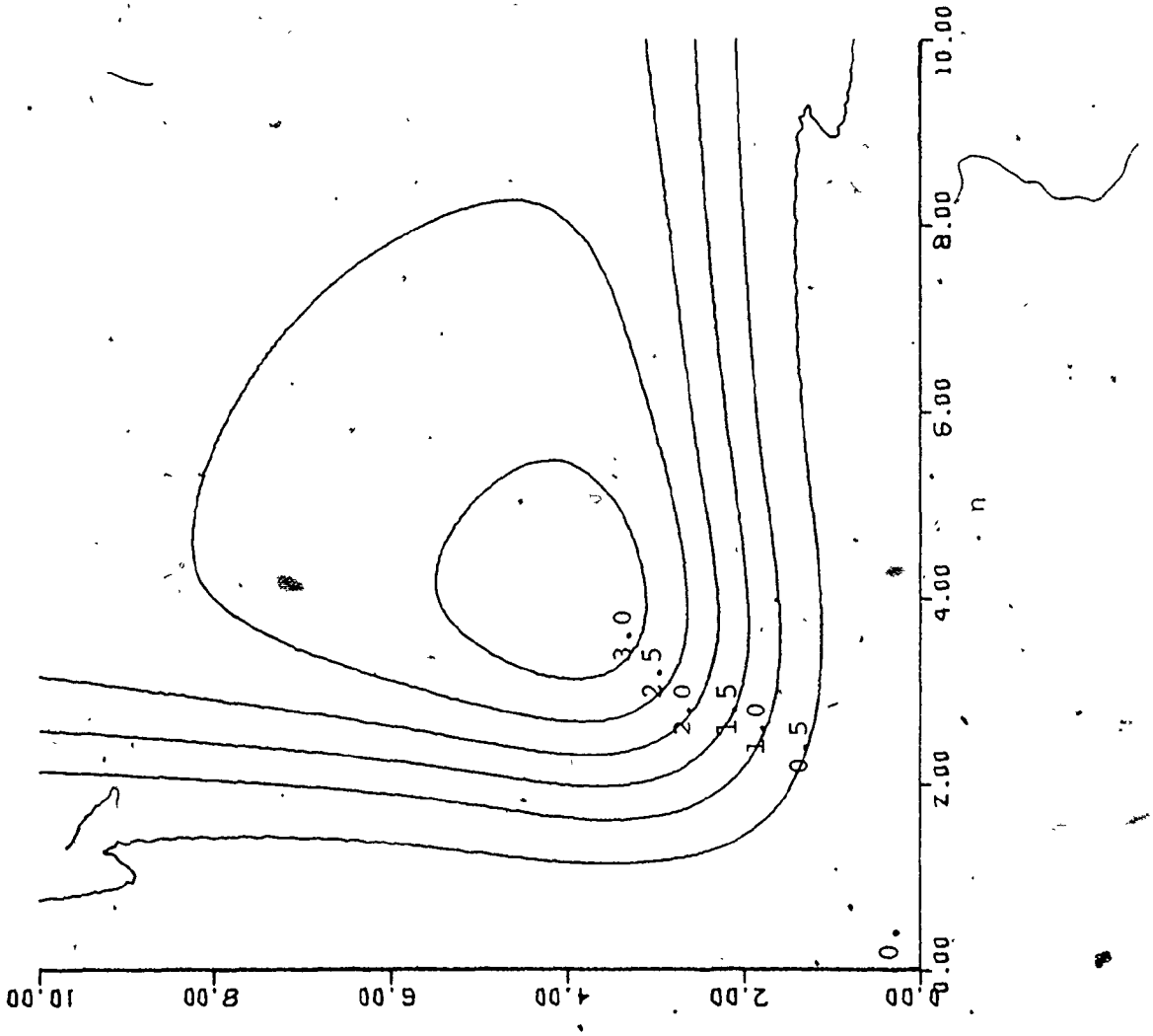

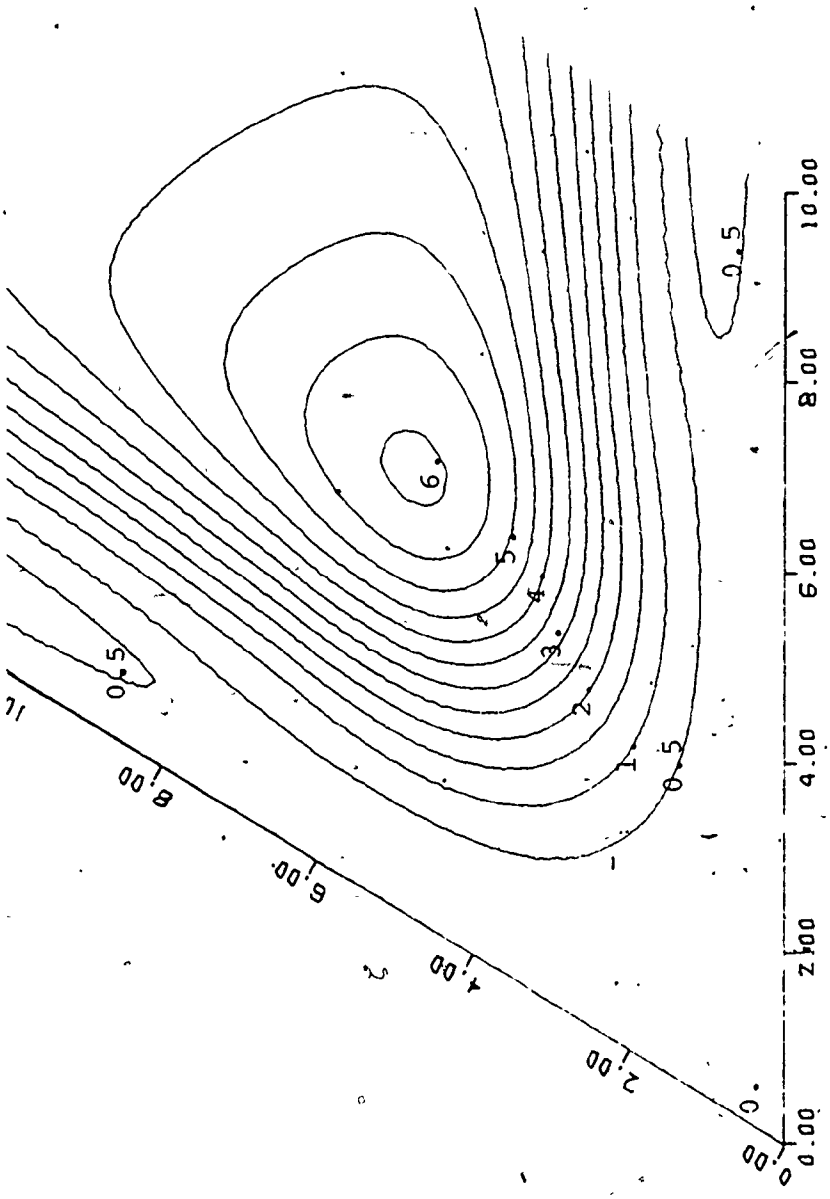

Figure 25 Contours of $r(\eta,\zeta)$ for $\alpha = 60^{\circ}$

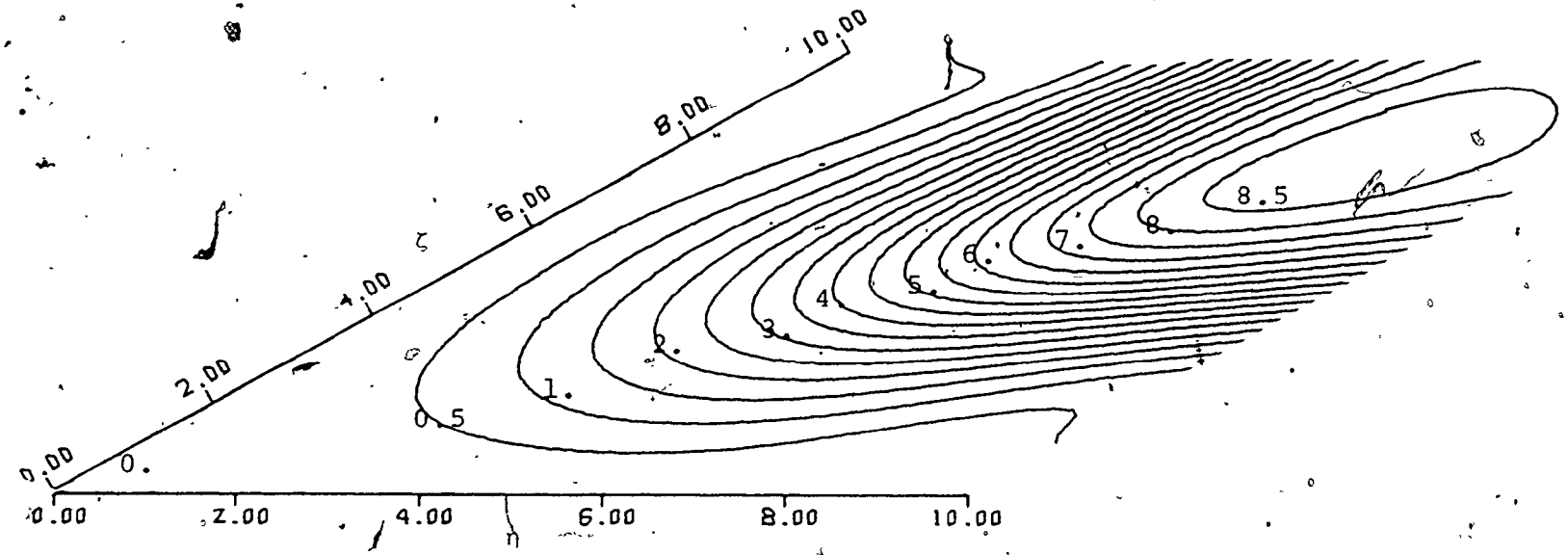

Figure 26

Contours of $r(\eta,\zeta)$ for

$\alpha = 30^{o}$

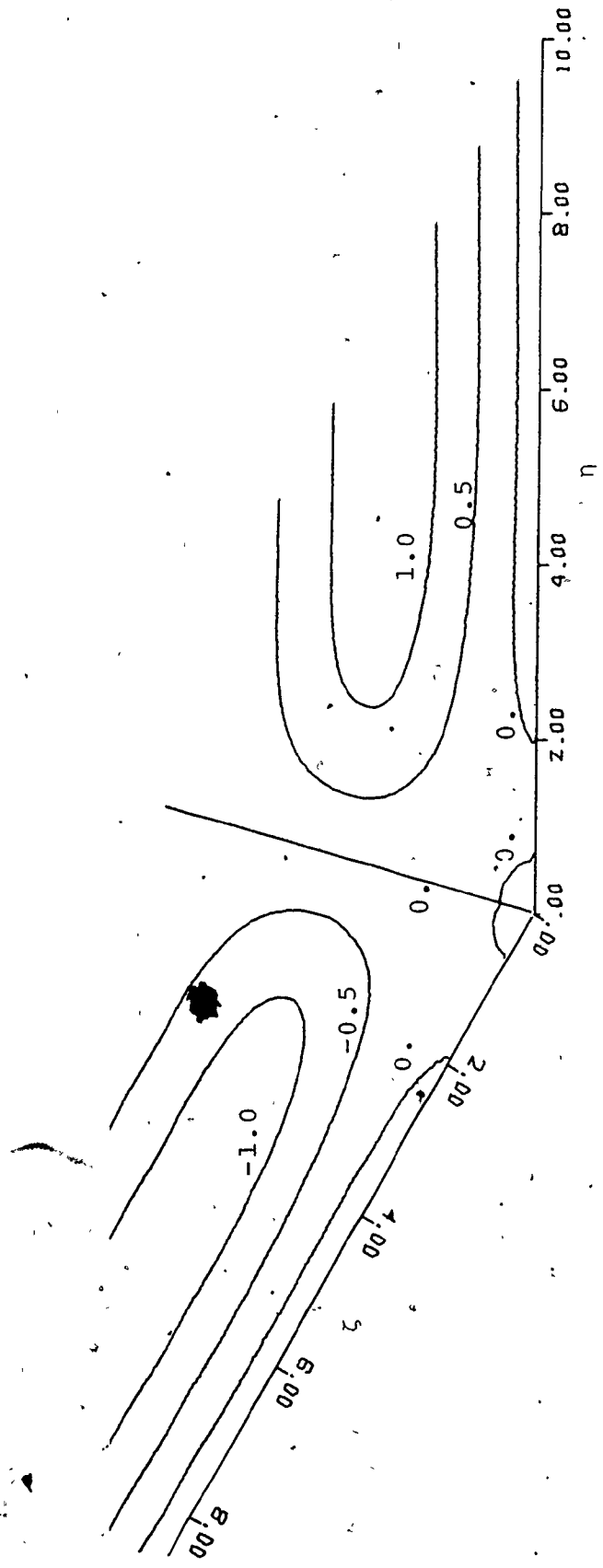

Figure 27 Contours of $\bar{A}(\eta,\zeta)$ for $\alpha = 150^0$

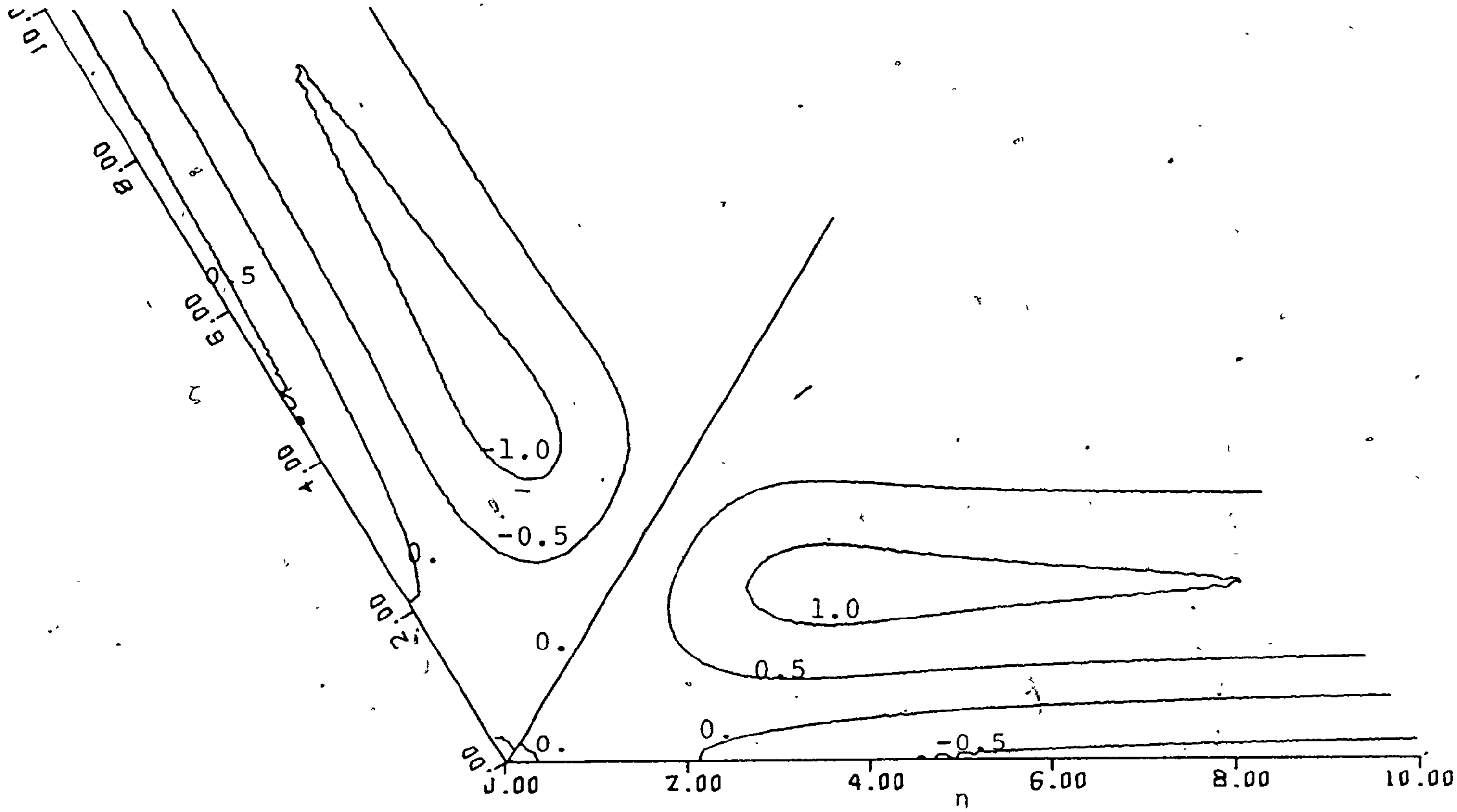

Figure 28. Contours of $\bar{A}(\eta,\zeta)$ for $\alpha = 120^{\circ}$

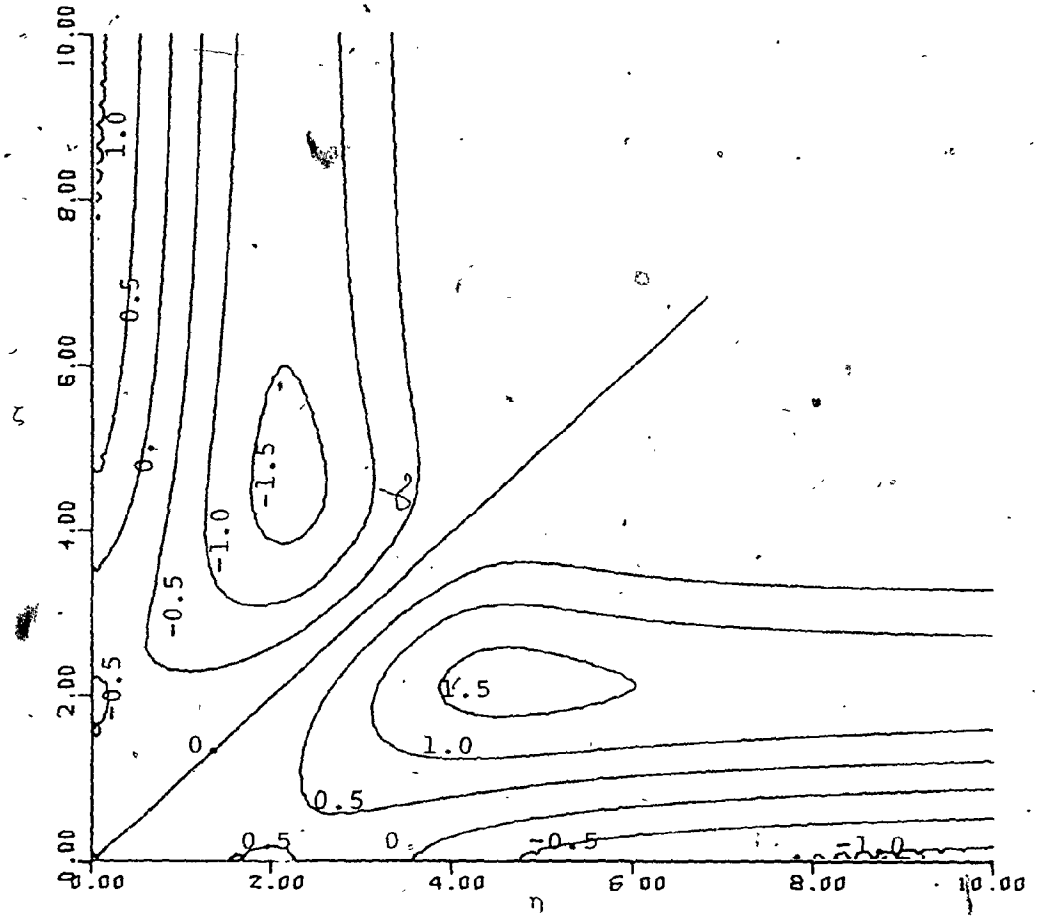

Figure 29

Contours of $\bar{A}(\eta,\zeta)$ for $\alpha = 90^{\circ}$

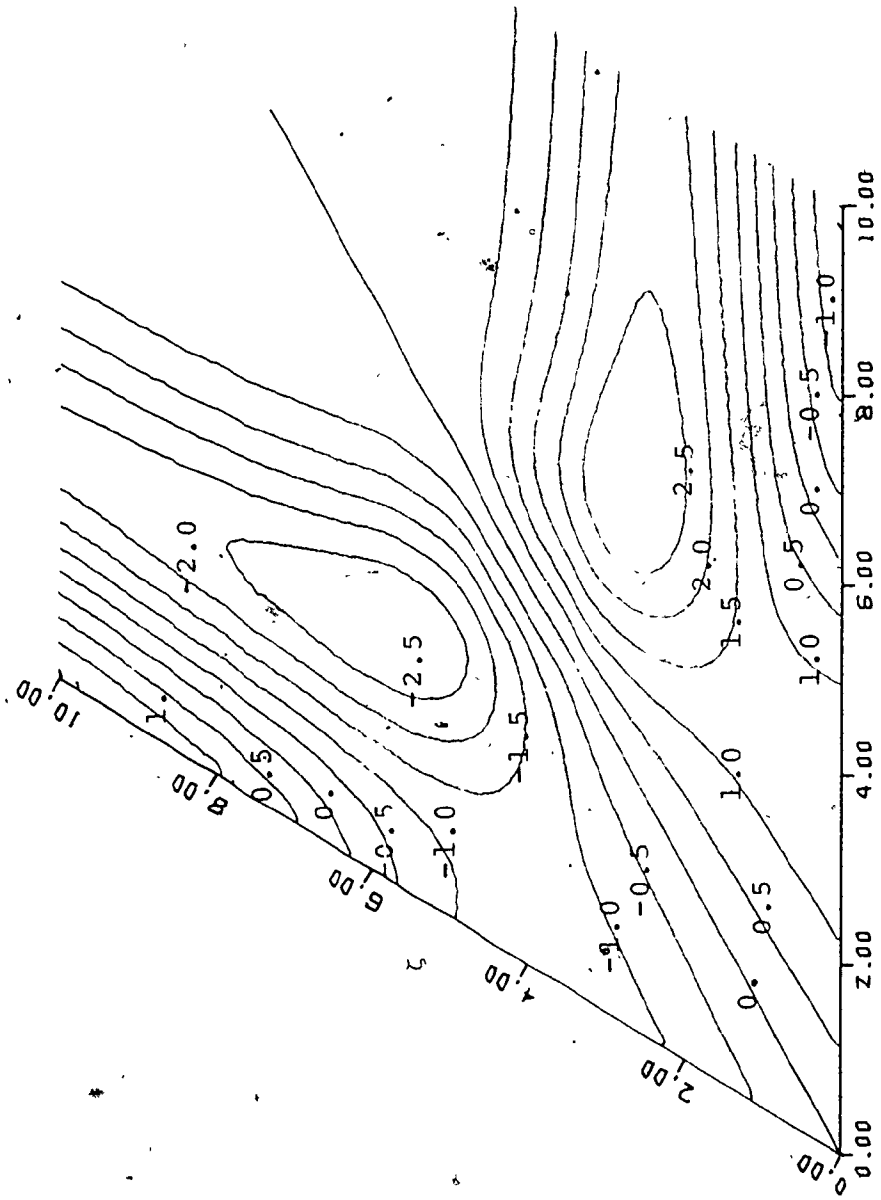

Figure 30 Contours of $\bar{A}(\eta,\zeta)$ for $\alpha = 60^{\circ}$

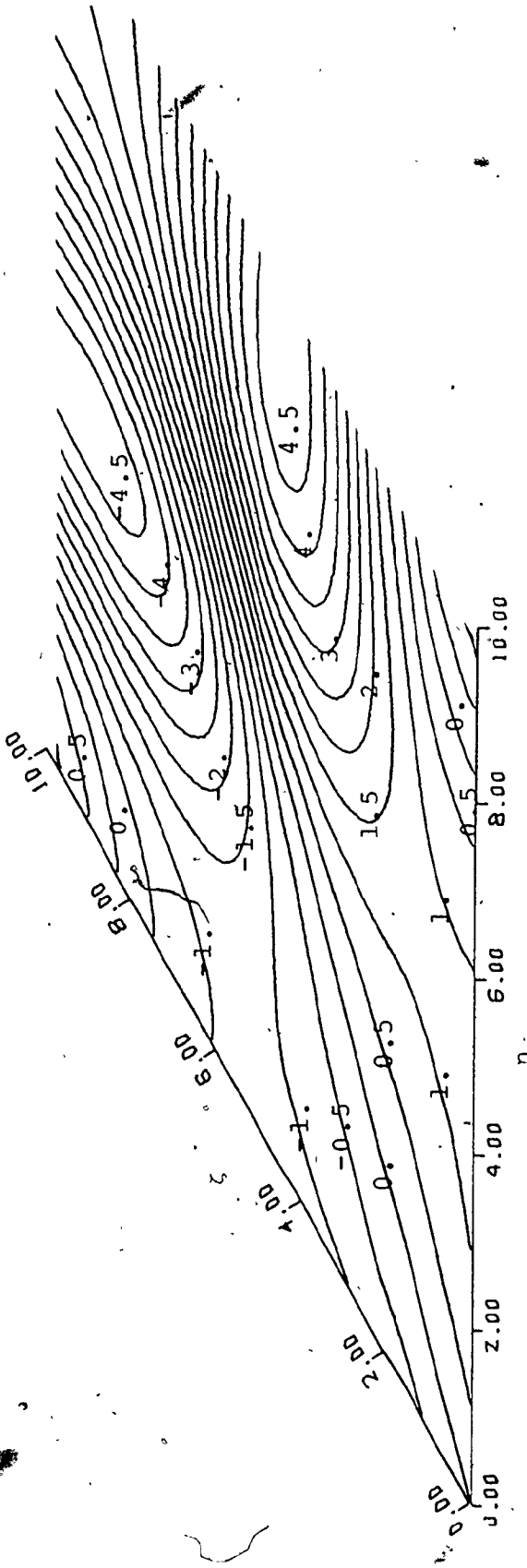

Figure 31 Contours of $\bar{A}(\eta,\zeta)$ for $\alpha = 30^{\circ}$

5. CONCLUSIONS

5.1 Conclusions of This Work

Development of the flow equations has generally followed that of Desai and Mangler (1974). A modified form of the non-orthogonal Cartesian coordinate system used by Barclay and Ridha (1980) was used in this work instead of the semi-curvilinear coordinate system used by Desai and Mangler (1974). For a right-angled corner, the modified coordinate system and the flow equations are identical to those used by Rubin and Ghia and their respective associates. This demonstrates that the analysis of Desai and Mangler (1974) is correct to this point.

While the basic method developed by Pal and Rubin (1971) for obtaining equations of the far-field boundary conditions was used by Desai and Mangler (1974), the actual boundary conditions used by the latter were different from those used elsewhere. This difference, noted by Barclay and Ridha (1980), is that Blasius flow is assumed by Desai and Mangler (1974) to be satisfied exactly, meaning that no cross-flow parallel to the wall is to exist. The coordinate transform of Sills (1969) and the redefinition of flow quantities (so that they remain bounded) are used by both Ghia (1975) and this work so that far-field boundary conditions could be applied at true infinity. Numerical results were obtained for concave corners of five different corner angles, including two angles less than 90^{o}.

The main features that the numerical results describe are the corner flow patterns, especially those of the secondary cross-flow, and how they change with changing corner angle. Such detailed knowledge of corner flow is important in order to set the stage for further investigation. The need for this is obvious since theoretical streamwise corner flow models do not predict the bulging mainstream isovel patterns that are found experimentally.

In practical situations, corner flow is influenced strongly by flow stability and pressure gradients as well as corner angle. Although Barclay and Ridha (1980) have stated that a significant cross-slow velocity directed at the corner enhances stability, and although this inward flow decreases with decreasing corner angle, the conclusion that streamwise corner flow tends toward instability with decreasing corner angle is qualitative at best and certainly poorly supported. The reason for this is that the present flow model is over-simplified and cannot answer questions concerning pressure gradient or stability. Similarity, as it is expressed in the coordinate transformations of (1.3.2) and elsewhere, implicitly assumes a zero pressure gradient. In order to account for non-zero pressure gradients, the flow equations must be modified beginning at this point. In addition, if stability and similarity are related as suggested by Zamir (1981), one needs a streamwise corner flow model that can account for dissimilar flow. Still another reason why the

results of the existing streamwise corner flow models do not show the bulging isovel pattern is that there may exist second-order terms, with respect to the inverse of the Reynolds number, that are large enough to affect the flow significantly. The Reynolds numbers describing the flow in the experimental studies are finite, after all, and may be small enough for second-order effects to be visible. This work will finish by illustrating these ideas further, and by suggesting areas of further study, in the next section.

5.2 Areas of Further Study

Even though the inverse of the Reynolds number may be small, the coefficients multiplying it may be large enough for the resulting product to be significantly large. One such possibility arises in the u-equation of (2.2.14), which would resemble the following equation had first and second-order terms been kept:

$$\nabla u + \phi u_{,2} + \psi u_{,3} = R_x^{-1}\{(q_{12} A_{,3} - q_{13} A_{,2}) + (\text{Other Trems})\} . \tag{5.2.1}$$

With the coordinate system of (2.3.1) and (2.3.3), the coefficient multiplying the second-order term is

$$(\eta + \zeta \cos\alpha) A_\zeta - (\eta \cos\alpha + \zeta) A_\eta . \tag{5.2.2}$$

From Figures 27 to 31 where $\bar{A}$ is plotted, at the point along the corner bisector where the contour lines are most dense, (5.2.2) is large and becomes larger with decreasing corner angle, provided A can be estimated by $\bar{A}$. The area where this occurs is the area where differences between theoretical

and experimental mainstream isovels are most apparent. In order to investigate this further, it would be necessary to discover all the second-order terms of all equations, including those arising from another outer and inner expansion of the perturbation process. Solutions for the new dependent variables that would appear would need to be obtained to make certain whether or not they might be large. It may be that other terms would cancel the one noted here. This perturbation expansion process becomes very tedious and still does not answer stability questions because similarity is still assumed valid.

In contrast, it is not difficult to modify the present streamwise corner flow model so that non-zero pressure gradients can be considered. It is well known (see Schlichting (1955)) that there exists a similarity transform for boundary layers with potential flow velocities of the form

$$U = U_o x^m , \qquad (5.2.3)$$

which corresponds to flow past a wedge-shaped boundary. The "m" in (5.2.3) is related to the angle of the point of the wedge, denoted by θ, through

$$m = \theta/(2 - \theta) . \qquad (5.2.4)$$

If (5.2.3) is used to approximate the potential flow arising from a streamwise corner with a non-zero angle of incidence, which would result in a favorable pressure gradient in an experiment, then the similarity transformation of the coordinates, compared with (1.3.2), are

$$x = x$$

$$y = \left(\frac{2\nu x}{(m+1)U}\right)^{\frac{1}{2}} \qquad (5.2.5)$$

$$z = \left(\frac{2\nu x}{(m+1)U}\right)^{\frac{1}{2}}$$

where U is given by (5.2.3). Starting at this point in the development of the flow equations, and proceeding as has been discussed in Sections 2 and 3 of Chapter 2, the system of equations corresponding to (2.3.5) becomes

$$\begin{aligned}
&u_{\eta\eta} - 2\cos\alpha\, u_{\eta\zeta} + u_{\zeta\zeta} + \sin\alpha\,(\phi u_\eta + \psi u_\zeta) \\
&\qquad = -\frac{2x\sin\alpha}{(m+1)\rho U^2}\,\frac{dP_o}{dx} \\
&A_{\eta\eta} - 2\cos\alpha\, A_{\eta\zeta} + A_{\zeta\zeta} + \sin\alpha\,(\phi A_\eta + \psi A_\zeta) \\
&\qquad + \frac{2\sin^2\alpha}{m+1}\,uA + 2u\sin\alpha\,\frac{(m-1)^2}{m+1} \qquad (5.2.6) \\
&\qquad ((\eta + \zeta\cos\alpha)u_\zeta - (\eta\cos\alpha + \zeta)u_\eta) = 0 \\
&\frac{2\sin\alpha}{m+1}\,u = \phi_\eta + \psi_\zeta \\
&\frac{\sin^2\alpha}{m+1}\,A = \psi_\eta - \phi_\zeta + \cos\alpha\,(\psi_\zeta + \phi_\eta).
\end{aligned}$$

The right-hand-side of the first equation of (5.2.6) is known from (5.2.3) and Bernoulli's equation, which is

$$U\frac{dU}{dx} = -\frac{1}{\rho}\frac{dP}{dx}\ , \qquad (5.2.7)$$

so that the equation becomes

$$\begin{aligned}
&u_{\eta\eta} - 2\cos\alpha\, u_{\eta\zeta} + u_{\zeta\zeta} + \sin\alpha\,(\phi u_\eta + \psi u_\zeta) \\
&\qquad = 2\sin^2\alpha\,\frac{m}{m+1}\ .
\end{aligned} \qquad (5.2.8)$$

Questions concerning stability still cannot be answered because similarity is still a basic assumption of this new system of equations. Rather than formulating the equations without similarity, an easier approach might be to introduce a non-similar perturbation into the above flow model. One location for such a perturbation is suggested by Zamir (1981), where it is noted that streamwise corner flow becones unstable as the angle of incidence (given by $\frac{\pi\theta}{2}$) decreases. One can postulate a pressure term consisting of similar and non-similar parts such as

$$2 \sin^2\alpha \frac{m}{m+1} + \varepsilon f(x) \qquad (5.2.9)$$

where f (= O(1)) is some function depending on the streamwise varaible x (and perhaps η, ζ, time t and corner angle α as well). The parameter ε represents the magnitude of the non-similar term of (5.2.9). For large θ and for ε chosen to be small, the first term of (5.2.9) would dominate, with the result that the overall flow is similar. With decreasing θ, however, the second term of (5.2.9) becomes more significant, and the flow becomes dissimilar. The expression (5.2.9) also suggests that the non-similar term becomes more significant as the corner angle α approaches zero. The fact that this is also the case as the corner angle opens up and approaches 180° is a fault of the coordinate system (which collapses in the same limit) and might be rectified by

insisting that

$$f \sim \frac{1}{\alpha} \quad \text{or} \quad f \sim (\pi - \alpha) \,. \qquad (5.2.10)$$

The form that the function f should take is a subject requiring further study. Physically, the function f may represent some fluctuation in the flow arising from any or all of the following causes:

1) a small degree of freestream turbulence,
2) a local phenomenon such as a separation bubble, or
3) a disturbance originating at the leading edge.

In conclusion, the method of the non-similar perturbation would probably be a much more fruitful area of investigation than that of continuing the singular perturbation expansion method.

APPENDIX I - FORMULATION OF DIVERGENCE

Before examining the divergence of a vector, the following result is needed. It is noted that the metric tensor is invariant with respect to covariant differentiation. This is given by

$$g_{ij}|_k = 0 \ , \qquad \text{(A.I.1)}$$

which becomes, upon expanding the derivative,

$$g_{ij,k} - g_{mj}\,\Gamma^m_{ik} - g_{im}\,\Gamma^m_{kj} = 0 \ . \qquad \text{(A.I.2)}$$

Multiplying both sides by g^{ij} and noting that

$$g^{ij}\,g_{jk} = \delta^i_k \ ,$$

where δ^i_k is the Kronecker delta, (A.I.2) becomes

$$g^{ij}\,g_{ij,k} - \Gamma^i_{ik} - \Gamma^j_{kj} = 0 \ . \qquad \text{(A.I.4)}$$

Since the Christoffel symbol Γ^i_{jk} is symmetric with respect to the indices j and k, and since the dummy indices (i.e. those to which the summation convention applies) can be renamed, then one obtains from (A.I.4) the following:

$$\Gamma^i_{ik} = \frac{1}{2}\,g^{ij}\,g_{ij,k} \ . \qquad \text{(A.I.5)}$$

The divergence of a vector can be written as

$$u^j|_j = u^j{}_{,j} + u^k\,\Gamma^j_{jk} \qquad \text{(A.I.6)}$$

which, by (A.I.5), becomes

$$u^j|_j = u^j{}_{,j} + \frac{1}{2}\,u^k\,g^{ij}\,g_{ij,k} \ . \qquad \text{(A.I.7)}$$

Adler et al (1965) present the following argument in order to simplify the last term. From matrix theory, g^{ij} is the

inverse of g_{ij} and can be written as

$$g^{ij} = \frac{\Delta ij}{g} \qquad \text{(A.I.8)}$$

where g and Δij are the determinant and cofactor of g_{ij}. The determinant is obtained from

$$g = g_{ij}\ \Delta ij \quad (i \text{ or } j \text{ not summed}) . \qquad \text{(A.I.9)}$$

Differentiating with respect to g_{ij} results in

$$\frac{\partial g}{\partial g_{ij}} = \Delta ij \ , \qquad \text{(A.I.10)}$$

since Δij does not contain the g_{ij} of (A.I.9). Substituting (A.I.10) into (A.I.8), one obtains

$$g^{ij} = \frac{1}{g} \frac{\partial g}{\partial g_{ij}} \ , \qquad \text{(A.I.11)}$$

which can be used to simplify (A.I.7) so that one obtains

$$\begin{aligned} u^j|_j &= u^j{}_{,j} + \frac{1}{2}\, u^k \frac{1}{g} \frac{\partial g}{\partial g_{ij}} \frac{\partial g_{ij}}{\partial \xi^k} \\ &= u^j{}_{,j} + \frac{1}{2}\, u^k\ (\ln(g))_{,k} \\ &= u^j{}_{,j} + u^k\ (\ln(g^{\frac{1}{2}}))_{,k} \\ &= u^j{}_{,j} + \frac{u^k\ (g^{\frac{1}{2}})_{,k}}{g^{\frac{1}{2}}} \end{aligned} \qquad \text{(A.I.12)}$$

where g is assumed greater than zero.

APPENDIX II - THE CONVECTIVE TERM

The first term of the Navier-Stokes equation of (2.1.1) can be expanded as follows. The covariant derivative is expanded so that the term in question becomes

$$u^j u_i|_j = u^j u_{i,j} - u^j u_k \Gamma^k_{ij} \qquad \text{(A.II.1)}$$

and the Christoffel symbol is written in terms of the metric tensor to get

$$\begin{aligned} u^j u_i|_j &= u^j u_{i,j} - \tfrac{1}{2} u^j u_k g^{km}(g_{jm,i} + g_{mi,j} - g_{ij,m}) \\ &= u^j u_{i,j} - \tfrac{1}{2} u^j u^m(g_{jm,i} + g_{mi,j} - g_{ij,m}) \\ &= u^j u_{i,j} - \tfrac{1}{2}(u^j u^m g_{jm,i} + u^j u^m g_{mi,j} \\ &\qquad - u^j u^m g_{ij,m}) . \end{aligned}$$

Derivatives of products are formed as follows:

$$\begin{aligned} u^j u_i|_j = u^j u_{i,j} - \tfrac{1}{2}\{&u^j(u^m g_{jm})_{,i} - u^j g_{jm} u^m{}_{,i} \\ &+ u^j u^m{}_{,} g_{mi,j} - u^j u^m g_{ij,m}\} , \end{aligned}$$

and the dummy suffices j and m of the last term only are renamed m and j respectively. The result is

$$u^j u_i|_j = u^j u_{i,j} + \tfrac{1}{2}(u_j u^j{}_{,i} - u^j u_{j,i}) . \qquad \text{(A.II.2)}$$

APPENDIX III - THE JACOBEAN

The determinant of g_{ij} can be found using (2.2.4) as follows:

$$g = \det(g_{ij}) = (1 + \frac{\nu}{Ux} q_{11}) (\frac{\nu x}{U})^2 (q_{22} q_{33} - (q_{23})^2)$$

$$- \frac{\nu^3 x}{U^3} q_{12}(q_{12} q_{33} - q_{13} q_{23})$$

$$+ \frac{\nu^3 x}{U^3} q_{13}(q_{12} q_{23} - q_{22} q_{13})$$

$$= (\frac{\nu x}{U})^2 (q_{22} q_{33} - (q_{23})^2) + \frac{\nu^3 x}{U^3} (q_{11} q_{22} q_{33}$$

$$- q_{11} (q_{23})^2 - q_{22} (q_{13})^2 - q_{33} (q_{12})^2$$

$$+ 2 q_{12} q_{13} q_{23}) .$$

Using the definitions implied in (2.2.3) for q_{ij}, this becomes

$$g = (\frac{\nu x}{U})^2 4\{(F_\eta^2 + G_\eta^2)(F_\zeta^2 + G_\zeta^2) - (F_\eta F_\zeta + G_\eta G_\zeta)\}$$

$$\frac{\nu^3 x}{U^3} \{2(F_\eta^2 + G_\eta^2)(F_\zeta^2 + G_\zeta^2)(F^2 + G^2) - 2(F_\zeta^2 + G_\zeta^2)$$

$$(F_\eta F_\zeta + G_\eta G_\zeta)^2 - 2(FF_\eta + GG_\eta)^2 (F_\zeta^2 + G_\zeta^2)$$

$$+ 4(FF_\eta + GG_\eta)(FF_\zeta + GG_\zeta)(F_\eta F_\zeta + G_\eta G_\zeta)$$

$$- 2(FF_\zeta + GG_\zeta)^2 (F_\eta^2 + G_\eta^2)\} .$$

If one expands the expressions inside the curly brackets and cancels the terms that subtract out, the expression simplifies to

$$g = 4(\frac{\nu x}{U})^2 (F_\eta G_\zeta - F_\zeta G_\eta)^2 . \qquad \text{(A.III.1)}$$

From (2.2.4), the expression for Q can be written as

$$Q = \det(t^i_j) = 2\,\frac{\nu x}{U}\,(F_\eta G_\zeta - F_\zeta G_\eta) \quad . \qquad \text{(A.III.2)}$$

By comparing (A.III.1) and (A.III.2), one notes that

$$Q = (g)^{\frac{1}{2}} \quad , \qquad \text{(A.III.3)}$$

therefore justifying the definition (2.1.7), at least in this case. By definition (A.III.2), one sees that Q is the Jacobean of the transformation.

APPENDIX IV - SECOND-ORDER EQUATIONS

In the following, references made to differentiation imply partial differentiation. Only the two first-order equations of (2.3.5) are required for consideration in this appendix. These equations are

$$2u \sin\alpha = \phi_\eta + \psi_\zeta \qquad \text{(A.IV.1)}$$

and $$A \sin^2\alpha = \psi_\eta - \phi_\zeta + \cos\alpha\ (\phi_\eta - \psi_\zeta)\ . \qquad \text{(A.IV.2)}$$

Once all the terms of the above equations are brought to the right hand side, each can be differentiated once by each of η and ζ to obtain the following four equations:

$$\phi_{\eta\eta} + \psi_{\eta\zeta} - 2u_\eta \sin\alpha = 0 \qquad \text{(A.IV.3)}$$

$$\phi_{\eta\zeta} + \psi_{\zeta\zeta} - 2u_\zeta \sin\alpha = 0 \qquad \text{(A.IV.4)}$$

$$\psi_{\eta\eta} - \phi_{\eta\zeta} + \cos\alpha\ (\phi_{\eta\eta} - \psi_{\eta\zeta}) - A_\eta \sin^2\alpha = 0 \qquad \text{(A.IV.5)}$$

$$\psi_{\eta\zeta} - \phi_{\zeta\zeta} + \cos\alpha\ (\phi_{\eta\zeta} - \psi_{\zeta\zeta}) - A_\zeta \sin^2\alpha = 0\ . \qquad \text{(A.IV.6)}$$

One now subtracts (A.IV.6) from (A.IV.3) to obtain

$$\phi_{\eta\eta} - \cos\alpha\ \phi_{\eta\zeta} + \phi_{\zeta\zeta} + \cos\alpha\ \psi_{\zeta\zeta} + A_\zeta \sin^2\alpha - 2u_\eta \sin\alpha = 0\ , \qquad \text{(A.IV.7)}$$

and (A.IV.4) is subtracted from (A.IV.5) to obtain

$$\psi_{\eta\eta} - \cos\alpha\ \psi_{\eta\zeta} + \psi_{\zeta\zeta} + \cos\alpha\ \phi_{\eta\eta} - A_\eta \sin^2\alpha - 2u_\zeta \sin\alpha = 0\ . \qquad \text{(A.IV.8)}$$

Both equations contain references to ϕ and ψ. To avoid this and make the cross-derivatives resemble those of the first two equations of (2.3.5) at the same time, (A.IV.4) is substituted into (A.IV.7) for $\psi_{\zeta\zeta}$ so that the equation becomes

$$\phi_{\eta\eta} - 2\cos\alpha\,\phi_{\eta\zeta} + \phi_{\zeta\zeta} + A_{\zeta}\sin^2\alpha - 2\sin\alpha\,(u_{\eta} - u_{\zeta}\cos\alpha) = 0 \quad . \tag{A.IV.9}$$

Similarly, if (A.IV.3) is used to substitute for $\phi_{\eta\eta}$ in (A.IV.8), then one has

$$\psi_{\eta\eta} - 2\cos\alpha\,\psi_{\eta\zeta} + \psi_{\zeta\zeta} - A_{\eta}\sin^2\alpha - 2\sin\alpha\,(u_{\zeta} - u_{\eta}\cos\alpha) = 0 \quad . \tag{A.IV.10}$$

These last two equations are now used along with the first two of (2.3.5) to form the set of four second-order partial differential equations of (2.3.6).

REFERENCES

Adler, R., M. Bazin and N. Schiffer (1965), Introduction to General Relativity, McGraw-Hill Book Co./Toronto, P. 71 - 72.

Barclay, W. H., and A. H. Ridha (1980), Flow in Streamwise Corners of Arbitrary Angle, AIAA Journal, 18, 1413.

Desai, S. S., and K. W. Mangler (1974), Incompressible Laminar Boundary-Layer Flow Along a Corner Formed by Two Intersecting Planes, Royal Aircraft Establishment Technical Report 74062.

Eichelbrenner, E. A. (1973), Three-Dimensional Boundary Layers, Annual Review of Fluid Mechanics, Van Dyke, M. and W. G. Vincenti (Editors), 5, 339.

Flugge, W. (1972), Tensor Analysis and Continuum Mechanics, Springer-Verlag/New York.

Ghia, K. N. (1975), Incompressible Streamwise Flow Along an Unbounded Corner, AIAA Journal, 13, 902.

Ghia, K. N., and R. T. Davis (1974a), A Study of Compressible Potential and Asymptotic Viscous Flows for Corner Regions, AIAA Journal, 12, 355.

Ghia, K. N., and R. T. Davis (1974b), Corner Layer Flow: Optimization of Numerical Method of Solution, Computers and Fluids, 2, 17.

Jones, C. W. and E. J. Watson (1963), Two-Dimensional Boundary Layers, Laminar Boundary Layers, Rosenhead, L. (Editor), Clarendon Press/Oxford, P. 224.

Libbey, P. A. and H. Fox (1963), Some Perturbation Solutions in Laminar Boundary Layer Theory, Part I: The Momentum Equation, Journal of Fluid Mechanics, 17, 433.

Mikhail, A. G. and K. N. Ghia (1978), Viscous Compressible Flow in the Boundary Region of an Axial Corner, AIAA Journal, 16, 931.

Pal, A. and S. G. Rubin (1971), Asymptotic Features of Viscous Flow Along a Corner, Quarterly of Applied Mathematics, 29, 91.

Rubin, S. G. (1966), Incompressible Flow Along a Corner, Journal of Fluid Mechanics, 26, 97.

Rubin, S. G. and B. Grossman (1971), Viscous Flow Along a Corner: Numerical Solutions of the Corner Equations, Quarterly of Applied Mathematics, 29, 169.

Schlichting, H. (1955), Boundary Layer Theory (First Edition) Kestin, J. (Translator), McGraw-Hill Book Co./New York, P. 116 - 120, 167 - 168.

Sills, J. A. (1969), Transformations for Infinite Regions and Their Applications to Flow Problems, AIAA Journal, 7, 117.

Stewartson, K. (1961), Viscous Flow Past a Quarter-Infinite Plate, Journal of Aeronautical Science, 28, 1.

Stewartson, K. (1974), Multistructured Boundary Layers on Flat Plates and Related Bodies, Advances in Applied Mechanics, Yih, C. S. (Editor), 14, 145.

Tokuda, N. (1972), Viscous Flow Near a Cornèr in Three Dimensions, Journal of Fluid Mechanics, 53, 129.

Van Dyke, M. (1975), Perturbation Methods in Fluid Mechanics (Annotated Edition), The Parabolic Press/Stanford, Cal., P. 121 - 147.

Zamir, M. (1970), Boundary-Layer Theory and the Flow in a Streamwise Corner, Aeronautical Journal, 74, 330.

Zamir, M. (1981), Similarity and Stability of the Laminar Boundary Layer in a Streamwise Corner, Proceedings of the Royal Society of London (Series A), 377, 269.

Zamir, M. and A. D. Young (1970), Experimental Investigation of the Boundary Layer in a Streamwise Corner, Aeronautical Quarterly, 21, 313.

Weinberg, B. C. and S. G. Rubin (1972), Compressible Corner Flow, Journal of Fluid Mechanics, 56, 753.

COMPUTER SOFTWARE

Mathematical routines used to find the far-field boundary values and to perform some of the data reduction are taken from the IMSL Library, Edition 8. These are listed as follows:

DVERK : Runge-Kutta Integration

IBCIEU : Bicubic Spline Interpolation .

The plotting routines used are CALCOMP routines. For the contour graphs, the program UCON2 is used. A source or reference for UCON2 is

UCON2 CONTOURING PROGRAM USER'S MANUAL
FOR USE ON THE CDC CYBER 73
Computing Center, The University of
Western Ontario,
London, Ontario, Canada (1973).

END

20-09183

FIN

The divergence of a vector can be written as

$$u^j|_j = u^j{}_{,j} + u^k \Gamma^j_{jk} \qquad \text{(A.I.6)}$$

which, by (A.I.5), becomes

$$u^j|_j = u^j{}_{,j} + \frac{1}{2} u^k g^{ij} g_{ij,k} . \qquad \text{(A.I.7)}$$

Adler et al (1965) present the following argument in order to simplify the last term. From matrix theory, g^{ij} is the

$$= u^j{}_{,j} + \frac{u^k (g^{1/2})_{,k}}{g^{1/2}} \qquad \text{(A.I.12)}$$

where g is assumed greater than zero.

renamed m and j respectively. The result is

$$u^j u_i|_j = u^j u_{i;j} + \frac{1}{2}(u_j u^j{}_{,i} - u^j u_{j;i}) \quad . \quad (A.II.2)$$